VIRUS-LIKE PARTICLES ELICIT ENHANCED IMMUNITY TO INFLUENZA AND PROVIDE THE SCAFFOLDING FOR A NOVEL VACCINE PLATFORM

by

Laura Elizabeth Richert

A dissertation submitted in partial fulfillment
of the requirements for the degree

of

Doctor of Philosophy

in

Immunology and Infectious Diseases

MONTANA STATE UNIVERSITY
Bozeman, Montana

August 2012

©COPYRIGHT

by

Laura Elizabeth Richert

2012

All Rights Reserved

APPROVAL

of a dissertation submitted by

Laura Elizabeth Richert

This dissertation has been read by each member of the dissertation committee and has been found to be satisfactory regarding content, English usage, format, citation, bibliographic style, and consistency and is ready for submission to The Graduate School.

Allen G. Harmsen

Approved for the Department of Immunology and Infectious Diseases

Mark Quinn

Approved for The Graduate School

Dr. Ronald W. Larsen

STATEMENT OF PERMISSION TO USE

In presenting this dissertation in partial fulfillment of the requirements for a doctoral degree at Montana State University, I agree that the Library shall make it available to borrowers under rules of the Library. I further agree that copying of this dissertation is allowable only for scholarly purposes, consistent with "fair use" as prescribed in the U.S. Copyright Law. Requests for extensive copying or reproduction of this dissertation should be referred to ProQuest Information and Learning, 300 North Zeeb Road, Ann Arbor, Michigan 48106, to whom I have granted "the exclusive right to reproduce and distribute my dissertation in and from microform along with the non-exclusive right to reproduce and distribute my abstract in any format in whole or in part."

Laura Elizabeth Richert

August, 2012

ACKNOWLEDGEMENTS

I would first like to thank my advisor, Dr. Allen Harmsen for his years of guidance, support, insight, and patience. His mentorship and wisdom have been of immense value to me. I would also like to thank my committee for their leadership in directing my project, as well as my career.

The Harmsen lab has provided a uniquely collaborative environment, and I have received help from each and every colleague here. I would like to especially thank Ann Harmsen who not only tirelessly counted my cells, but who also microdissected iBALT with me, all the while managing to provide excellent conversation. I would also like to specifically thank Dr. Agnieszka Rynda-Apple. She advised my very first rotation project with great patience and has been an amazing mentor, role model, and friend to me ever since.

I would like to thank my parents, sister and grandparents for their support throughout many years. I would have never made it as far as I have without their love. Finally, I would like to thank my amazing fiancé, Joshua for being by my side throughout my entire graduate career. He has made the last five years enjoyable and exciting, and has always known when I need to blow off some steam on my mountain bike or skis. Without his late night cell counts and lymph node plucking, many of the “unfavorably timed” kill dates would never have happened.

TABLE OF CONTENTS

1. INTRODUCTION TO DISSERTATION 1

Overview of Dissertation 2

2. BACKGROUND 5

Influenza Virus Background 5
Influenza Virus Genetics 5
Influenza Virus Epidemiology 8
IAV Vaccines 13
Current Antivirals and Resistant IAV Strains 16
Pulmonary Mucosal Immunity 17
Innate Immune Responses to Influenza Infection 17
Adaptive Immune Responses to Influenza 22
Damage Control 26
Inducible Bronchus-Associated Lymphoid Tissue (iBALT) 28
Innate Imprinting 34
Virus-Like Particles and Nanoparticles 37
Virus-Like Particle Vaccines 38
Small Heat-Shock Protein G41C (sHspG41C) 39
Bacteriophage P22 VLP 40

3. VIRUS-LIKE PARTICLES PRIME LUNG DENDRITIC CELLS FOR ACCELERATED PRIMARY ADAPTIVE IMMUNE RESPONSES TO INFLUENZA 43

Contributions of Authors and Co-Authors 43
Manuscript Information Page 44
Abstract 45
Introduction 45
Results 49
Exposure of the Lungs to VLPs Causes Enhanced DC Migration Which Correlates With Accelerated Viral Clearance 49
Exposure of the Lungs to VLPs Causes Enhanced Antigen Processing in Response to an Unrelated Challenge 53
Exposure of the Lungs to VLPs Results in Accelerated Virus Clearance 55
VLP-Exposure Alters the Activity of $CD11c^{+}$ Cells 56
$CCR2^{-/-}$ mice are Delayed in Influenza Clearance Due to Impaired APC Trafficking 59
Enhanced Expression of VCAM-1 and ICAM-1 on DC's Facilitates T Cell Co-stimulation and Activation in VLP-Exposed Mice 62
Exposure of the Lungs to VLPs Promotes the Expansion, and Alters the Trafficking of Flu-Specific $CD4^{+}$ T Cells 64

TABLE OF CONTENTS-CONTINUED

CD8$^+$ T Cell Responses are Not Altered by VLP-Exposure....66
Non-Specific iBALT is an Inductive Tissue, as Well as an Effector Tissue.....67
Discussion....69
Methods....76
Virus-Like Particle Production and Purification....76
Influenza Viruses. 76
Animals and *in vivo* Procedures....76
iBALT Microdissection. 79
FACS Staining and Antibodies. 80
Histology. 80
ELISA. 81
Serum Albumin and Lactate Dehydrogenase Concentration Determination....82
Plaque Assay. 82
Statistics. 82
Supplementary Material....83
Acknowledgements....84

4. A VIRUS-LIKE PARTICLE VACCINE PLATFORM ELICITS HEIGHTENED AND HASTENED LOCAL LUNG MUCOSAL ANTIBODY PRODUCTION AFTER A SINGLE DOSE....85

Contributions of Authors and Co-Authors....85
Manuscript Information Page 87
Abstract....88
Introduction....89
Materials and Methods....92
Production of Small Heat-Shock Protein Cage Nanoparticle (sHsp) 92
OVA Preparation 93
P22 Preparation....94
Optimization of OVA-sHsp Conjugation 94
Synthesis and Purification of the OVA-sHsp Conjugate....95
Limulus Amebocyte Lysate Assay 97
Confirmatory Analysis....97
Western Blots....98
Influenza Virus....98
Mice, Pretreatment, and Challenges 98
Immunostaining and Flow cytometry 100
ELISA 101
Statistics....102
Results....102
Conjugation of OVA to sHsp....102
Characterization of the OVA-sHsp Conjugate 103

TABLE OF CONTENTS-CONTINUED

The Immune Response to OVA-sHsp is Quick and Intense After Only a Single Intranasal Dose....107
The Conjugation of an Antigen to sHsp Results in the Generation of the Same Immune Response to that Antigen as sHsp Itself....110
sHsp Can Act as an Adjuvant in the Lungs....112
sHsp-Treatment Induces Local IgA Responses....116
sHsp Pretreatment of the Lungs Enhances Influenza-Specific Antibody Responses and Changes the Lung Environment, Making it More Conducive to Local Antibody Responses....117
Discussion....121
Acknowledgements....126
Supplementary material....127
Optimization of OVA-sHsp Conjugation....127

5. CONCLUSIONS AND FUTURE STUDIES....134

Future Studies....138
Receptor Recognition of VLPs....138
Differential Functions of iBALT?....139
Governance of Trafficking....140
Regulatory Mechanisms....141
iBALT-Independent Immune Mechanisms....142
Illustrative Mechanism....143

REFERENCES....146

LIST OF FIGURES

Figure Page

3.1. Exposure of the Lungs to VLPs Causes Enhanced DC Migration Which Correlates with Accelerated Viral Clearance 53

3.2. Exposure of the Lungs to VLPs Causes Enhanced Antigen Processing in Response to an Unrelated Challenge 55

3.3. Exposure of the Lungs to VLPs Results in Accelerated Virus Clearance.....57

3.4. VLP Exposure Alters the Activity of $CD11c^{+}$ Cells.....59

3.5. $CCR2^{-/-}$ Mice are Delayed in Influenza Clearance Due to Impaired APC trafficking 62

3.6. Enhanced Expression of VCAM-1 and ICAM-1 on DC's Facilitates T cell Co-stimulation and Activation in VLP-Exposed Mice.....64

3.7. Exposure of the Lungs to VLPs Promotes the Expansion, and Alters the Trafficking of Flu-Specific CD4+ T Cells 66

3.8. $CD8^{+}$ T Cell Responses are not Altered by VLP-Exposure 68

3.9. Non-Specific iBALT is an Inductive Tissue, as well as an Effector Tissue.....69

3.S1. VLP-Exposure Alters the Activity of $CD11c^{+}$ Cells 84

3.S2. VLP-Exposure Reduces Collateral Damage in the Lungs of Both WT and $CCR2^{-/-}$ Mice 84

4.1. OVA was Conjugated to the sHsp S121C Platform 106

4.2. The Immune Response to sHsp is Accelerated and Intensified After Only a Single Intranasal Dose 109

4.3. The Conjugation of an Antigen to sHsp Results in the Generation of the Same Immune Response to that Antigen as sHsp Itself 112

LIST OF FIGURES – CONTINUED

Figure Page

4.4. sHsp Can Act as an Adjuvant in the Lungs 115

4.5. sHsp Treatment Induces Local IgA Responses 118

4.6. sHsp Pretreatment Accelerates the Onset of Influenza-specific IgG in BALF 119

4.7. sHsp Pretreatment of the Lungs Leads to an Even Faster Response to Subsequent Antigens 121

4.S1. Anion Exchange Chromatography Was Utilized to Separate sHsp, OVA, and the Conjugated Species.....130

4.S2. sHsp Pretreated TLR4$^{-/-}$ Mice are Protected from Influenza-Associated Weight Loss 130

4.S3. SDS-PAGE Gel Showing the Ovalbumin Sample Prior to Conjugation with SM(PEG)$_n$ Linkers and OVA Labeled with SM(PEG)$_6$.....131

4.S4. The Ratio of OVA to sHsp Cage Within the Mixed Sample was Determined by Densitometry Analysis of Western Blots.....131

4.S5. The Molecular Weights of Cross-Linked Proteins Within the Linked Sample Were Determined by SDS-PAGE.....131

4.S6. Size Exclusion Chromatography was Utilized to Compare the Sizes of Particles Within the Samples used for *in vivo* Experiments.....132

4.S7. Dynamic Light Scattering Measurements Show the Average Diameter of the Particles Within the Solutions used for *in vivo* Experiments.....132

4.S8. The Relative Conjugation Efficiency of OVA to sHsp for a Matrix of Reaction Conditions was Analyzed via SDS-PAGE.....133

4.S9. A Representation of the Positions of the Reactive Cysteines on the sHsp Crystal Structure for S121C, E102C, and G41C is Shown.....133

LIST OF FIGURES – CONTINUED

Figure Page

4.S10. Western Blots Were Utilized to Identify OVA and sHsp Within the Protein Bands at Higher Molecular Weights 134

5.1. Mechanism of Dissertation 145

ABSTRACT

We first show that the intranasal delivery of virus-like particles (VLPs), which bear no antigenic similarities to respiratory pathogens, prime the lungs to facilitate heightened and accelerated primary immune responses to high-dose influenza virus challenge. These responses were characterized by accelerated $CD103^+$ and $CD11b^+$ dendritic cell trafficking to the local tracheobronchial lymph node (TBLN). Furthermore, both alveolar macrophages and dendritic cells of VLP-exposed mice processed both a model antigen, and influenza virus in the lungs and TBLNs significantly earlier than controls. Additionally, VLP-primed $CD11c^+$ cells that trafficked in a CCR2-dependent manner, and upregulated T cell co-stimulatory molecules were associated with enhanced viral clearance. Influenza-specific $CD4^+$ T cell proliferation and activation were significantly accelerated in both inducible bronchus-associated lymphoid tissues (iBALT) and the TBLNs of VLP-exposed mice. Finally, pulmonary epithelial expression of the polymeric Ig receptor allowed for the enhanced luminal presence of anti-influenza antibody, and these responses were further supported by germinal center B cells and T_{FH} cells in the lung. Thus, the exposure of the lungs to VLPs resulted in enhanced antigen processing abilities, causing accelerated influenza-specific primary immune responses in both the iBALT and TBLNs, which resulted in accelerated viral clearance.

We next show that a model antigen, ovalbumin (OVA), can be chemically conjugated to the exterior of our VLP, the small heat-shock protein (sHsp). When conjugated OVA-sHsp was delivered intranasally to naïve mice, the resulting immune response to OVA was accelerated and intensified, and OVA-specific IgG1 responses were apparent within 5 days after a single immunizing dose. If animals were pretreated with a disparate VLP, P22 (a non-replicative bacteriophage capsid), before OVA-sHsp conjugate immunization, OVA-specific IgG1 responses were apparent already by 4 days after a single immunizing dose of conjugate in OVA-naïve mice. Additionally, the mice pretreated with P22 produced high titer mucosal IgA, and isotype-switched OVA-specific serum IgG. Thus, VLP-treatment elicited quick and intense antibody responses and these accelerated responses could similarly be induced to an antigen chemically conjugated to the sHsp VLP, demonstrating the utility of conjugating antigens to VLPs for pre-, or possibly post-exposure prophylaxis of lung, all without the need for adjuvant.

CHAPTER ONE

INTRODUCTION TO DISSERTATION

The influenza A virus (IAV) annually infects an estimated three to five million people worldwide, resulting in up to 500,000 deaths (WHO; http://www.who.int/mediacentre/factsheets/fs211/en/), thus representing a persistent and prominent concern of immense global impact. While preventative vaccines for IAV are available (to certain populations), viral escape mutants which evade the specific immune responses engaged by vaccination breach the effectiveness of this strategy. Furthermore, the currently available vaccines may have poor efficacy (or contraindication) in at risk populations including the very young, very old, and immunocompromised[3-5]. Finally, while influenza infection may be usually resolved with palliative care in otherwise healthy adolescents and adults, influenza-associated collateral pulmonary damage is known to predispose even healthy individuals to secondary bacterial pneumonias, constituting a considerably more serious situation.

The immune mechanisms responsible for the clearance of the influenza virus are relatively well-studied. However, little is known about how the virus affects a primed lung (as could be expected for human adults), as many of these studies have been performed in the lungs of naïve mice and ferrets. Significantly, it has previously been determined that infection with IAV results in the formation of a tertiary lymphatic tissue in the lungs termed inducible bronchus-associated lymphoid tissue (iBALT)[6]. Moreover, the presence of influenza-specific memory cells harbored in iBALT areas are protective

against a subsequent re-challenge with influenza[6]. Similarly, it is known that the specific sequence of pulmonary encounters with pathogens and antigens may significantly alter the outcome of a subsequent exposure to an antigenically distinct allergen or pathogen via a phenomenon referred to as "innate imprinting"[7]. Thus, pulmonary immune "education" largely dictates the outcome of a challenge with an inhaled pathogen. In this regard, studying immune responses to the influenza virus in the context of pre-existing pulmonary priming carries weighty implications for the determination of vaccination outcomes, as well as the course of the disease and its resolution. Thus, we herein describe how immunity to IAV is altered (to great benefit to the host) when the lungs of mice have been previously exposed to a non-pathogenic priming agent. We have established this state of priming by utilizing virus-like particles (VLPs) which bear no antigenic similarities to agents of future exposure, and show that the inhalation of VLPs elicited pulmonary priming (including the formation of iBALT) which is protective against a subsequent high-dose influenza virus challenge. We have furthermore characterized the underlying immunological mechanisms defining these host-pathogen interactions, which will be described in the following text.

Overview of Dissertation

We have evaluated the use of virus-like particles (VLPs) as a novel vaccine platform for the prevention of influenza virus infection. In the majority of the work we have focused on utilizing the VLPs to induce a state of pulmonary priming, which included the formation of inducible bronchus-associated lymphoid tissue (iBALT).

Primed lungs were then challenged with high-dose influenza virus. Using this model system, we determined the innate and adaptive immune components involved in the clearance of influenza virus in the presence of pre-formed iBALT, as well as other pulmonary augmentations. In a related group of studies, we determined the capacity for utilizing VLPs as antigen delivery vehicles. Here ovalbumin (OVA) was conjugated to the VLPs and we characterized the ability of the VLPs to augment immunity to OVA.

In chapter two, a review of relevant literature as background for the subsequent chapters is provided. In chapter three, we describe the mechanisms by which the administration of prophylactic VLPs to the lungs altered a subsequent immune response to the influenza virus. We found that the intranasal administration of VLPs acted to prime the lungs to facilitate heightened and accelerated primary immune responses to high-dose influenza challenge. These responses were characterized by accelerated $CD103^+$ and $CD11b^+$ dendritic cell trafficking to the local tracheobronchial lymph node (TBLN). Furthermore, both alveolar macrophages and dendritic cells of VLP-exposed mice cleaved both a model antigen (OVA-DQ), and influenza virus in the lungs and TBLNs significantly earlier than controls. Additionally, VLP-primed $CD11c^+$ cells that trafficked in a CCR2-dependent manner, and upregulated T cell co-stimulatory molecules were associated with enhanced viral clearance. Finally, influenza-specific $CD4^+$ T cell proliferation and activation were significantly accelerated in both inducible bronchus-associated lymphoid tissues (iBALT) and the TBLNs of VLP-exposed mice. Thus, the exposure of the lungs to VLPs resulted in enhanced antigen processing abilities, causing

accelerated influenza-specific primary immune responses in both the iBALT and TBLNs, which resulted in accelerated viral clearance.

Chapter four details the use of the VLPs as an antigen delivery platform. We show that VLPs can act as an adjuvant for a normally innocuous protein (OVA), inciting the production of high-titer antibodies within 5 days after a single dose. We further show that when mice are pretreated with a disparate VLP, we can further heighten the responses to a subsequent (unrelated) OVA-VLP conjugate. These heightened responses included the production of mucosal IgA and the recruitment and organization of germinal center B cells and T follicular helper cells.

In chapter five, a summary of the conclusions of the project is provided, followed by potential avenues for future directions. The total references of this dissertation follow chapter five.

CHAPTER TWO

BACKGROUND

Influenza Virus Background

Influenza A virus (IAV), a member of the *Orthomyxoviridae* family, is an enveloped negative sense single-stranded RNA virus that causes respiratory infection in humans, and may result in significant morbidity and mortality for individuals of all immune statuses and ages worldwide[8]. In this regard, the world health organization (WHO) estimates that infection with seasonally circulating IAV strains results in three to five million cases of severe illness, and about 250,000 to 500,000 deaths annually (WHO; http://www.who.int/mediacentre/factsheets/fs211/en/). Furthermore, highly pathogenic pandemic strains of IAV may be substantially more devastating, as was experienced during the Spanish influenza outbreak of 1918[9]. Thus, IAV is a continuingly significant public health concern.

Influenza Virus Genetics

The genome of IAV is composed of 8 disconnected segments which encode 12 viral proteins via post-translational modifications[10, 11]. Two surface proteins, hemagglutinin (HA) and neuraminidase (NA), constitute the major immunodominant surface-displayed antigens[12]. Additionally, HA and NA subtypes are used in viral strain identification and designation (i.e. H1N1). Sixteen subtypes of HA and 9 subtypes of NA have been identified to date, although most circulating human strains are composed of

HA1-3 and NA1-2 with the remaining subtypes being more highly represented in ducks and other aquatic birds[12-14]. Remaining IAV proteins include the nucleoprotein (NP), matrix proteins (M1 and M2), nonstructural proteins (NS1 and NS2), polymerase basic proteins (PB1, PB2, and PB1-F2), and the polymerase acidic protein (PA)[12, 15], each of which plays an essential role in infection and virulence. The HA protein is responsible for viral attachment and membrane fusion to the host cell, by binding host cell sialic acid. Thus, single amino acid substitutions in HA can be directly related to increased pathogenicity of the virus, as has been recognized in certain highly pathogenic strains of IAV[9, 15, 16]. The viral RNA polymerase complex (composed of PB1, PA, and PB2) is responsible for viral transcription and replication, and as such, gain of function mutations in the RNA polymerase complex may result in enhanced viral replication capacity. Additionally, PB1-F2 is a well-established virulence factor, as it induces host cell apoptosis, and can upregulate proinflammatory cytokine production in certain highly pathogenic strains of IAV[15]. The M1 protein provides structure to the IAV virion, while the M2 protein forms an ion channel which conducts protons into the virion core, allowing for the fusion of lysosomal and virion membranes, which facilitates the release of viral RNA into the cytoplasm for transport into the nucleus[17]. NA is required for the liberation of progeny viruses by cleaving sialic acid residues, thus allowing for viral spread. Finally, NS1 antagonizes type one interferon production in infected host cells[15]. Thus, many of the IAV proteins represent both important virulence factors, as well as potential targets of antiviral strategies.

IAV has a tropism for a diverse range of hosts and is known to naturally infect waterfowl, humans, pigs, horses, dogs, cats, minks, seals, whales, tigers, leopards, and terrestrial birds and poultry[18-20]. Interestingly, however while mammalian infection results in upper respiratory tract distress, in waterfowl, IAV manifests as an intestinal tract infection, is spread primarily via the fecal-oral route, and is largely asymptomatic[20]. IAV infectivity per species is largely controlled by the identity of the host cell surface oligosaccharides that terminate in specific sialic acid modifications[20]. For example, human viruses preferentially bind to terminal α2,6-galactose linkages, while avian viruses bind to terminal α2,3-galactose linkages[20-22]. Furthermore, whereas pig tracheal epithelial cells contain both terminal α2,6- and α2,3-linkages, human and avian tracheal epithelium exclusively display either α2,6- or α2,3-linkages, respectively[23-25]. In this regard, avian viruses replicate more than 100-fold less efficiently in humans and other primates[26, 27], and human viruses replicate poorly in waterfowl[28], whereas pigs may be equally infected with both avian and human-specific viruses[29, 30]. Thus pigs provide a pivotal reservoir for potential co-infection and the opportunity for viral reassortment[20, 25, 31].

Antigenic Shift and Drift. As has been recently highly publicized, newly emerging strains of IAV with varying levels of pathogenicity and transmissibility surface and circulate each year. There are two major mechanisms by which newly emerged IAV strains may come to circulate. The IAV RNA-dependent RNA polymerase is highly error prone, and given that no proof-reading mechanisms exist, it is estimated that the replication error rate of insertions, deletions, and mutations is on the order of 1 in 10^4 bases[32-34], resulting in only a fraction of viral progeny particles being infectious[12]. Thus,

point mutations may lead to mutant viruses ranging from uninfectious and unstable to highly pathogenic. Such replication error, resulting in slightly altered mutant strains given by single amino acid substitutions, is referred to as antigenic drift, and underlies the necessity for yearly vaccination. More drastic changes to the viral identity however, can be achieved by genetic reassortment, referred to as antigenic shift. If two or more viruses of alternative strains co-infect the same host cell, significant potential for chromosomal mixing among the viruses occurs. Importantly, if these events occur in the swine population, avian-, swine-, and human-derived viruses may combine to produce viral progeny very unlike the parental strains—indicating an obvious public health concern[10, 35]. As such, pigs have been recognized as "mixing vessels" for various viral strains[36], and it has been shown that indeed a variety of avian and human influenza viruses replicate in pigs both experimentally and naturally[29, 30]. Furthermore, it is now well documented that co-infecting viruses may reassort in pigs[37], and the resultant progeny viruses can be naturally transmitted to humans[25, 38]. Thus, novel strain emergence via reassortment events allow for transgression of the species barrier, and represent an increased likelihood for pandemic potential, given the lack of pre-existing immunity to such novel strains in humans[25].

Influenza Virus Epidemiology

IAV infects individuals of all ages and immune statuses, making it one of the most prominent diseases worldwide. In the United States, it is estimated that 10-15% of the total population will become infected with IAV each year. However, this estimate may rise up to 40% during outbreaks—with the highest rate of infection in young

children and the elderly[8]. Notably, whereas the elderly represent the highest rate of influenza-related mortality, the attack rate in the elderly is actually less than in the very young, which is likely due to partial protection from pre-existing antibodies in the older populations[39, 40]. While most IAV infections are self-limiting in otherwise healthy adults, infants, elderly, asthmatic, immunocompromised, and pregnant individuals are at greater risk for increased morbidity and mortality, indicating the importance for efficient vaccination strategies[41, 42]. Finally, various strains of IAV possess alternative levels of pathogenicity, as has been recently noted for the 2009 pandemic H1N1 virus, which tended to infect individuals with an average age of 29 in contrast to other seasonal strains in which the average age of infection is 59[8]. Furthermore, the demographics of infection also were unexpected as compared to other recently circulating seasonal strains, characterized by a tendency to preferentially target the morbidly obese, African Americans, and Native Americans and Alaskan Natives[43-45]. Thus, immune status, ethnicity, and the infecting strain of IAV can determine the outcome of infection.

In temperate climates, the rate of IAV infection cycles with the seasons, showing an increase during the colder winter months, while in equatorial climates IAV epidemics are less obvious. Importantly, IAV particles are cold-tolerant, stable in low humidity, and can persist as fomites on surfaces for hours[46]. Thus, it is assumed that a major factor in IAV seasonality is indoor crowding—allowing for better transmission through close contact of respiratory secretions by coughing and sneezing, and surface contamination[8, 46].

Upon infection, IAV requires a 2-5 day incubation period during which IAV proliferates in the airway epithelium prior to the onset of symptoms[47]. After incubation however, an extremely rapid development of symptoms is highly characteristic, and aids in distinguishing IAV infection from other respiratory viruses[8]. Predominant symptoms are high fever (>90% of cases), dry cough (>80% of cases), nasal congestion and rhinorrhea (>80% of cases), and may also include headache, myalgia, malaise and fatigue[8].

IAV is a cytolytic virus and also evokes strongly proinflammatory immune responses. As such, infection with IAV holds the potential to significantly damage the delicate pulmonary architecture. Importantly, 7-21 days after the resolution of IAV infection, susceptible individuals may develop a secondary bacterial infection, which are majorly caused by *Staphylococcus aureus*, *Streptococcus pneumonia*, *Hemophilus influenza*, and group A β-hemolytic streptococci[42, 48]. Such secondary infections may occur due to an influenza-related loss of mucociliary clearance, a compromised respiratory epithelium, or impaired neutrophil, macrophage, and lymphocyte function[48-50]. In this regard, it is now recognized that secondary bacterial infections were an important factor in the extremely high rate of mortality during the 1918 Spanish influenza pandemic[51].

Pandemic Strains of IAV. Pandemic strains of IAV have significant historical impact, resulting in millions of deaths worldwide. Historic pandemics strains of IAV include Spanish (1918), Asian (1957), Hong Kong (1968), and Russian (1977) reassortments. Notably, the Spanish flu of 1918 was the most deadly worldwide outbreak

of any pathogen to date, resulting in an estimated 500 million infections and 20-100 million deaths[52, 53]. Worldwide transmission of the virus was probably accentuated by World War I, as troops were in close contact with each other, and much travel back and forth to population dense warzones with suboptimal sanitation practices was occurring. Additionally, the microbiology, transmission and necessary sanitation practices for prevention were poorly understood. Furthermore, it is of note that this pandemic occurred in the pre-antibiotic era.

Via sequencing strategies, we have now identified the causative 1918 IAV strain as an H1N1 virus[51, 52, 54-58]. It is thought to have avian origin, and has been hypothesized to have been passed directly from birds to humans, although this remains to be debated. In support of this theory however, is the increasingly high pathogenicity of the virus as it was propagated by human-to-human transmission in several "waves" of epidemics. In the early 1918 summer wave, H1N1 IAV mortality rates were of the expected seasonal magnitude (although the associated morbidity was comparatively heightened). However, by the fall and winter of 1918, sufficient human-to-human passage had likely allowed for the acquisition of better replication in the human respiratory tract, leading to augmented mortality worldwide[52]. Thus, compared to seasonal IAV H1N1 strains, the 1918 H1N1 was much more pathogenic, causing enhanced infection in young healthy adults, and eliciting a violent pneumonia, often with pulmonary edema and hemorrhage, which frequently led to death within only five days[59].

Such extreme pathogenicity is now known to have resulted from mutations in several Spanish IAV proteins. While generally, IAV replicates in the upper respiratory

tract, the variant 1918 RNA polymerase complex allowed for a higher replication efficiency specifically in the deep lungs. This capability was then compounded by the mutant PB1-F2 and NA proteins which augmented the replication capacity of the virus, allowing for an increase in pulmonary pathology. Finally, the Spanish IAV NS1 elicited enhanced type one interferon inhibition, thus disarming early innate immune responses which are known to be of the utmost importance in infection outcome[52, 60]. While the Spanish IAV HA gene did not contain a mutation which has been specifically recognized to increase viral pathogenesis, when it was experimentally cloned into a contemporary influenza virus, the resultant virus replicated to a higher degree, and caused significant cellular influx into the lungs, resulting in extensive pulmonary damage[9, 16]. Thus, viral gain of function mutations in several of the Spanish IAV proteins lead to strong proinflammatory responses, which elicited extreme pulmonary damage and mortality.

More recently, in 2009 the emergence of a novel H1N1 influenza strain, thought to originate from domestic Mexican swine, resulted in its transmission to 214 countries and caused >18,000 confirmed deaths within one year[23]. This virus was derived from the triple-reassortment of the PB2 and PA genes from an avian virus, the PB1 gene from a human virus, and the remaining gene segments from two distinct lineages of swine viruses[20, 23, 61]. Like the 1918 H1N1 strain, young adults (<35 years of age) appeared to be more permissive to infection as compared to older adults (>65 years of age), however it was later acknowledged that many older adults must have been previously exposed to an antigenically similar virus, as a large percentage of this population harbored cross-reactive antibodies to the novel 2009 H1N1 strain[23]. Finally, while it was originally

feared that the 2009 H1N1 would carry a similar transmissibility, infectivity, and morbidity profile as the 1918 H1N1 strain, these predictions never came to fruition. Additionally, worldwide vaccination programs expedited the production of a vaccine which was quickly delivered to at risk individuals, and was later incorporated into the seasonal influenza vaccine preparation.

Emerging Highly Pathogenic Strains of IAV. A second strain of IAV which has received much recent attention is the highly pathogenic avian H5N1 IAV strain which was first reported to infect poultry in Guangdong, China in 1996[20, 62]. While this virus has become endemic in poultry since then, and continues to be an avian virus to date, there remains grave concern about reassortment events with human viruses, especially given the often close quarters of farmers and animals in endemic areas. Additionally, while the H5N1 strain preferentially infects birds, to date the WHO has reported 566 human infections, with an alarmingly high (60%) mortality rate (WHO; http://www.who.int/influenza/human_animal_interface/H5N1_cumulative_table_archives/en/)[20], although the current H5N1 virus remains to be poorly transmitted between people, as well as between experimental mammalian models[63, 64]. Regardless, in areas where the highly pathogenic H5N1 virus is endemic, the vaccination of poultry is now considered to be a preventative or adjunct control measure[20, 65, 66].

IAV Vaccines

Preventative annual influenza vaccination is the cornerstone for disease control[5, 20]. Four vaccine strategies, including the intramuscularly-delivered trivalent inactivated

influenza vaccine (TIV), the nasally-delivered live attenuated influenza vaccine (LAIV), a newly added quadrivalent LAIV, and an inactivated H5N1 monovalent vaccine which is being stockpiled by the CDC, are the current FDA-approved options (FDA; http://www.fda.gov/BiologicsBloodVaccines/SafetyAvailability/VaccineSafety/ucm110288.htm). Additionally, several groups are currently evaluating the efficacy of delivering the standard split-virus vaccines intradermally, which appears to be quite promising, and is thought to be potentially advantageous due to the abundance of Langerhans dendritic cells present in the skin, which allow for a decreased required dose[3].

With the exception of the H5N1 vaccine, all currently available vaccines contain at least three strains of influenza (four in the quadrivalent LAIV) which are predicted to circulate in the upcoming flu season. The TIV is composed of formalin- or β-propriolactone-inactivated strains of influenza[67], which allow for the safe vaccination of at-risk populations including pregnant women[68]. The TIV is the longest-standing traditional influenza vaccine, and has been shown to be about 80% effective in healthy individuals ages 16-65, given that the infecting strain was included in the vaccine formulation. Pitfalls of the TIV include its significantly reduced efficacy in children and the elderly, and the required needle-based delivery[3, 4].

The LAIV constituents are live attenuated viruses which have been cold-adapted and engineered via reverse genetic technology[69]. Thus, while the LAIV viruses may feebly replicate in the nasal mucosa, they cannot replicate in the lower respiratory tract, given the increased temperature of this site[5, 69]. The LAIV was originally predicted to provide superior protection as compared to the TIV, given that LAIV influenza proteins

are presented to the immune system in their native form. Furthermore, because it is delivered intranasally directly to the mucosa, it should provide a better mimic of natural infection. Indeed, the LAIV has been shown to elicit excellent local mucosal IgA, and strong cell-mediated immune responses[70-72]. However, an unforeseen confounding factor for immunizing adolescents and adults who have been previously exposed to influenza with the LAIV is the presence of pre-existing hemagglutination-inhibiting antibodies, which may disallow LAIV to "protect by infecting"[5, 73]. In children however, the LAIV has been shown to be more effective than the TIV, although it is not recommended for use in infants and toddlers[5].

As mentioned above, the viral strains which are incorporated into both the seasonal TIV and the LAIV are selected based on a predictive model for determining the most likely representative strains circulating in the upcoming flu season. While this predictive strategy is relatively effective, it leaves obvious gaps in protection which are easily breached as newly emerging strains of influenza are introduced, as was experienced in the 2009 H1N1 pandemic. Additionally, both the TIV and LAIV are produced in eggs, which requires a 1 (LAIV) -2 (TIV) year lead time for the production of an ample national vaccine supply[5], again allowing for vulnerability in our current strategy. Importantly, the production of the LAIV requires about half the time to produce equivalent doses to the TIV, given that the expected yield per egg exceeds that of the TIV by 30-50 times[5]. Thus, the LAIV may provide an important advantage during shortages, and furthermore, may provide a more economical option in countries with limited

financial resources[5]. Unfortunately, for both the LAIV and the TIV, the egg-based production process precludes those with egg allergies from vaccination.

Current Antivirals and Resistant IAV Strains

Currently approved antiviral drugs, which are primary utilized in post-exposure prophylaxis, include the adamantanes (amantadine and rimantadine), which inhibit the M2 proton channel of the influenza virus, and the neuraminidase inhibitors (oseltamivir and zanamivir)[74, 75]. Both classes of drugs have been shown to limit the length and severity of infection, with the most efficacious prophylaxis being achieved if the antivirals are administered within 48 hours of infection[8].

Adamantanes block the IAV M2 ion channel protein, which is known to be essential to viral replication[76]. While the adamantanes are highly effective in the prevention of infection[8], single amino acid changes in the viral M2 protein can confer resistance, as has now been widely observed[8, 77]. Furthermore, the adamantanes are not well tolerated due to side effects, especially in the elderly[8]. Thus, while highly effective against susceptible strains, the adamantanes are no longer recommended for IAV prophylaxis.

Neuraminidase inhibitors (NAIs) impede the viral NA enzyme by mimicking sialic acid (its natural substrate)[74]. As such, if progeny viruses cannot be liberated from the host cells, the viral load is decreased[75]. NAIs have a more favorable drug profile, with few side-effects as compared to the adamantanes. Importantly, NAIs have been shown to reduce hospitalizations, secondary bacterial infection and resultant antibiotic use, and additional sequelae for at-risk populations, as well as overall survival, even in the

elderly[8, 78]. Like the adamantanes, resistance to NAIs (especially oseltamivir) can also occur via a single amino acid substitution[79]. From 2007 to 2009 the global frequency of oseltamivir-resistant IAV strains rose from 16% to a staggering 95%[8, 80]! Interestingly however, with the emergence of the NAI-susceptible pandemic H1N1 2009 strain, the concern of NAI-resistance became less spotlighted, and to date, most of the clinical isolates of the 2009 H1N1 remain NAI-susceptible[81, 82]. Vigilant global monitoring however, will continue to be necessary to maintain the efficacy of our best antivirals to date[8, 83, 84].

Pulmonary Mucosal Immunity

Innate Immune Responses to Influenza Infection

Physical Barriers, Small Proteins, and Receptors. Because the respiratory tract is constantly exposed to inhaled foreign particulate of both pathogenic and innocuous forms, it is well-equipped with physical and chemical defense mechanisms, as well with sophisticated antigen recognition. Anatomical barriers of the lung include the mucociliary escalator which transports inhaled particulate antigens that have been captured by the mucous/surfactant layer, to the throat by the unidirectional beating of ciliated epithelial cells. Antigens that arrive in the throat are then swallowed, where they will be likely denatured by the highly acidic stomach environment. Also contributing to pathogen capture are the collectins (surfactant proteins-A and D), which act to opsonize or agglutinate inhaled particulate to enhance uptake by antigen presenting cells (APCs).

Additionally collectins may act to inhibit the growth of certain bacteria, and augment the action of other antimicrobial peptides, such as the α-defensins[85]. The complement system also aids in influenza viral clearance, as has been demonstrated by the increased morbidity and mortality of mice lacking either the C5 or C3 complement proteins[86, 87]. Despite these physical safeguards, some free virus may remain. Thus, virus particles that survive the initial clearance strategies attach to and infect respiratory epithelium, alveolar macrophages, and sentinel airway dendritic cells[15, 88-90].

Pathogen recognition receptors (PRRs), which are majorly expressed on dendritic cells (DCs), alveolar macrophages (AMs), and epithelial cells in the lung, are the second line of pathogen defense, acting to initiate an immune response (or induce tolerance to innocuous antigens). Three types of PRRs are important in viral recognition: Toll-like receptors (TLRs), retinoic acid-inducible gene I (RIG-I)-like receptors (RLRs), and nucleotide oligomerization domain (NOD)-like receptors (NLRs)[91, 92]. The interaction of the TLRs and RLRs on APCs with their ligands initiates a signaling cascade which elicits the production of IFNα/β and activation of NF-κB[93-97]. NF-κB activation then leads to the downstream production of IL-1β, IL-6, IL-8, TNF-α, CCL2 (MCP-1), CCL3 (MIP-1a), CCL5 (RANTES), CXCL10 (IP-10), and increased expression of co-stimulatory molecules including CD40, CD80, and CD86[97-100]. Specifically, cell surface-expressed TLR2 and TLR4 have been shown to be essential to influenza virus recognition and clearance through their recognition of viral envelope proteins[92, 97, 101, 102]. In addition, TLR7 and TLR9, which are both cytoplasmic receptors, are responsible for recognizing viral ssRNA and unmethylated CpG DNA, respectively, thus indicating their antiviral

functions intracellularly[97]. Similarly, the RLRs are also cytoplasmic receptors that recognize viral RNA, indicating an important redundancy in viral recognition[97]. NLRs are a combination of scaffolding and sensing proteins that detect danger signals, thereby initiating the formation of a large cytoplasmic complex called the inflammasome. The inflammasome then acts to bridge the gap between microbial product- and metabolic stress-sensing to the proteolytic activation of IL-1β and IL-18 into their mature forms[97, 103]. The influenza virus specifically engages the NLRP3 inflammasome complex through its viral M2 channel activity in infected DCs and AMs[93, 104-107], thus initiating downstream defense mechanisms.

Antigen Presenting Cells. Two classes of antigen presenting cells (APCs) are majorly implicated in antigen uptake, processing, and presentation in the lung—dendritic cells (DCs) and alveolar macrophages (AMs). Dendritic cells are further divided into two major subsets, conventional DCs (cDC), and plasmacytoid DCs (pDC), based upon their surface expression of various cluster of differentiation (CD) antigens, their location, and their functional characteristics[108]. Although plasmacytoid DCs are known to be potent producers of IFNα/β during viral infection[97], their role in antigen uptake, processing, and presentation is diminuted as compared to conventional DCs[89, 108, 109], which will be the focus of the remaining discussion here. Conventional DCs express high levels of the integrin CD11c and are uniformly negative for expression of the lectin Siglec-F (allowing for their distinction from alveolar macrophages, which also express CD11c)[110-112]. By flow cytometry, DCs are low in the autofluorescent channels, and as they mature, they upregulate MHC II and co-stimulatory molecules (CD40, CD80, CD86, ICAM-1), and

secrete cytokines including IL-12 and IL-1β[109, 113, 114]. Conventional DCs are further subdivided into airway resident DCs, which express high levels of CD103 ($\alpha_E\beta_7$ integrin), and do not express CD11b, whereas parenchymal (or interstitial) DCs have the opposite pattern ($CD103^-CD11b^{hi}$)[111, 113, 115]. Both subpopulations of cDCs have been shown to be essential to pulmonary viral immunity. Sentinel $CD103^+$ DCs are located throughout an interdigitating network along the epithelium and mucosa of the airways. They express tight junction proteins that allow them to extend "periscoping" projections up between airway epithelial cells, where they sample bypassing inhaled luminal antigens[110, 111, 113]. $CD11b^+$ parenchymal dendritic cells are mostly located in the submucosa and parenchyma of the lung and have been similarly shown to efficiently capture exogenous antigen, including influenza virus[109].

Upon antigen capture, DCs (both $CD103^+$ and $CD11b^+$) upregulate the C-C chemokine receptor 7 (CCR7), and thus migrate towards the receptor's ligands, C-C chemokine ligand 19 and 21 (CCL19 and CCL21) via a chemokine gradient. CCL19 and CCL21 are secreted by the lymphatic endothelium, lymph node stromal cells and lymph node endothelial cells, as well as by DCs themselves, in an autocrine manner[116, 117]. As antigen-harboring DCs arrive in the lymph node, they additionally "mature" by upregulating the expression of co-stimulatory molecules and MHC II[114, 118]. Thus, DCs may present their processed antigen to $CD4^+$ and $CD8^+$ T cells in a cognate fashion. It is of note that certain subsets of DCs have been suggested to be better equipped to activate $CD4^+$ versus $CD8^+$ T cells, however, there is still much contradiction on the matter within the literature, which is likely due to the route of delivery and identity of the antigen

utilized in each scenario, as well as advances in phenotyping parameters by flow cytometry[88, 109, 115, 119-125].

The second prominent class of pulmonary APC is the alveolar macrophage. AMs are situated in the deep lung where they are exposed directly to inhaled pathogens and non-pathogenic particulates. While dogmatically, AMs are thought to be immunosuppressive, both historic and recent evidence has revealed that during infection AMs are highly phagocytotic and efficiently carry antigen to the draining lymph node[126-128]. Thus, both $CD103^+$ and $CD11b^+$ DCs, as well as AMs, are highly implicated in viral uptake and trafficking of antigen to the local lymph node[88, 109, 115, 119-123, 127, 128].

Finally, an additional subset of APCs that has been categorized both as a monocyte and DC by various groups has gained much recent recognition[129-135]. This subset has been referred to as "inflammatory monocytes (IMCs)"[131, 134, 136], "inflammatory DCs (IDCs)"[136, 137], "monocyte-derived DCs (moDCs)"[132, 138], "TNF/iNOS-producing DCs (TipDCs)"[129, 139], "exudate macrophages"[133, 135], "myeloid-derived suppressor cells"[140, 141], and "myeloid-derived regulatory cells"[142] by various groups. All of these groups however, report that these populations are CD11c negative and Ly-6G negative, but express high levels of Ly-6C, CCR2, and often, CD11b. Additionally, most studies agree that these Ly-$6C^{hi}CD11b^+$ monocytes are largely precursors of macrophages[143-145] and dendritic cells[144-146], are derived from the bone marrow, and egress from the bone marrow to sites of infection in a CCR2-dependent manner[130, 147]. Furthermore, this population appears to be the dominant population responsible for repopulation of the lungs during pulmonary inflammation/infection.

Functionally, the role for Ly-6C^{hi}CD11b^{+} monocytes in mediating the clearance of pathogens including *Mycobacterium tuberculosis*[148], *Cryptococcus neoformans*[131], *Listeria monocytogenes*[129], and many others[132] has been well documented, however there remains some debate about the contributions of Ly-6C^{hi}CD11b^{+} monocytes during influenza infection. While some groups deem these cells to be necessary for influenza clearance[135, 139], others attribute their role solely to increasing damage in the lungs[133, 149]. As such, Ly-6C^{hi}CD11b^{+} monocytes have been shown to be both proinflammatory[133, 139, 149] and suppressive[136, 139, 140, 142], however perhaps the most insightful study would argue that they exert both proinflammatory and suppressive functions in the context of the timing of infection[136].

Adaptive Immune Responses to Influenza

CD4^{+} and CD8^{+} Effector T Cells.

Within the T cell zones of the tracheobronchial lymph node (TBLN), antigen-loaded DCs interact with T cells, eliciting T cell proliferation and activation[150, 151]. Importantly, while it was previously thought that antigen transfer to lymph node resident CD8α^{+} DCs must occur for antigen presentation in the lymph node[152, 153], recent evidence refutes this necessity. Ballesteros-Tato *et al*. have shown that CD11b^{+} DCs can directly cross-prime CD8^{+} T cells[109], although competing studies would argue that CD103^{+} DCs (and the recently described interferon killer DCs)[154] in fact are the only subsets capable of expanding naïve CD8^{+} T cell populations[88, 115]. CD103^{+} airway dendritic cells are indeed the most susceptible of the DCs to viral infection, and have also been implicated in the efficient expansion of CD4^{+}

T cells[90, 110, 125, 155]. Thus, additional work must be done to resolve these discrepancies. Regardless of DC phenotype, T cells which have interacted with the appropriate DCs and have received appropriate co-stimulation undergo clonal expansion and acquire effector functions over the course of several days[156-158]. Primed effector T cells then exit the lymph node through the efferent lymphatics and the thoracic duct where they may join the bloodstream to traffick to the site of infection (lung).

Effective immunity to influenza utilizes all three major components of adaptive immunity—$CD8^+$ T cell responses, $CD4^+$ T cell responses, and antibody (B cell responses)[159]. As such, mice lacking either $CD4^+$ or $CD8^+$ T cells show a delay in viral clearance, but do not succumb to infection when other immune components are intact[160, 161]. In contrast, however, mice lacking B cells rapidly succumb to infection, despite their ability to mount an efficient $CD8^+$ T cell response, indicating the especially essential function of antibody[162, 163].

Major mechanisms of $CD8^+$ T cell antiviral responses to influenza include the direct lysis of virus-infected cells by the exocytosis of perforin- and granzyme-containing granules[164-166], and the initiation of apoptosis of infected cells by FAS ligand, or TNF-related apoptosis-inducing ligand (TRAIL)[167]. Additionally, although it has been well documented that $CD8^+$ T cell secrete proinflammatory cytokines such as IFN-γ, recent evidence has revealed that these effector T cells may co-produce IL-10, but do so only in the infected lung[168]. In a sister study, it was further recognized that the production of regulatory IL-10 by $CD8^+$ effector T cells required IL-2, which was produced by $CD4^+$ effector T cells, and IL-27 which was produced by inflammatory monocytes, and

neutrophils[169]. Thus, while $CD8^+$ effector T cells are largely thought to exude pro-inflammatory and lytic functions, and there appears to be a previously unappreciated role for regulatory $CD8^+$ effector T cell functions in mediating inflammation at the site of infection. Such regulation is essential to protection of the lung from collateral damage, which will be further discussed below.

$CD4^+$ T cells have been extensively shown to be essential in immunity to influenza by eliciting high affinity antibody production through B cell help[170], and are also known to produce high titers of cytokines including IFN-γ, which drives antibody class-switching to a protective IgG2a subtype[1, 171, 172]. Moreover, most $CD4^+$ effector T cells exhibit T_H1-polarized characteristics and express T-bet in response to influenza infection in an IL-2, and type one- and type two-interferon-dependent fashion[173, 174]. More recently, $CD4^+$ T cells have been shown to have direct cytotoxicity function in the lung via perforin and granzyme B production, thus implicating $CD4^+$ effector T cells as multidimensional contributors to antiviral immunity[175-178]. In addition, recent reports have indicated that T_H17 cells may play a role in the clearance of several viruses, including influenza[174, 179]. And although it remains to be formally demonstrated, T_H17-associated cytokines such as IL-22, have been suggested to be involved in the upregulation of defensins and the promotion of tissue repair[174].

B Cell-Mediated Immunity. Strong neutralizing antibody responses are the cornerstone of antiviral immunity, as well as vaccine production and licensing. Importantly, $CD4^+$ T cells are required for appropriate B cell reactions and stimulation, as in their absence, B cells will undergo apoptosis, irrespective of an ongoing infection[180].

$CD4^+$ T cells that enter B cell follicles and initiate the formation of germinal centers are referred to as T follicular helper (T_{FH}) cells[181, 182]. T_{FH} cells migrate into germinal center areas via the expression of CXC-chemokine receptor 5 (CXCR5). They additionally are defined by their expression of high levels of inducible T cell co-stimulator (ICOS), programmed cell death one (PD1), the transcriptional repressor B cell lymphoma 6 (BCL-6), as well as their production of IL-21 and IL-4[183]. Within the germinal center, the interactions of CD40 on B cells and CD40 ligand (CD40L) on T_{FH} cells initiate B cell proliferation and class-switching[174, 183]. Thus, the interactions of T_{FH} cells with B cells promote the generation of high-affinity class-switched antibody, and long-lived antibody secreting plasma cells.

Neutralizing antibodies to influenza virus are those specific for the HA and NA proteins. HA-neutralizing antibodies may inhibit the function of HA either by directly binding to the receptor attachment site (inhibiting the recognition of host sialic acid residues), or by sterically hindering the conformational changes required for membrane fusion[184]. Neutralizing NA antibodies hamper the budding of virions. Interestingly, while the induction of neutralizing antibodies is the gold standard for measuring vaccine efficacy, in fact, most human antibodies produced in response to influenza vaccination and natural infection are non-neutralizing[185-187]. While these antibodies do not directly bind and inhibit the influenza virus, they do provide protection by three main mechanisms[184]. In FcR-mediated phagocytosis opsonized virus is cleared by the binding of the antigen-antibody complex to Fc receptors expressed on APCs[188]. In antibody-dependent cell-mediated cytotoxicity (ADCC), antigen-antibody complexes bind FCRγIII

on natural killer cells which then kill virions and infected cells. Finally, in complement-dependent cytotoxicity (CDC) antigen-antibody complexes activate host serum complement protein components which eventually assemble to puncture the lipid membrane of the infected cell. Thus, both neutralizing antibodies, and antibodies that act via alternative pathways may elicit sterilizing immunity to viral infection. Importantly, while the historic goal for vaccine design relied on the production of antibodies against the globular head of HA, many groups have been re-evaluating this strategy[184]. In a recently published article, Corti *et al*. describe their discovery of a neutralizing antibody against the conserved stalk region of the HA protein, thus implicating this region of HA as an important target, given that it is less prone to antigenic drift and shift[189].

Damage Control

Immunity in the lung requires that a rapid and efficient immune response occur to provide sterilizing immunity without causing extensive inflammation and collateral damage due to either host or pathogen actions. Furthermore, well-orchestrated repair mechanisms must be in place to maintain efficient oxygen exchange. Influenza virus progeny hijack host plasma membranes by budding, and as such the influenza virus is highly destructive to the respiratory epithelium solely by its replication, and the release of progeny viruses. As infected cells undergo cell death, cellular debris is released into the airways and parenchyma of the lung. In the case that the cell has undergone apoptosis, slightly less damage can be expected. However, if the cell was lysed prior to sequestering

its cellular components into less inflammatory packages, the result can be quite proinflammatory.

Host responses, however, can be equally destructive. The exuberant release of proinflammatory cytokines (especially NOS2 and TNF-α)[126], and cytotoxic granules, the induction of apoptosis, and the recruitment and accumulation of immune cell infiltrate into the lungs can be highly detrimental. Thus, collateral damage from infection is a risk factor for significant morbidities. Luckily, several strategies to regulate and ameliorate host- and pathogen-derived collateral damage exist. As above-mentioned, $CD8^+$ and $CD4^+$ T effector cells not only produce IFN-γ, but can co-produce IL-10, which is an important regulatory cytokine[168]. Also present during influenza infection are regulatory T cells (Tregs). In this regard Antunes *et al*. have recently reported that the adoptive transfer of $CD4^+CD25^+$Forkhead box $P3^+$ ($FoxP3^+$) Tregs ameliorated IAV-associated morbidity in *Rag1-/-* mice while effector $CD4^+$ T cells did not facilitate the same protection[190]. Furthermore, while regulatory cytokines (IL-10 and IL-35) have been implicated in the amelioration of infection in other systems[168, 191], Antunes and coworkers report that the mechanism of Treg cell suppression was not cytokine dependent, and instead Tregs acted to alter the number and distribution of monocytes and macrophages via alterations in recruitment.

Finally, as IAV is cleared, lung tissue is repaired and remodeled to return to homeostasis. Importantly, Monticelli *et al*. have recently defined at least one of the mechanisms by which a damaged lung is repaired. In an exhaustive study they define a novel population of pulmonary innate lymphoid cells (ILCs) ($Lineage^-CD90^+CD25^+$

$CD127^{+}IL\text{-}33R^{+}$) which are similar to the previously described populations of natural helper cells or nuocytes of the intestine[192-195]. These pulmonary ILCs produce an epidermal growth factor family protein, amphiregulin, that acts to restore epithelial integrity[196]. Thus, while an efficient early proinflammatory response must occur to clear IAV, it is equally important for regulatory and remodeling responses to follow, dampening damage associated with both IAV and the immune system itself.

Inducible Bronchus-Associated Lymphoid Tissue (iBALT)

Dogmatically, pulmonary immunity is instigated by the migration of antigen-bearing APCs to the local lymph node where they promote T cell expansion. Antigen-specific T cells are thus recruited back to the lungs where they exert their antiviral functions and then undergo apoptosis (contraction). However, recent evidence would suggest that tertiary lymphatic tissue present in the lung, termed inducible bronchus-associated lymphoid tissue (iBALT) also plays a critical role in the induction and execution of immunity in the lungs. iBALT is the pulmonary component of the common mucosal immune system which includes all mucosa-associated lymphoid tissues (MALT) such as is found in the gut (GALT), nose (NALT), and genitourinary tract (GUALT). However, unlike other MALT, iBALT is not constitutively present in the lungs of healthy adults, but in fact may be induced to develop given antigenic stimulus[197]. As such, iBALT may be equally referred to as a tertiary lymphatic organ (TLO), or ectopic (or effector) lymphoid tissue (ELT).

Stimuli Required for the Formation of iBALT. Like adult humans, the lungs of mice do not contain areas of iBALT under homeostatic conditions[197]. However, iBALT has been experimentally shown to develop in response to infection with influenza virus[6, 198], a replication-deficient modified vaccinia virus Ankara[199], virus-like particles[200], the neonatal exposure to inhaled lipopolysaccharide[201], exposure to other toll-like receptor ligands[202], small proteins[200, 203], diesel exhaust[204], organic dust[205], and cigarette smoke[206, 207]. Importantly, in many of these cases, iBALT organization wanes after the antigenic stimulus is removed and enough rest time is given. Spontaneous iBALT development has also been associated with certain autoimmune disorders including rheumatoid arthritis[208] and Sjögren syndrome[209]. In this regard, animal models have revealed that intact Treg cell function is required for pulmonary homeostasis, as in the absence of appropriate Treg numbers as is observed for $CCR7^{-/-}$ mice (and often in autoimmunity), iBALT may develop spontaneously[210]. Finally, in certain cases, patients with chronic obstructive pulmonary disorder (COPD)[211, 212], idiopathic lung disorders[213, 214], or other pulmonary dysfunction[215-217] are known to develop iBALT. In contrast to adults, the presence of iBALT in children appears to be normal[197, 218, 219], thus emphasizing the importance of local immunity during immune development. The presence of iBALT in fetal lungs however, is largely associated with co-morbidities such as intrauterine pneumonia[220]. Finally, other species such as rabbits and pigs are known to constitutively maintain iBALT structures, independently of antigenic stimulus[221].

Organization of iBALT. Areas of iBALT are generally located at airway bifurcations where branching airways allow for easy antigen deposition[200, 222], and are adjacent to high endothelial venules (HEVs) and lymphatic ducts[6, 223]. iBALT areas are composed of T_{FH} cell[224] and germinal center B cell areas[6], surrounded by interdigitating follicular dendritic cells, as well as CD11c-expressing dendritic cells[6, 198, 200]. Thus, iBALT is organized similarly to secondary lymphoid tissues, although iBALT areas lack encapsulation. Once formed, iBALT-resident DCs efficiently collect antigens from the airways and prime naïve T and B cells[6, 199]. Furthermore, iBALT has been reported to generate memory lymphocytes including long-lived plasma cells[2, 198]. Finally, in LT-$\alpha^{-/-}$ mice which lack other secondary lymphoid tissues, the formation of iBALT is both protective against influenza, and alleviates associated collateral damage[6]. In this regard, iBALT-mediated immunity likely represents an important component of developing immunity for children as well as compensatory mechanism for infection clearance.

Development and Maintenance of iBALT. Many of the molecular signaling pathways required for the development of secondary lymphoid organs (SLOs) are also necessary for the development of ectopic lymphoid tissues[225, 226]. During SLO development lymphoid tissue-inducer (LTi) cells interact with stromal organizer cells to recruit lymphoid cells and initiate SLO formation and organization[203, 227]. As such, it has been recently demonstrated that LTi cells are governed by the transcription factors Id2 and ROR-γt, and mice lacking either transcription factor are unable to develop lymph nodes, Peyer's patches, isolated lymphoid follicles, or NALT[228-230]. Interestingly however, neither the lack of Id2 or ROR-γt expression, nor the lack of LTi cells negate

the formation of tertiary lymphoid tissues, thus implicating a yet undefined population of cells for this role, which likely include IL-17-producing cells[201, 203, 227, 231].

During the formation of SLOs, the interactions of LTi cells with stromal cells result in the expression of homeostatic and recruitment chemokines including CXCL12, CXCL13, CCL19 and CCL21[203]. Similarly, during tertiary lymphoid organ neogenesis CXCL13 (the ligand for CXCR5) is similarly expressed by follicular dendritic cells[232] and as CXCL13 is a potent B cell and T_{FH} cell chemoattractant[233, 234], the overexpression of CXCL13 results in spontaneous lymphoid neogenesis[235]. Similarly, the overexpression of the ligands for CCR7 (CCL19 and CCL21) or lymphotoxin-α (LT-α) also results in the development of ectopic lymphoid organs[236, 237 235], and conversely, their blockade results in follicle disruption[238, 239]. Strikingly, the loss of CXCL13 does not impact iBALT formation[240]. Additional organizational factors have recently been identified by Rangel-Moreno *et al*. who have demonstrated that $CD4^+$ T cell- and γδ T cell-produced IL-17 is also necessary for the formation of iBALT[201]. Furthermore, they found that IL-17 acts to trigger the expression of CXCL13 and CCL19 via an LT-α-independent mechanism, although lymphotoxin is required for the maintenance of pre-formed iBALT.

Dendritic cells are known to be important cellular components of iBALT areas, and have been widely implicated in the local presentation of antigen[241]. However, emerging evidence would additionally indicate a role for DCs in the organization and homeostasis of iBALT areas. We and others have found that in the absence of DCs, the contributions of iBALT in fighting infection significantly wanes[198, 199, and Richert *et al.* unpublished data]. Importantly, GeurtsvanKessel *et al.* show that during influenza infection the

loss of DCs leads to a downstream loss of virus-specific plasma cells and a decrease in mucosal IgA titers[198]. As such, GeurtsvanKessel *et al*., and others additionally demonstrated that DCs potently express CXCL12, CXCL13, CCL19, and CCL21 and furthermore that their expression is augmented by viral stimulus[113, 198], thus implicating TLO resident DCs as multifunctional organizers as well as antigen presenters.

While DCs may promote the formation and maintenance of iBALT, $CD4^{+}CD25^{+}FoxP3^{+}$ Tregs appear to be the counteracting balance in this pathway. The Tregs present in $CCR7^{-/-}$ mice have an intrinsic homing defect, as under normal homeostatic circumstances Tregs express high levels of CCR7[242]. Tellingly, $CCR7^{-/-}$ mice spontaneously develop iBALT without the introduction of environmental exacerbants, while the adoptive transfer of wild-type Tregs inhibits iBALT formation[210]. Lastly, in an alternative argument, Tregs have been shown to differentiate into T_{FH} cells which support germinal center reactions and the production of IgA in SLOs[243]. Thus, Tregs are also highly implicated as multidimensional contributors to the regulation of iBALT.

Role of iBALT in Immunity. There remains some debate about the benefits and drawbacks of the presence of iBALT in terms of both its role in the clearance of infection, as well as potential exacerbation of autoimmune disorders. Notably, it has been reported that the presence of iBALT correlates with increased disease severity for COPD[212] and rheumatoid arthritis patients[209]. It has also been suggested that iBALT may provide a reservoir in which latent microorganisms may reside[244]. However, we and many others would argue for the benefits of iBALT-mediated local immunity during infection. Moyron-Quiroz *et al*. have demonstrated that mice which lack secondary

lymphoid organs, but are able to develop iBALT in response to influenza infection, clear influenza virus (albeit delayed as compared to fully immunocompetent controls) and exhibit reduced collateral damage to great benefit[6]. In a second publication, Moyron-Quiroz *et al*. went on to demonstrate that iBALT may serve as a site for antigen persistence, providing a niche for resting memory lymphocytes, thus allowing for a jump start during rechallenge[2]. Van Panhuys *et al.* further argue that effector lymphoid tissue at the site of pathogen entry is of crucial benefit, as its location at sites of repeated pathogen entry may allow for the local sequestration of antigens and pathogens, thereby limiting the ability of the invader to access the lymph node where it may inspire unnecessary inflammation[245]. In this regard, it is known that B cell-deficient mice (which cannot form organized iBALT) that are infected with *Mycobacterium tuberculosis* are more susceptible to disease pathology, and furthermore that iBALT can be found in both humans and wild-type mice infected with *M. tuberculosis*[225, 246], indicating its role in disease mediation. Similarly, mice which are immunized with antigen to develop iBALT, and subsequently challenged with *Francisella tularensis* are protected from both morbidity and mortality[247]. Finally, in a slightly eccentric study, Trouvanziam *et al*. show that the transplantation of human fetal bronchial tissue into SCID mice allowed for the induction of iBALT which then mediated a robust subsequent T cell response to *Pseudomonas aeruginosa* infection[248]. These and other studies would indicate that iBALT may serve as a general priming site by which T cells may be activated by DCs, regardless of the antigen specificity which had induced the formation of iBALT[198, 199]. In this regard, it has been suggested by many groups that iBALT holds potential for

exploitation as a site for the delivery of drugs and vaccines[249, 250], and furthermore, that a locally-regulated response to infection is correlative with decreased collateral damage[200, 251].

Importantly, while iBALT may provide local immune support during infection, it may play an alternative role during autoimmunity and cancer. Thus, experts in these fields would suggest that TLOs may be detrimental in terms of facilitating epitope spreading during autoimmunity, or may allow for the progression of B cell-mediated (and other) lymphomas[252]. Thus, perhaps the disruption or establishment of TLOs could be equally beneficial depending on an individual's immune status[253].

Innate Imprinting

Immune homeostasis in the lung requires a delicate balance of tolerance and infection fighting signals to achieve the appropriate outcome given the immune stimulant. While it is known that events such as secondary bacterial co-infection during active influenza virus infection are highly detrimental to health, it remains relatively undefined how previous infections (complete with efficient clearance and recovery) affect the outcome of future infections. Importantly, each individual will develop a unique profile of previous pathogen exposure in a personally distinctive sequential order throughout a lifetime of "colds", "allergies", and "flu-seasons". Thus, the immune system becomes primed or tolerized to a unique set of antigens, which affects the outcome of downstream challenges to newly encountered antigens in a phenomenon referred to as "innate imprinting"[7, 254]. Importantly, innate imprinting does not rely on specific memory lymphocyte responses, and strikingly, immunological outcomes will vary greatly given

the exact order of previous pathogen exposure[255]. For example, it is known that a prior lung infection with IAV protects mice against respiratory syncytial virus (RSV)-associated pathology, and also limits the replication of vaccinia virus[256-258]. Conversely, prior IAV infection exacerbates lymphocytic choriomeningitis virus (LCMV)-associated pathology in mice[258]. Furthermore, autoimmune diseases may be linked to an individual's infection history via a similar mechanism, as it has been shown by many groups that the acquisition of certain infections within the first years of life decreases the risk of developing type one diabetes, inflammatory bowel disease, and multiple sclerosis[255, 259-261]. Conversely, RSV infection early in life is thought to be a risk factor for the development of childhood asthma[262]. Thus, innate imprinting appears to rely on both the pulmonary microenvironment, as well as innate immune cells themselves, but does not rely on adaptive memory. In this regard, it has been shown that pulmonary priming with microbial products resulted in downstream protection from several respiratory pathogens[263, 264]. Similarly, we and others have noted that the presence of iBALT is associated with (and likely is one mechanism of) innate imprinting and as such, the antigen utilized to establish the formation of iBALT may be completely unrelated to those of future challenge[7, 200, 251, 265]. Furthermore, as it is thought that local iBALT-mediated pathogen clearance is less damaging than systemic immune activation, innate imprinting also allows for a more succinct immune response with less collateral damage, indicating a close relationship between these two concepts[263]. Related mechanisms of innate imprinting additionally include lasting alterations in pulmonary epithelial cells, heightened DC activity, and innate (natural) antibody[7, 266-269]. Taken together, there is

much evidence in support of innate memory or imprinting that is characterized by a conglomeration of mechanisms including innate immune cell function, natural antibody, and the organization of effector lymphoid tissues.

Heterologous Immunity. Heterologous immunity is related to innate imprinting in that a previous infection with one virus may affect the outcome of future challenges; however the mechanisms for heterologous immunity are distinct for those of innate imprinting. While innate imprinting relies on an alert state of the innate immune cells, in heterologous immunity, cross-reactive T cells (notably $CD8^+$ T cells) which have been established in response to a primary challenge agent provide protection (to some degree) against a secondary pathogen via promiscuous epitope recognition. Given T cell receptors may recognize up to 10^6 different peptides, some level of cross-reactivity is inherent[270, 271]. Heterologous T cell and B cell immunity has been demonstrated for protection between various strains of influenza virus[272]—and more impressively across different viruses altogether[273]. Examples of this include cross-reactive immunity between LCMV and vaccinia virus[274], influenza and hepatitis C virus[275], influenza and Epstein-Barr virus[276], influenza and human immunodeficiency virus[277], and human papillomavirus and a coronavirus[278]. Importantly however, the sequence of infection significantly impacts the outcome by either exacerbating the outcome of a challenging virus or ameliorating it[258, 273]. The mechanisms underlying such distinctively opposite results are still largely undefined, but may involve the timing of recovery and challenge, private T cell repertoires of the individual[279, 280], and differential normal flora[281, 282]. While a complete

consideration of each of these is not in the scope of this discussion, these mechanisms are all likely contributing to each individual's continually evolving immune status.

Virus-Like Particles and Nanoparticles

The application of virus-like particles (VLPs) and nanoparticles to medicine has received much recent attention. While the terms "VLP" and "nanoparticle" encompass a broad spectrum of biologically and functionally diverse molecules, these compounds are related to each other both by their small size (nanometer scale), and by the current interest in exploiting these containers for both medicine and industry. Virus-like particles are derived from viruses, and may be composed of viral capsid or envelop proteins[283]. Importantly however, VLPs do not traditionally contain genetic material, and are therefore not infectious. Interestingly, the antigenicity of VLPs is preserved due to the retained presence of surface-expressed viral epitopes, as was elegantly demonstrated for the human papilloma virus VLP[284, 285]. Due to their empty interior, VLPs may be utilized as delivery platforms for diverse cargo including antigens, adjuvants, peptides, or proteins[283]. Additionally, foreign molecules may be attached to the VLP surface in which case, the natural tissue tropisms for various types of VLPs may be exploited for site-specific targeting[283]. Finally, VLPs are often resistant to degradation via temperature or pH changes, can be produced in high yield, and have intrinsically low toxicity in vivo, thus providing highly advantageous properties for clinical application[286].

While VLP platforms are generally comprised of manipulated, naturally occurring viruses, nanoparticles may include many different molecular compositions and

symmetries. Popular nanoparticles include quantum dots, dendrimers, polymer vesicles, liposomes, and protein-based nanostructures, which will be the topic of further discussion here[286]. Like VLPs, nanoparticles are currently being evaluated for their ability to deliver a compound of choice, which has proven to be quite fruitful. One major caveat of nanoparticle platforms however, is their increased toxicology profile as compared to VLPs. Thus, nanoparticle delivery strategies must be carefully assessed for their *in vivo* safety prior to broad utilization.

Virus-Like Particle Vaccines

The recent utilization of virus-like particles as vaccine delivery strategies has proven to be highly rewarding. In this regard, two VLP-based vaccines are commercially available and FDA-approved (Hepatitis B virus vaccine and Human Papilloma virus vaccine), while a host of others (Norovirus, Hepatitis E virus, Hepatitis C virus, Human and Simian Immunodeficiency viruses (HIV and SIV) Rift Valley fever virus, Influenza virus, Bluetongue virus, Rota virus) are in various stages of research and development[287-293]. VLPs are advantageous for vaccine delivery because they engage evolutionarily conserved surface PRRs, allowing for the stimulation of natural pathways and pre-programmed immune responses. Interestingly however, due to their lack of genomic materials, VLPs do not contain ligands for intracellular TLRs or RLRs, thus the underlying mechanisms by which VLPs drive strong innate immunity are still being determined. One of these mechanisms may involve the incorporation of byproducts leftover from VLP expression systems, such as baculovirus or yeast proteins[294]. Additionally, it is known that the particulate nature of VLPs allows for their efficient

uptake by resident APCs, and furthermore that the highly ordered and repetitive nature of their architecture engages B cell receptors to drive potent humoral immunity[295-298]. Thus, with the strategic addition of adjuvants to the interior or exterior of VLPs, VLPs may provide equally efficacious immunity as native viruses without causing infection[299]. Finally, whereas live-attenuated virus-based vaccines may be contraindicated in certain subpopulations including the very young, very old, and immunocompromised, a non-replicative VLP vaccination strategy may represent an efficacious alternative[97].

Small Heat-Shock Protein G41C (sHspG41C)

In the following studies (described in chapters 3-5) we have utilized the small heat-shock protein cage nanoparticle G41C (sHsp), which we refer to here as a VLP. We note here that while we recognize that the biochemical and structural identity of the sHsp nanoparticle is distinct from virus-like particles, we find that immunologically, the result of delivering sHsp into the lung very closely parallels the result of delivering other "true" virus-like particles such as the P22 bacteriophage (discussed below) and the Cowpea Chlorotic mottle virus (CCMV) (data not shown) to the lung. Furthermore, the immune responses observed in this regard can be better compared to VLP delivery strategies than nanoparticle delivery strategies described in the literature[289, 300, 301]. Thus, in order to create a common theme and best relate our work to comparable strategies and resultant immunological outcomes in the literature, we refer to the sHsp nanoparticle as a virus-like particle throughout the following results.

sHsp was originally isolated from the deep sea hyperthermophilic archaeon, *Methanococcus jannaschii*. When its subunits are expressed in an *E. coli* expression

system, they self-assemble to comprise a hollow 12 nm cage with 24 identical faces[302]. Previous studies by Flenniken *et al*. have shown that sHsp can be genetically and biochemically manipulated to produce clinically relevant sHsp variations[303-305]. Studies from our lab have further shown that when sHsp is administered to mice via several different routes, it is quickly cleared from the body, and does not bioaccumulate with multiple doses[306]. Importantly, no adverse side effects were noted in these studies, even upon repeated dosing[200, 224, 265, 306]. Since the initial characterization and safety evaluation of sHsp in our lab, we have utilized sHsp extensively and have found that the repeated intranasal administration of sHsp induces the formation of iBALT[200] as well as other immunological changes[265]. Significantly, the immune enhancements afforded by sHsp have no cross-reactivity with antigens of future challenge, yet still provide exquisite protection from high dose challenge with certain lung pathogens[200, 224, 265]. Furthermore, as discussed above, and as has been reported by others, this locally-mediated pathogen clearance is less damaging[200, 265]. Finally, in a collaborative effort with the lab of Dr. Trevor Douglas, we have found that when sHsp is conjugated to the model antigen ovalbumin (OVA), and delivered intranasally to mice, these mice generate high titer anti-OVA antibody[224], thus demonstrating the broad utility for sHsp as a more specific VLP platform. The immunological mechanisms governing these results will be further discussed in the following chapters.

Bacteriophage P22 VLP

Our second VLP of use here is the bacteriophage P22[307-309]. P22 naturally infects *Salmonella typhimurium* when intact tail fibers are present. However the P22 VLP of use

here is comprised solely of the phage head lacking all genetic material, therefore rendering it uninfectious. The P22 VLP is produced in an *E. coli* expression system and assembles into a *T=7* icosahedral capsid of 420 copies of the 46.6 kDa coat protein with an external diameter of 58 nm[310, 311]. Like other VLPs described in the chapters to follow, the intranasal delivery of P22 to the lungs of mice elicits the formation of highly organized iBALT, as well as other pulmonary changes. As will be further discussed in the final chapter, we have yet to define the cell surface (or cytosolic) receptors responsible for the recognition of our VLPs. We hypothesize that the highly repetitive faces may engage B cell receptors to elicit T-independent B cell responses; however we also find that T cells are required for VLP-mediated immunity to the influenza virus. We additionally hypothesize that these VLPs may be exhibiting pathogen-associated molecular patterns (PAMPs) or damage-associated molecular patterns (DAMPs) and thus may be signaling through companion pattern recognition receptors (PRRs)[312]. Importantly, while we have used the naked P22 here, this platform is highly amenable to manipulation, thereby providing much potential for vaccine design exploitation[307, 310, 313].

Role of Lipopolysaccharide in VLPs. Because our VLPs are produced in an *E. coli* expression system, we have found that residual lipopolysaccharide (LPS) is likely adjuvanting the effects of the VLPs. Importantly, while there remains legitimate hesitation in the delivery of LPS to the lung, in fact the lung is constantly exposed to LPS through the inhalation of environmental particulate. As such, the lung is intrinsically tolerant to relatively high-doses of LPS[314, 315]. Thus, in line with other VLP strategies including the licensed Human Papilloma virus vaccine[316-318], our VLPs contain an

adjuvant, which boosts the immune responses above those expected when the VLPs are delivered alone. Finally, while we acknowledge that a detoxified version of LPS (monophosphoryl lipid A (MPL)) would likely be a better candidate TLR-agonist for translational and preclinical studies, we find that our current preparation is acceptable for the interpretation of the results to follow. Finally, while we utilized various PRR knockout mice to attempt to tease out the individual contributions of the VLPs and adjuvant in the context on an influenza virus challenge, the results in these studies were confounded by the fact that APCs recognize the influenza virus through TLR2 and TLR4[101, 102]. Furthermore, the induction of the IFNα/β response, as well as $CD4^+$ T cell and B cell responses to influenza virus infection are abrogated in the absence of MyD88 signaling[97, 319].

CHAPTER THREE

VIRUS-LIKE PARTICLES PRIME LUNG DENDRITIC CELLS FOR ACCELERATED PRIMARY ADAPTIVE IMMUNE RESPONSES TO INFLUENZA

Contributions of Authors and Co-Authors

Manuscript in Chapter 3

Author: Laura E. Richert

Contributions: Contributed to designing studies, collected and analyzed data, and wrote the manuscript.

Co-author: Agnieszka Rynda-Apple

Contributions: Contributed to experimental design, data collection, analysis, and interpretation, and critically read and edited the manuscript.

Co-author: James A. Wiley

Contributions: Contributed to funding the research, designing studies, collecting data, and critically read and edited the manuscript.

Co-author: Ann L. Harmsen

Contributions: Contributed to collecting data and critically read and edited the manuscript.

Senior Co-author: Trevor Douglas

Contributions: Obtained funding for virus-like particle production, facilitated the production of virus-like particles, and critically read and edited the manuscript.

Senior Co-author: Allen G. Harmsen

Contributions: Obtained funding for the studies, conceived and designed studies, contributed to data analysis and interpretation, and critically read and edited the manuscript.

Manuscript Information Page

Laura E. Richert, Agnieszka Rynda-Apple, James A. Wiley, Ann L. Harmsen, Trevor Douglas, Allen G. Harmsen
Journal Name: *Mucosal Immunology*

Status of Manuscript:
__ Prepared for submission to a peer-reviewed journal
_X Officially submitted to a peer-reviewed journal
__ Accepted by a peer-reviewed journal
__ Published in a peer-reviewed journal
Published by: Nature Publishing Group
Submitted July 9, 2012

The following chapter has been submitted to the journal *Mucosal Immunology* and appears in this dissertation with the permission of Nature Publishing Group.

Abstract

The intranasal delivery of virus-like particles (VLPs), which bear no antigenic similarities to respiratory pathogens, acted to prime the lungs to facilitate heightened and accelerated primary immune responses to high-dose influenza challenge. These responses were characterized by accelerated $CD103^+$ and $CD11b^+$ dendritic cell trafficking to the local tracheobronchial lymph node (TBLN). Furthermore, both alveolar macrophages and dendritic cells of VLP-exposed mice cleaved both a model antigen, and influenza virus in the lungs and TBLNs significantly earlier than controls. Additionally, VLP-primed $CD11c^+$ cells that trafficked in a CCR2-dependent manner, and upregulated T cell co-stimulatory molecules were associated with enhanced viral clearance. Finally, influenza-specific $CD4^+$ T cell proliferation and activation were significantly accelerated in both inducible bronchus-associated lymphoid tissues (iBALT) and the TBLNs of VLP-exposed mice. Thus, the exposure of the lungs to VLPs resulted in enhanced antigen processing abilities, causing accelerated influenza-specific primary immune responses in both the iBALT and TBLNs, which resulted in accelerated viral clearance.

Introduction

Respiratory immunity requires a rapid and highly regulated execution of unique molecular signaling and cellular recruitment events that then promote appropriate interactions with the invader. Like other mucosal surfaces, the lungs are constantly exposed to antigens, both pathogenic and harmless. However, unique to the lung is the essential maintenance of efficient oxygen exchange during local immune responses.

These criteria require that clearance of pathogens and responses to environmental allergens in the lung occur without unnecessary inflammation or the incursion of inappropriate reactions that may delay sterilizing immunity and the return to homeostasis. Recent evidence suggests that each antigen exposure in the lungs may impact the immunological identity (skewing) and vigor of subsequent unrelated responses, as has been documented for sequential combinations of challenges with many diverse pathogens[7, 254-256, 320]. Pathogen or antigen challenges may thus either augment or dampen future heterologous challenges, depending on the individual's history of previous pathogen exposure[279, 280]. While these responses may be partially governed by cross-reactive T cells[257, 273] or haplotype anomalies[280], heterologous innate immunity also plays an important role in pathogen clearance in a process referred to as innate imprinting[7, 254, 321]. Thus, while we still do not fully understand many of the underlying cellular mechanisms which govern alternative responses to identical challenges, we do recognize the clinical significance of an individual's immune history, especially in consideration of designing new vaccination strategies. Here, we report a mechanism by which the intranasal delivery of virus-like particles (VLPs), which bear no antigenic similarities to agents of future challenge, modulate the pulmonary microenvironment to great benefit, and thus facilitate an enhanced and accelerated level of protection against subsequent high-dose influenza challenge.

The immune response in the lung is dogmatically initiated when sentinel airway dendritic cells sample and internalize inhaled antigen or pathogen, and then migrate through the afferent lymphatics to the local lymph node[116, 118, 322, 323]. Within the lymph

node, newly migrated dendritic cells present their antigens to T cells which then migrate, as effectors, back to the site of infection. Interestingly however, recent evidence has revealed that an immune educated lung, like other mucosal tissues, may in fact be an effector site which is capable of clearing pathogens independently from the lymph node[2, 6, 199, 324], thus suggesting that a second pathway for the initiation and execution of respiratory immunity exists. In this regard, the exposure of the lung to an antigen often elicits the formation of local lymphoid satellite islands termed inducible bronchus-associated lymphoid tissue (iBALT). Organized iBALT is usually found in areas around the bronchioles and adjacent to arteries, and has been reported to be induced in response to diverse respiratory stimuli including viral infection[6], neonatal exposure to inhaled LPS[201], toll-like receptor ligands[202], small proteins[200, 325], cigarette smoke[206, 207], or as a result of certain autoimmune disorders[209, 253]. Importantly, we have previously shown that exposure of the lungs to VLPs also induces the formation of iBALT[200]. Structurally, iBALT is organized similarly to a lymph node, with antigen presenting cells[198, 199], high endothelial venules (HEV's)[326], and germinal center B cells surrounded by follicular dendritic cells, and T follicular helper cell zones[6, 200, 224]. It has been established that iBALT may serve as a site of viral antigen persistence, providing a niche for resting memory lymphocytes which are important in subsequent pathogen exposures[2]. However, little is known about how the presence of iBALT, induced by a stimulus unrelated to the subsequent challenge agent, influences an antigenically distinct primary immune response. Additionally, little is known about how (or if) the presence of iBALT modulates the local lymph nodes' responses to immune challenge, whether it be

independent, antagonistic, or synergistic. We herein describe the immune mechanisms by which pulmonary immune education (or innate imprinting) can be achieved through the intranasal instillation of non-pathogenic VLPs, which act to modulate a subsequent primary immune response to the H1N1 influenza virus (PR8).

The VLPs used here are derived from the small heat shock protein nanoparticles[302, 303, 327], which as we have demonstrated in earlier work, can be safely administered into the lung, and do not bioaccumulate with multiple doses[200, 306]. Moreover, we have shown that the intranasal delivery of these VLPs elicit pulmonary education, which provides subsequent protection against diverse high-dose primary pathogen challenges, while ameliorating collateral damage[200, 224, 265]. We demonstrate in the following studies that VLP-instillation facilitated accelerated influenza virus clearance and enhanced immunity through accelerated airway ($CD103^+$) and parenchymal ($CD11b^+$) dendritic cell trafficking and antigen processing. These responses were dependent upon the presence of $CD11c^+$ cells which had been directly exposed to VLPs, migrated in a CCR2-dependent manner, and transiently upregulated the co-stimulatory molecules intracellular adhesion molecule-1 (ICAM-1) and vascular cell adhesion molecule-1 (VCAM-1).

The initial innate responses to influenza challenge were then followed by an accelerated expansion of influenza-specific $CD4^+$ T cells in both iBALT and the local tracheobronchial lymph node (TBLN), as compared to control mice. The combination of these events resulted in accelerated viral clearance and significantly ameliorated host-derived collateral damage, as previously demonstrated in this system[200]. Furthermore,

using the sphingosine-1-phosphate receptor-1($S1P_1$) agonist FTY720 to block lymphocyte egress out of secondary lymphoid tissues and therefore inhibit cellular recruitment to the lung[328-330], we show that a primed lung, which had not been exposed to any influenza proteins, was efficient at clearing virus, independently of secondary lymphoid help.

Thus, we demonstrate a mechanism of innate imprinting by which a VLP-primed lung, lacking any memory cells to agents of subsequent challenge, elicited alternative cellular trafficking and expansion patterns, and thus allowed for viral clearance at an accelerated rate, with less harmful consequence. Importantly, it has been suggested by us[200, 224], and others[203, 250, 251, 331, 332] that such harnessing of local mucosal immunity, and specifically iBALT function, may in fact pose an important clinical approach to the augmentation of pathogen clearance. And given that we do not exist in a sterile environment, understanding the interplay between pulmonary immune education and disease processes could provide significant insight in clinical application.

Results

Exposure of the Lungs to VLPs Causes Enhanced DC Migration Which Correlates With Accelerated Viral Clearance

Sentinel respiratory dendritic cells (DC's) are the first line of airway defense, sampling inhaled antigen and thereby initiating primary immune responses. Additionally, DC's have been shown to be essential constituents of iBALT[198, 199]. We therefore determined the migration patterns of respiratory DC's in response to influenza virus in

VLP-exposed versus naïve lungs, and the corresponding viral load. In order to establish a state of priming which was not specific to a particular pathogen, and therefore did not harbor pathogen-specific memory lymphocytes, we intranasally (i.n.) instilled virus-like particles (VLPs)[302, 303, 306, 327] (or DPBS) into wild-type mice five times, as we have previously described[200]. Mice were then rested for 72 hours, and challenged with 1.5 X 10^3 plaque-forming units (pfu) of A/PR/8/34 (PR8) influenza virus i.n. Groups were killed at intervals during a 7-day infection course, and the viral load at each time point was determined (Figure 1a). Importantly, we found that VLP-exposed mice had an accelerated rate of viral clearance, showing a significant reduction already by day 4 post-infection, whereas virus continued to replicate/linger in the controls throughout day 7. This result suggested that the early innate immune events are key to enhanced downstream viral clearance. The corresponding trafficking patterns of resident airway[110, 111, 113] ($CD11c^+Siglec\text{-}F^-CD103^+CD11b^-$) and parenchymal ($CD11c^+Siglec\text{-}F^-CD103^-CD11b^+$)[110, 111, 113] DC's from the lungs into the local tracheobronchial lymph nodes (TBLNs) were also altered by VLP exposure (Figure 1b-e). Not surprisingly, in mice that had been primed with VLPs, both the lungs and TBLNs were populated with about 10-fold more DC's, even prior to infection. Strikingly however, both $CD103^+$ and $CD11b^+$ DC's in the lungs of VLP-exposed mice peaked in number, and began migrating from the lungs into the TBLNs between days 1 and 2 post-influenza infection (Figure 1b-e). Furthermore, in VLP-exposed mice we observed a repeatable and sizable loss (or efflux) of both $CD103^+$ and $CD11b^+$ DC's from the TBLNs between 12 and 24 hours, which was recovered over the subsequent 24 hours (Figure 1d-e). As will be further discussed later,

such dynamic DC trafficking, and efflux/loss has been broadly reported by others[118, 333, 334], however the underlying mechanisms governing the rapid decline in trafficking into the lymph node, egress from the lymph node, or apoptosis of DC's remain unclear. A similar pattern to VLP-exposed mice was observed for the $CD103^+$ DC population in the lungs of contr ol mice, albeit at a lower magnitude (Figure 1b). Interestingly, $CD11b^+$ DC's in both the lungs and TBLNs of control mice did not display the same efflux/loss pattern as was observed in VLP-primed mice, and instead $CD11b^+$ DC's steadily accumulated in both sites over the 7-day infection (Figure 1c and e). In the TBLNs of control mice however, while the pattern of expansion and efflux/loss of $CD103^+$ DC's trended similarly to VLP-exposed mice, the timing was delayed until day 4 post-infection (Figure 1d). Taken together, the accelerated rate of DC migration and the resultant enhanced viral clearance in VLP-exposed mice indicated that the rapidity of the innate immune response to a primary influenza challenge is impacted by previous lung priming, regardless of the antigenic specificity.

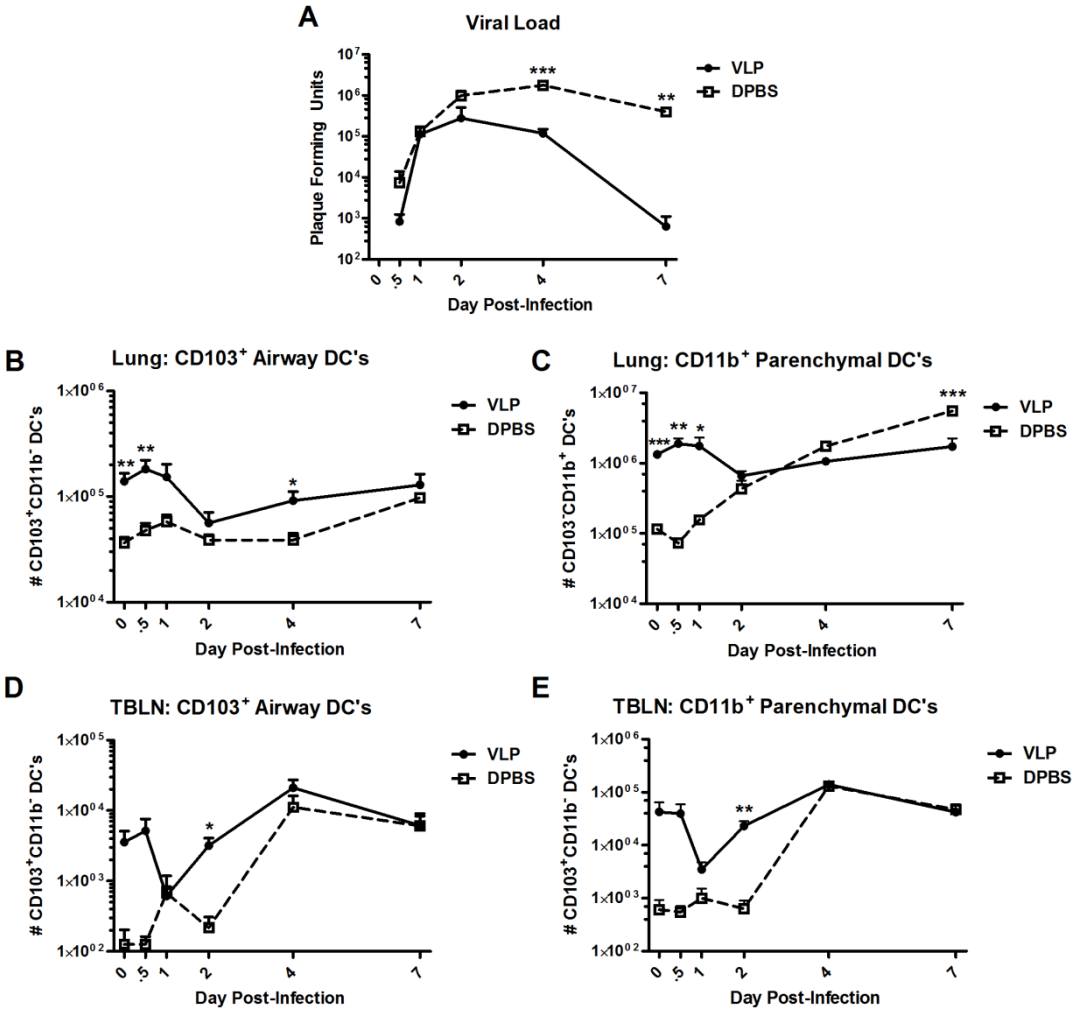


Figure 1 Exposure of the lungs to VLPs causes enhanced DC migration which correlates with accelerated viral clearance. Mice were exposed to VLPs or vehicle i.n. All mice were then challenged with 1.5 X 10^3 pfu PR8 influenza and sacrificed at designated times. (a) Viral load was determined by plaque assay from lung homogenate of the left lung lobe. (b and d) $CD11c^+Siglec\text{-}F^-CD11b^-CD103^+$ resident airway dendritic cells and (c and e) $CD11c^+Siglec\text{-}F^-CD103^-CD11b^+$ parenchymal dendritic cells in the multilobe of the lungs and whole TBLNs were quantified by FACS and total cell counts. A *t*-test was utilized to determine statistical significance at each timepoint. * $P<.05$, ** $P<.01$, *** $P<.001$.

Exposure of the Lungs to VLPs
Causes Enhanced Antigen Processing
in Response to an Unrelated Challenge

Since enhanced dendritic cell trafficking to sites of antigen presentation strongly correlated to the kinetics of viral clearance in VLP-primed mice, we sought to define the potential functional differences in the antigen uptake and processing capacity of DC's elicited by VLP-exposure. As above, we treated mice with 5 i.n. doses of VLPs, or vehicle, rested them for 72 hours, challenged all groups with 100 μg ovalbumin-DQ (OVA-DQ) or control ovalbumin (cold OVA) i.n., and then killed groups at different times after challenge. OVA-DQ is self-quenched in its native form and fluoresces only after it has been proteolytically cleaved, as is accomplished by antigen processing. We therefore were able to directly measure antigen uptake and processing by DC's and alveolar macrophages (AM's) in the lungs. Indeed, we found that both the DC's ($CD11c^{+}Siglec\text{-}F^{-}$) (Figure 2a-b) and resident alveolar macrophages ($CD11c^{+}Siglec\text{-}F^{+}$) (Figure 2c-d) of VLP-primed mice took up and processed antigen with a faster rate and greater efficiency, thereby allowing a jump-start in antigen clearance. In the lungs of VLP-treated mice, as early as 6 hours post-OVA-DQ instillation, DC's and AM's had already begun cleaving OVA-DQ, and this response peaked at 12 hours post-challenge. These events were unparalleled by control mice which never achieved the same level of antigen uptake and processing (Figure 2a and C). Furthermore, as seen previously, the loss of fluorescence indicated that these cells were either migrating away from the delivery site, or alternatively were clearing the antigen by excretion-- both of which are important components in achieving immunity to invading pathogens. Similarly, in the

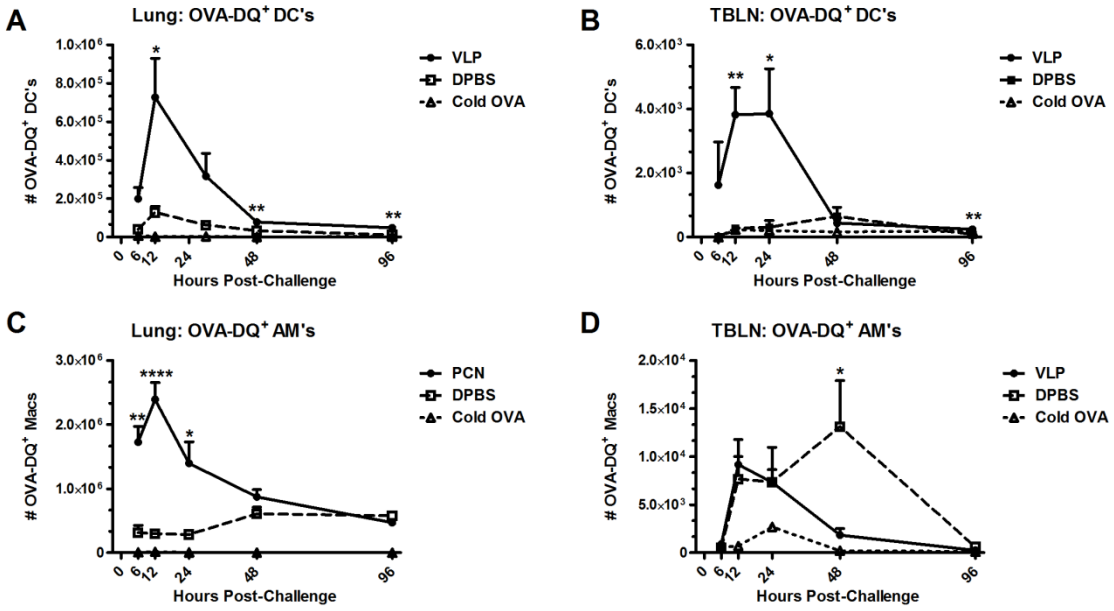


Figure 2 Exposure of the lungs to VLPs causes enhanced antigen processing in response to an unrelated challenge. Mice were exposed to VLPs or vehicle i.n. Mice were then challenged with 100 μg Ovalbumin-DQ, or unlabeled regular "cold" OVA as a staining control i.n., and sacrificed at designated timepoints. (a-b) OVA-DQ$^+$ dendritic cells (DC's) and (c-d) alveolar macrophages (AM) in whole lungs and TBLNs were quantified by FACS and total cell counts. A *t*-test was utilized to determine statistical significance at each timepoint. * $P<.05$, ** $P<.01$, **** $P<.0001$.

TBLNs of VLP-exposed mice DC's were highly active, processing antigen to a significantly higher degree than control mice, and clearing processed antigen already by 48 hours (Figure 2b). Alveolar macrophages in the TBLNs of VLP-exposed mice exhibited less dramatic early differences, however while the DC's and AM's of VLP-treated mice had mostly resolved their activity by 48 hours post-OVA-DQ challenge (Figure 2a-c), migratory macrophages in the TBLNs of control mice were finally able to achieve a similar peak of processing at 48 hours. Therefore not only were both the DC's and AM's in the primed lungs exhibiting alternative and accelerated trafficking patterns, they were also functionally enhanced. However, while OVA is a useful model antigen,

we repeated these studies using an influenza-GFP[335] model to recapitulate these events in an infected lung.

Exposure of the Lungs to VLPs Results in Accelerated Virus Clearance

Given that the timing of an immune response to a pathogen is of the utmost importance to the outcome, we determined if similarly heightened antigen processing occurred in VLP-exposed mice in response to influenza virus infection. Mice were instilled with VLPs or DPBS, rested, then challenged with $1X10^6$ pfu NS1-GFP PR8 influenza, in which the viral GFP expression is dependent on the NS1 promoter[335]. Mice were killed at 1, 2, 3, 4, and 7 days post-infection and the total number of GFP-expressing $CD11c^+$ cells in lung homogenates and bronchoalveolar lavage fluids (BALF) was determined by FACS. Similar to what we observed using OVA-DQ, total $CD11c^+$ cells (including both DC's and AM's) in the lung interstitium of VLP-exposed mice took up the NS1-GFP PR8 virus more rapidly, and processed and cleared the virus, thus quickly degrading the GFP signal (Figure 3a). However, $CD11c^+$ cells of control mice incurred a protracted viral clearance process, resulting in a peak in the GFP signal at day 4. A similar pattern was observed in the BALF, again indicating the importance of the contributions from primed alveolar macrophages (Figure 3b). We further confirmed our FACS results by fluorescent histology in which we observed a similar degradation of NS1-GFP PR8 in VLP-exposed mice over the course of the infection, while the GFP signal remained elevated in control mice throughout the experiment (Figure 3c).

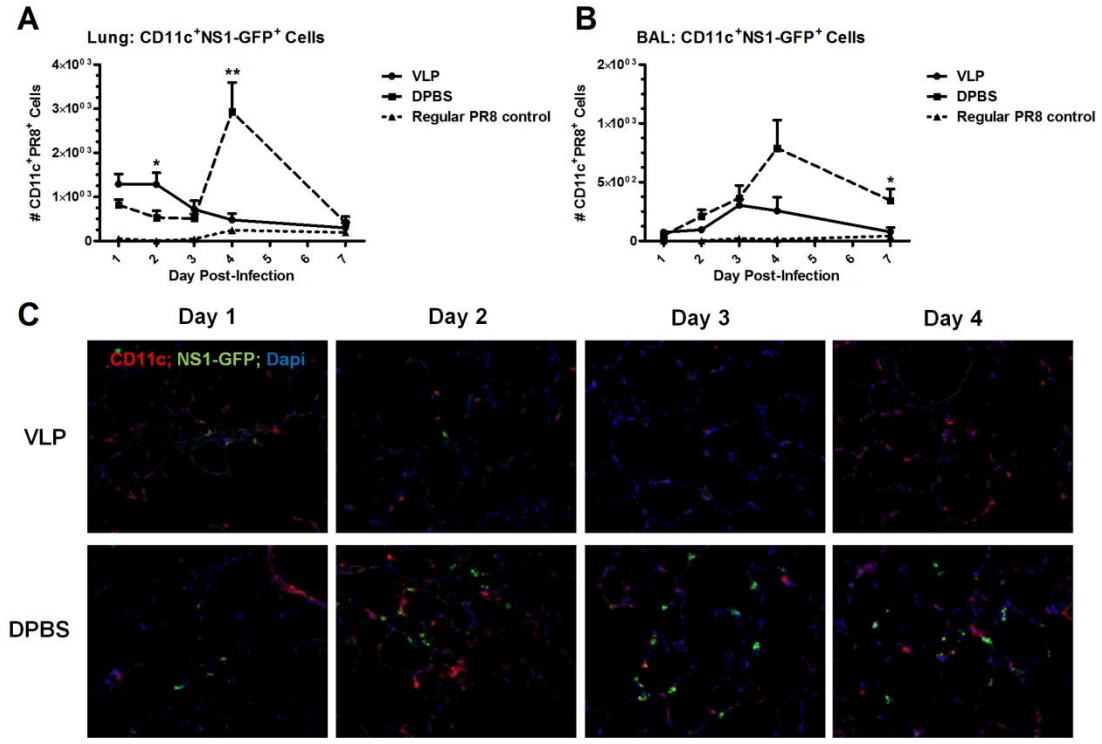


Figure 3 Exposure of the lungs to VLPs results in accelerated virus clearance. Mice were exposed to VLPs or vehicle i.n. All mice were then challenged with $1X10^6$ pfu NS1-GFP PR8 or 1.5 X 10^3 pfu regular PR8 (as control) i.n., and sacrificed at designated timepoints. (a) Total $CD11c^+NS1\text{-}GFP^+$ cells in the multilobe of the lungs and (b) bronchoalveolar lavage (BAL) were determined by FACS and total cell counts. (c) Frozen section histology further revealed that virus was being degraded in VLP-exposed mice, while it continued to replicate in controls throughout day 4 post-infection. A *t*-test was utilized to determine statistical significance at each timepoint. * $P<.05$, ** $P<.01$.

VLP-Exposure Alters the
Activity of $CD11c^+$ Cells

Because we found that both trafficking and antigen processing were accelerated in VLP-exposed mice we next determined whether the observed enhancement of DC and AM function was required for the accelerated viral clearance. We therefore treated CD11c-diptheria toxin receptor transgenic (CD11c-DTR)[336, 337] or wild-type (WT) mice with VLPs, or DPBS, and allowed them to rest for 72 hours. We then administered 100

n.g. of diphtheria toxin intratracheally (i.t.) to all groups to deplete total $CD11c^+$ cells from CD11c-DTR mice. Finally, we allowed new DC's and AM's to reestablish in the lungs by resting the mice for 9 days. Some of the mice were killed before influenza infection to determine DC repopulation whereas other mice were killed at 7 days after infection to determine viral pfu. We thus created fully immunocompetent mice, which had been treated with VLPs, but which contained DC's and AM's that had accumulated in the lungs in the absence of VLPs and thus lacked the primed $CD11c^+$ cells which are normally present in the VLP-exposed mice. DC's and AM's in both the lungs and TBLNs of reconstituted (uninfected) mice were quantified by FACS (Figure 4a-b). Whereas dendritic cell numbers of depleted and reconstituted mice did not return to the lung to the degree seen in VLP-exposed WT mice, presumably because the reestablishment of DC's was not under the influence of VLPs in the lungs, DC numbers in the VLP-exposed CD11c-DTR mice, and in the DPBS-exposed WT and CD11c-DTR mice were not significantly different from each other. This suggested that the repopulation of DC's in the VLP-exposed CD11c-DTR mice was similar to that in mice not exposed to VLPs. There were no significant differences in the total number of DC's in the TBLNs (Figure 4a), and AM's similarly returned equally in all groups in both the lungs and TBLNs (Figure 4b). Similar reconstitution at day 9 was also observed in a complimentary experiment utilizing WT mice treated with an α-CD11c-depleting antibody (Supplementary Figure S1) Hematoxylin and Eosin-stained sections additionally revealed that iBALT was still present in CD11c-DTR mice after reconstitution but tended to be

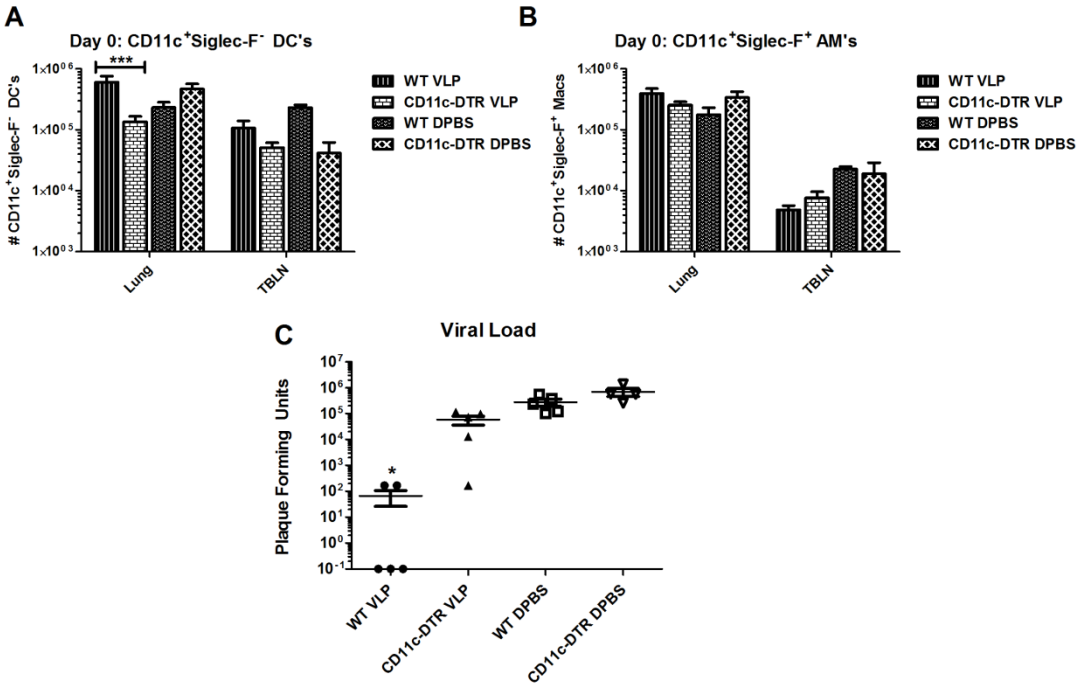


Figure 4 VLP exposure alters the activity of $CD11c^+$ cells. C57BL/6 (WT) or CD11c-DTR mice were exposed to VLPs or vehicle i.n., rested for 72 hours, and then treated with 100 ng diphtheria toxin (DT) intratracheally (i.t) to deplete $CD11c^+$ cells. Next, all groups were rested for 9 days to allow for $CD11c^+$ cell reconstitution from the bone marrow, and finally challenged with 1.5 X 10^3 pfu PR8 influenza. (a-b) At day 9 (day 0 of infection), uninfected, reconstituted mice were sacrificed and (a) total $CD11c^+Siglec\text{-}F^-$ DC's and (b) $CD11c^+Siglec\text{-}F^+$ AM's were quantified from the multilobe of the lungs and whole TBLNs. (c) At day 7 post-infection the remaining groups were sacrificed and the total viral load was determined from the left lobe of the lung. A one-way ANOVA followed by a Bonferroni post-test between groups was utilized to determine statistical significance. * P<.05, *** P<.001.

slightly smaller in size than in non-depleted mice, while no such structures were visualized in controls prior to influenza challenge (not shown). Functionally however, we found that the mice repopulated with naïve $CD11c^+$ cells had lost the enhanced protection from viral challenge afforded by the VLP-exposure. In this regard, at day 7 post-influenza infection, the viral titers in reconstituted CD11c-DTR mice were only slightly

decreased as compared to DPBS-exposed control mice (both WT and CD11c-DTRs) (Figure 4c). These results indicated that the protective effects observed by priming the lungs with VLPs required $CD11c^+$ cells that accumulated in response to or were exposed directly to VLPs. Thus, we next determined how interference of the migration of $CD11c^+$ cells contributes to the observed protection in VLP-treated mice.

$CCR2^{-/-}$ Mice are Delayed in Influenza Clearance Due to Impaired APC Trafficking

The chemokine receptor CCR2 interacts with its ligands MCP-1 (CCL2), and MCP-3[147], to facilitate the migration of macrophage precursors out of the bone marrow and into sites of inflammation[130, 147]. Additionally, CCR2 is required for CCL19 production and subsequent CCR7-dependent migration[338], which is known to be highly important in influenza virus responses. Thus, the interactions between CCR2 and its ligands are integral to the cellular trafficking responses during infection. Given that we have found that very early AM and DC recruitment and movement in the lungs and TBLNs is more active in mice exposed to VLPs (Figure 1), we next determined whether this enhanced migration was responsible for the observed enhanced viral clearance by utilizing $CCR2^{-/-}$ mice. We found that proficient early macrophage trafficking, specifically to iBALT areas, was associated with viral clearance in VLP-exposed mice (Figure 5). $CCR2^{-/-}$ or WT mice were exposed to VLPs or vehicle, challenged with influenza virus, weighed daily, and killed at day 7 post-infection. We found that VLP-exposed $CCR2^{-/-}$ mice were not protected from influenza infection (Figure 5a), and that they were only partially protected from influenza-associated morbidity, as indicated by

weight loss (Figure 5b). We next characterized the trafficking patterns in VLP-exposed $CCR2^{-/-}$ mice. Surprisingly, we found only subtle differences in numbers of DC's and AM's recovered in the lungs and TBLNs of each group during the 48 hours following infection (Figure 5c-f). However, we saw striking differences between $CCR2^{-/-}$ mice and WT mice in numbers of recruited Ly-$6C^{hi}CD11b^{+}$ monocytes. In both the lungs (Figure 5g) and the TBLNs (Figure 5h), we found that regardless of treatment with VLPs, $CCR2^{-/-}$ mice lacked migratory Ly-$6C^{hi}CD11b^{+}$ monocytes (as has been similarly reported by others[130, 147]). Additionally, only in WT VLP-exposed mice did we find recruited Ly-$6C^{hi}CD11b^{+}$ monocytes in the TBLNs over the first 48 hours of infection (Figure 5h). Finally, we examined the cellular trafficking of DC's and AM's directly into areas of iBALT. At 12 hours post-infection, VLP-exposed or control mice were sacrificed, and areas of iBALT were specifically microdissected from live lung sections and prepared for FACS. While DC trafficking into iBALT areas was not noticeably impaired in $CCR2^{-/-}$ mice (Figure 5i), importantly, AM's in $CCR2^{-/-}$ mice accumulated in the iBALT at significantly decreased numbers in both VLP-exposed and control mice (Figure 5j). Thus, the delay in early recruitment of alveolar macrophages ($CD11c^{+}$Siglec-F^{+}) into iBALT areas and inflammatory monocytes (Ly-$6C^{hi}CD11b^{+}$) into the lungs and TBLNs was likely detrimental to downstream viral clearance. Taken together, when early monocyte/macrophage trafficking was impaired or delayed, the protection afforded by VLP-priming was lost. However, intermediate morbidity was observed, indicating that enhanced APC trafficking capabilities are likely not the sole immunological mechanism at play. We thus determined how the enhancement of early events, including macrophage

Figure 5

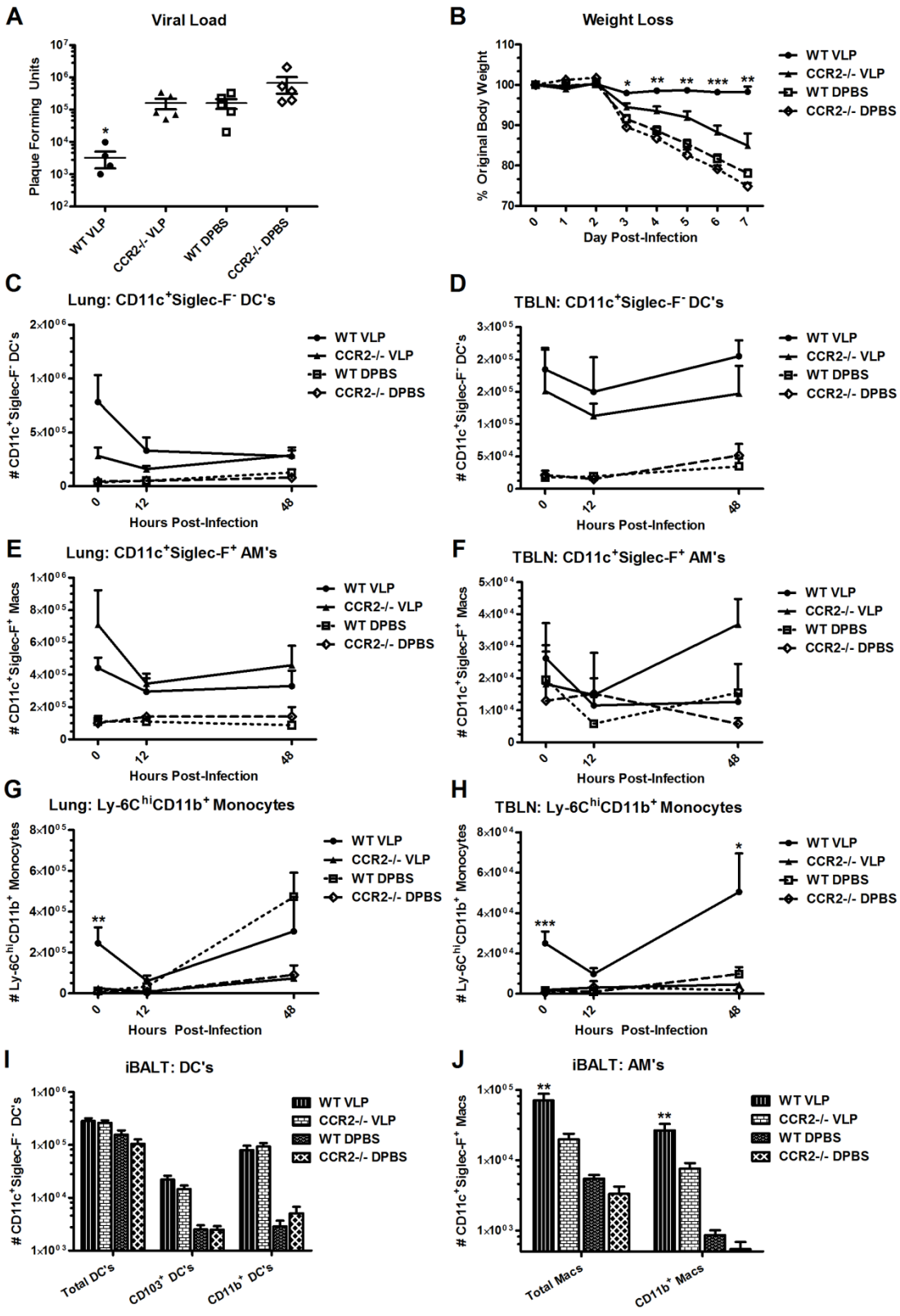

A
Viral Load
Plaque Forming Units
WT VLP
CCR2-/- VLP
WT DPBS
CCR2-/- DPBS
B
Weight Loss
% Original Body Weight
Day Post-Infection
C
Lung: CD11c+Siglec-F- DC's
CD11c+Siglec-F- DC's
Hours Post-Infection
D
TBLN: CD11c+Siglec-F- DC's
E
Lung: CD11c+Siglec-F+ AM's
CD11c+Siglec-F+ Macs
F
TBLN: CD11c+Siglec-F+ AM's
G
Lung: Ly-6Chi CD11b+ Monocytes
Ly-6Chi CD11b+ Monocytes
H
TBLN: Ly-6Chi CD11b+ Monocytes
I
iBALT: DC's
Total DC's
CD103+ DC's
CD11b+ DC's
J
iBALT: AM's
Total Macs
CD11b+ Macs

Figure 5-Continued $CCR2^{-/-}$ mice are delayed in influenza clearance due to impaired APC trafficking. C57BL/6 (WT) or $CCR2^{-/-}$ mice were exposed to VLPs or vehicle i.n. Mice were rested for 72 hours, and then challenged with 1.5 X 10^3 pfu PR8. (a) At day 7 post-infection, mice were sacrificed, and viral load was determined from the left lobe of the lungs. (b) Mice were weighed daily over the course of the infection. (c-h) Additional groups of mice were used to determine the cellular trafficking at early timepoints after infection. At 0, 12 hours, and 48 hours post-infection mice were sacrificed and the multilobe of the lungs and whole TBLNs were collected and prepared for FACS. Tissues were stained for (c-d) DC's, (e-f) AM's, and (g-h) Ly-$6C^+CD11b^+$ monocytes. Also at the 12 hour post-infection timepoint, the lungs from some groups of mice were inflated with agarose, sectioned, and iBALT areas were specifically microdissected from whole lungs. Total (i) DC's and (j) AM's in iBALT areas were quantified by FACS and total cell counts. A one-way ANOVA followed by a Bonferroni post-test between groups was utilized to determine statistical significance for each timepoint. * $P<.05$, ** $P<.01$, *** $P<.001$, **** $P<.0001$.

and dendritic cell recruitment, trafficking, and antigen processing impacted downstream antigen presentation, and subsequent T cell expansion.

Enhanced Expression of VCAM-1 and ICAM-1 on DC's Facilitates T Cell Co-stimulation and Activation in VLP-Exposed Mice

Vascular cell adhesion molecule-1 (VCAM-1) and intracellular adhesion molecule-1 (ICAM-1) are expressed on dendritic cells and are required for the co-stimulation of T cells to facilitate proliferation[339-342] and form a functional immunological synapse complex[343-345]. We therefore determined the expression patterns of both VCAM-1 and ICAM-1 on dendritic cells from lungs or TBLNs of VLP-exposed or control mice, at different times after influenza infection. In the lungs of mice exposed to VLPs, the expression of both VCAM-1 and ICAM-1 were significantly upregulated at twelve hours post-influenza infection, indicating tightly regulated, enhanced co-stimulatory activity directly in the lungs (Figure 6a). By 24 hours post-infection, both receptors were

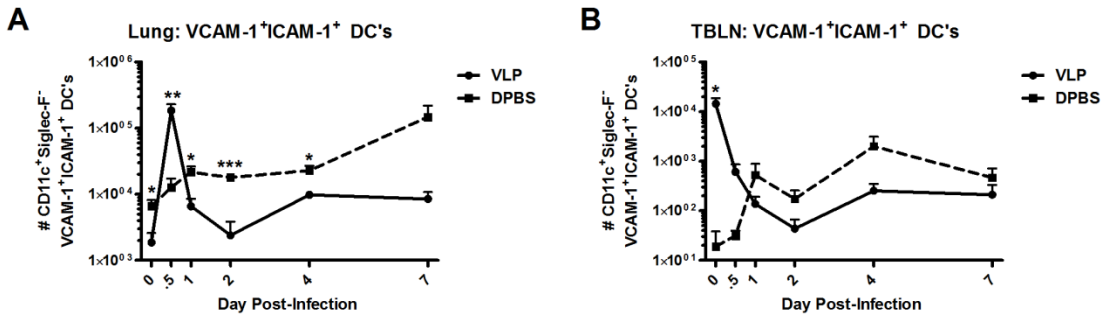


Figure 6 Enhanced expression of VCAM-1 and ICAM-1 on DC's facilitates T cell co-stimulation and activation in VLP-exposed mice. Mice were exposed to VLPs or vehicle i.n. Mice were rested for 72 hours, and then challenged with 1.5 X 10^3 pfu PR8. (a-b) At 0, 12 hours, and 1, 2, 4, and 7 days post-infection mice were sacrificed and $CD11c^+Siglec\text{-}F^-VCAM\text{-}1^+ICAM\text{-}1^+$ DC's were quantified from (a) the multilobe of the lungs and (b) whole TBLNs by FACS and total cell counts. A *t*-test was utilized to determine statistical significance at each timepoint. * $P<.05$, ** $P<.01$, *** $P<.001$.

substantially down-regulated, perhaps indicating both the declining need for such heightened expression, and a profoundly regulated expression. Conversely, the DC's of control mice achieved no such peak, and in fact displayed an opposite trend, as they continued to slowly and progressively upregulate the expression of co-stimulatory molecules throughout the course of the 7-day infection. In the TBLNs, we found that in VLP-primed mice VCAM-1 and ICAM-1 are already highly expressed at day 0 (uninfected), and furthermore, that the number of DC's expressing co-stimulatory molecules declines over the course of infection, which is again an opposite response from control mice, whose lungs and TBLNs respond very similarly (Figure 6b). Taken together, VLP-exposed DC's in the lungs rapidly (by 12 hrs.) upregulate the expression of surface co-stimulatory molecules ICAM-1 and VCAM-1and subsequently rapidly down regulate these co-stimulatory molecules. However in the TBLN, there is a rapid loss of co-stimulatory molecule-expressing DC's in first 24 hrs. This is consistent with

the early loss of DC numbers from the TBLN of VLP-instilled mice as seen in Figure 1. Thus, we next determined whether VLP-exposed mice were more efficient at activating and expanding T cells, which could explain the profound reduction in viral load at early timepoints in these mice.

Exposure of the Lungs to VLPs Promotes the Expansion, and Alters the Trafficking of Flu-Specific $CD4^+$ T Cells

VLP- or DPBS-exposed mice were adoptively transferred with CFSE-labeled naïve transgenic $CD4^+$ T cells specific to the influenza hemagglutinin ($HA_{126-138}$) peptide from HNT mice[1]. Twenty-four hours after the adoptive transfer, all mice were infected with 1.5 X 10^3 pfu PR8, and the transferred T cells were followed by FACS over the infection course to determine division and activation. We determined the $CD4^+$ T cell responses specifically in the iBALT, as well as in the lung, BAL, TBLN, and spleen (Figure 7). Flu-specific $CD4^+$ T cells migrated into areas of iBALT, and expanded to a peak response at day five, as characterized by a loss of CFSE and upregulation of CD44 (Figure 7a). This indicated that a highly potent and adept $CD4^+$ T cell response was occurring, specifically within areas of iBALT in VLP-instilled mice and was subdued in DPBS-instilled mice. Additionally, this $CD4^+$ T cell expansion in the VLP-instilled mice was tightly regulated and as viral load was beginning to be controlled, $CD4^+$ T cells were significantly contracted. In whole lung homogenate, the pattern was slightly different—while the same peak response was observed at day five in the lungs of VLP-exposed

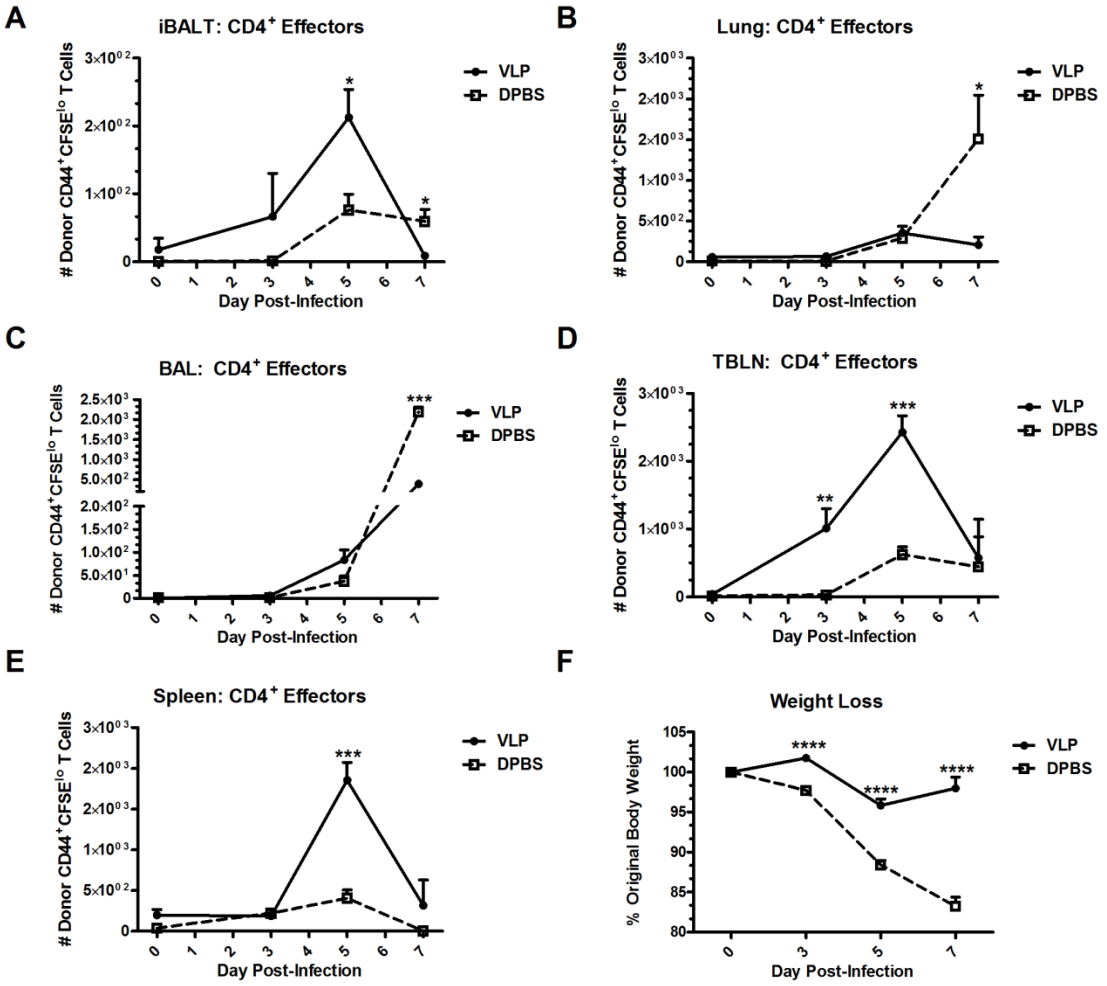


Figure 7 Exposure of the lungs to VLPs promotes the expansion, and alters the trafficking of flu-specific $CD4^+$ T cells. 1.2 X 10^7 naïve CFSE-labeled influenza-transgenic $CD4^+$ T cells from HNT mice[1] were transferred intravenously (i.v.) into Thy1.1 recipients which had been exposed to VLPs or DPBS i.n. Recipient mice were rested for 24 hours post-transfer, then infected with 1.5 X 10^3 pfu PR8. At days 0, 3, 5, and 7 post-infection one group was sacrificed and $CD4^+Thy1.2^+CD44^{hi}CFSE^{lo}$ donor T cells were quantified by FACS and total cell counts from (a) microdissected iBALT (b) total lung homogenate from the multilobe of the lung (c) BAL (d) TBLN and (e) spleen. (f) Body weights were determined over the 7 day infection course. A *t*-test was utilized to determine statistical significance at each timepoint. * $P<.05$, ** $P<.01$, *** $P<.001$, **** $P<.0001$.

mice, the control animals were obligated to continue to mount a response throughout day 7, again indicating differences in viral load and the necessity for effector $CD4^+$ T cells to be present in the lung for an extended time (Figure 7b). $CD4^+$ T cells present in the lavage appeared to have roughly the same pattern as in the lung, with no early significant differences between groups (Figure 7c). In the TBLN, donor $CD4^+$ T cells were considerably more rapid in division, and the upregulation of CD44, achieving a significantly more robust early response already by day 3 post-infection (Figure 7d). As was seen in iBALT areas, total numbers of activated T cells peaked at day 5 and had been contracted significantly already by day 7 post-infection. Finally, we noted that the effects of VLP-instillation are not exclusive to the respiratory tract, and in fact promote immunity in distal sites, such as the spleen (Figure 7e), which exhibited an almost identical pattern of expansion, activation, and contraction as we had observed in the local lymphoid sites of the lungs, including iBALT. Finally, as expected, VLP-exposed mice were protected against influenza-associated weight loss (Figure 7f). Thus, the priming of the lung with VLPs accelerated the expansion of flu-specific $CD4^+$ T cells in the lung and TBLN, speeding the rate of activation and resulting in enhanced viral clearance.

$CD8^+$ T Cell Responses are Not Altered by VLP-Exposure

In a similar study, without adoptive transfer, we determined the kinetics of influenza-specific $CD8^+$ T cells specifically within iBALT areas and TBLNs through combined H-$2D^b$ $NP_{366-374}$ (NP) and H-$2D^b$ $PA_{224-233}$ (PA) MHC I influenza tetramer staining and FACS analysis. While $CD8^+$ T cells have historically been shown to be

important in viral clearance of influenza, neither their function[200] nor their associated kinetics (Figure 8) seemed to be altered by VLP-exposure. Thus, it appeared that enhanced antiviral T cell responses after VLP-exposure were a contribution of the accelerated $CD4^+$ T cell trafficking and division only, and were not dependent upon an enhancement of $CD8^+$ T cell activity.

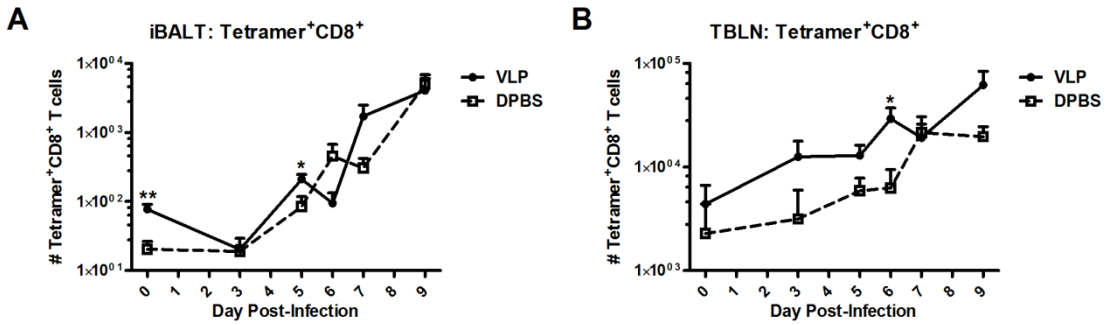


Figure 8 $CD8^+$ T cell responses are not altered by VLP-exposure. Mice were exposed to VLPs or vehicle i.n, rested for 72 hours, and then challenged with 1.5 X 10^3 pfu PR8. (a-b) Total MHC I influenza NP and PA $tetramer^+CD8^+$ T cells were quantified from (a) microdissected iBALT and (b) TBLNs over 9 days of infection. A *t*-test was utilized to determine significance at each timepoint. * $P<.05$, ** $P<.01$.

Non-Specific iBALT is an Inductive Tissue, as Well as an Effector Tissue

Dogmatically, a primary immune response in a naïve lung requires cellular trafficking of antigen presenting cells to the draining lymph node in order for T cell activation and recruitment back to the effector site. However, previously reported data have indicated that the TBLN may not be of crucial importance in the presence of iBALT[2, 6, 200]. We therefore determined how the primary antiviral immune response was impacted by the TBLN's input in immunocompetent animals. In order to isolate the

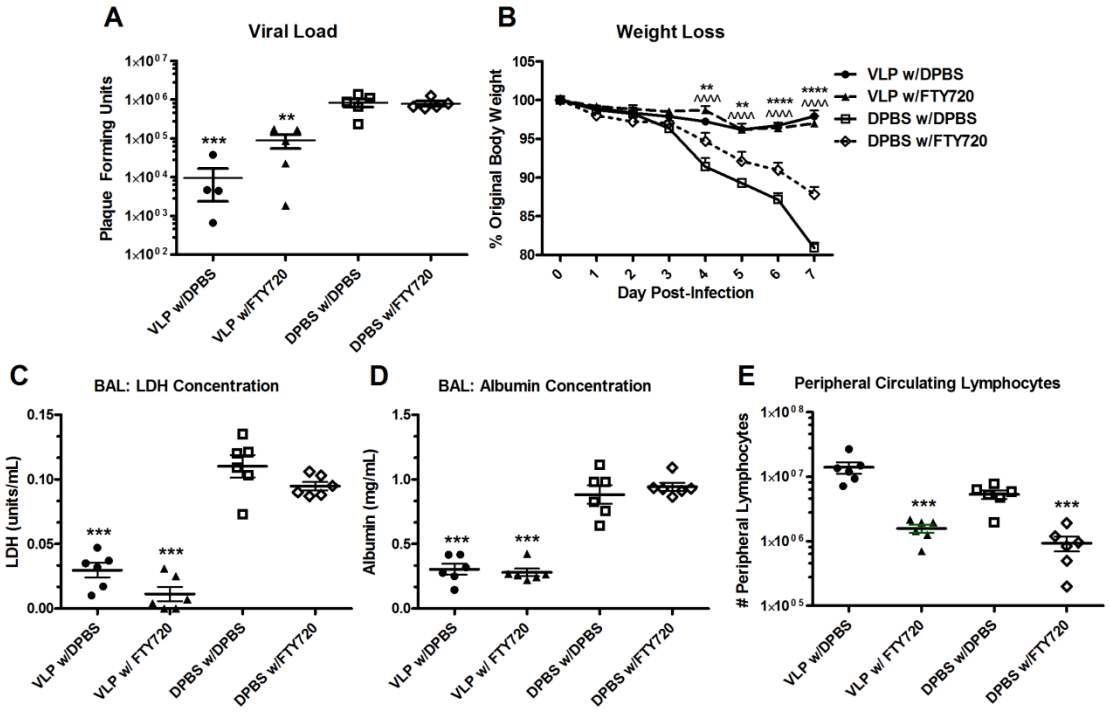


Figure 9 Non-specific iBALT is an inductive tissue, as well as an effector tissue. Mice were exposed to VLPs or vehicle i.n, rested for 72 hours, and then treated with FTY720 (4 mg/kg)[2] or vehicle intraperitoneally (i.p.) 6 hours prior to challenge with 1.5 X 10^3 pfu PR8. Daily FTY720 (or DPBS) was administered over the infection course to maintain lymphocyte sequestration into secondary lymphoid organs. (a) Viral load was determined from the left lung at day 7 post-infection. (b) Mice were weighed daily over 7 days. (c-d) The concentration of damage indicators (c) lactate dehydrogenase and (d) serum albumin were measured from 2 mL BALF at day 7 post-infection. (e) Peripheral lymphocytes in the blood were quantified from each group to ensure depletion by FTY720 treatment. A one-way ANOVA followed by a Bonferroni post-test between groups was utilized to determine statistical significance. ** P<.01, *** P<.001, **** P<.0001.

iBALT's local antiviral responses from the TBLN's contributions, we instilled mice with either VLPs or DPBS as above, then administered the sphigosine-1-phosphate receptor 1 ($S1P_1$) inhibitor, FTY720, or DPBS i.p. 6 hours prior to infection, and then again daily over the course of influenza infection to continually sequester lymphocytes into lymphoid

tissues, and prohibit egress and trafficking from peripheral sites[2, 329]. Importantly, mice that had been instilled with VLPs, with or without FTY720 treatment, were able to clear influenza infection to a significantly higher degree than mice instilled with DPBS (Figure 9a). Furthermore, those mice treated with VLPs, followed by FTY720, did not lose weight over the infection timecourse (Figure 9b), and showed decreased lung damage, as indicated by the reduced concentration of lactate dehydrogenase (LDH), and albumin in the bronchoalveolar lavage fluid (BALF) as compared to controls (Figure 9c-d). We also evaluated the completeness of lymphocyte sequestration by FTY720 administration by enumerating peripheral blood lymphocytes and found that they were significantly decreased to levels considered to indicate biologically relevant depletion[2] (Figure 9e). Thus, the lung achieved a protective immune response, without cellular trafficking from the TBLN or periphery, and without out the aid of any memory responses.

Discussion

Our understanding of the mechanisms by which remarkably divergent responses to identical pathogens may occur at the individual level, based upon past exposure events remains to be fully developed. In our current studies, we have described a model of innate imprinting by which the instillation of VLPs, which bear no antigenically similar components to influenza, protected naïve mice against subsequent high-dose flu challenge. Importantly, differential DC trafficking from the lungs into the TBLN accelerated the onset of the primary immune response. Dendritic cells are known to be essential to both influenza virus clearance[119] and the maintenance of iBALT[198, 199], which

we have previously shown is a result of VLP-exposure[200]. Additionally, viral infection is known to increase the number and rate of DC trafficking from the lungs to the lymph node, which is especially dynamic at early stages of infection[267, 333]. In fact, it has been reported that upon influenza infection the turnover of upper airway DC's is 80% within the first 18 hours of infection[267, 333], with an 18% DC increase in the TBLN. In the time following this initial burst of trafficking, the capacity for further DC accumulation in the lymph node reaches a choke point, and cannot continue indefinitely[346, 347]. Recently accumulated DC's then undergo apoptosis (or a low percentage of cells may egress through efferent lymph[118]) to result in a significant drop by 24 hours post-infection, only to return to homeostasis by 48 hours post-infection[333]. The mechanisms which control this dynamic trafficking are still debated, and may include differential signal expression[334], or differential regulation of anti-apoptotic genes of DC's within the TBLN[346]. Consistent with the literature, we observed an accumulation of DC's (both airway and parenchymal) into the TBLNs after influenza infection. In addition we observed a quick loss and recovery of DC's, which was much more pronounced in VLP-exposed mice. Thus, our model of innate imprinting altered the tempo of normal DC trafficking in response to influenza virus challenge, by accelerating and augmenting normal DC responses in VLP-exposed mice. Finally, $CD103^+$ DC's have been shown to be not only most permissive to influenza infection, but also best at activating T cells in the lymph node[88, 89], and as is suggested by our data and has been previously suggested by others, the accelerated presence and migration of the $CD103^+$ population may represent an important contribution to enhanced viral immunity[110]. Since a rapid and

efficient innate immune response dictates a more favorable outcome for the host, the mechanisms controlling the differential timing could be important in understanding individualistic immunity.

Through VLP-exposure, we not only accelerated the rate of DC migration into the TBLNs, but we also enhanced the antigen processing capacity of both DC populations, and alveolar macrophages, as demonstrated by the degradation of GFP-expressing influenza, and the accelerated processing of OVA-DQ. Alveolar macrophages are also known to be important in antigen translocation from the airways [127, 128], and in the control of a steady state lung. While AM's generally express a suppressive function, they may play a dynamic role in initiating, or controlling inflammation. Additionally, the pathogen exposure history of DC's and AM's may be long-lasting and provide innate imprinting/memory[7, 321]. For both DC's and AM's, the presence of iBALT seems to be an important common thread in the mechanisms of innate imprinting. In our model, we find that DC's and AM's of VLP-primed mice exert a significantly enhanced ability to take up and process antigen, and migrate into the TBLN, which was of great benefit when these mice were challenged with influenza.

We additionally found that VLP-exposure directly impacted the ability of $CD11c^+$ cells to react to downstream challenges, and in fact, that naïve $CD11c^+$ cells were unable to achieve a similar result when faced with influenza virus challenge. This was indicated by our finding that mice exposed to VLPs, subsequently depleted of $CD11c^+$ cells, and allowed to be repopulated with $CD11c^+$ cells, lost the protective imprinting phenotype. Thus, the mechanism of innate imprinting in these studies was dependent on the priming

of $CD11c^+$ cells. While it is known that DC's are necessary to maintain the organization of iBALT[198, 199], we found that upon $CD11c^+$ cell depletion, iBALT remained relatively intact. This may have been the result of the quick CD11c repopulation of the lung in our model. Because iBALT structures are known to be important in the clearance of influenza virus[6, 203, 225], we cannot fully preclude the possibility that the effects of the $CD11c^+$ cell depletion upon the iBALT may have partially negated the protection afforded by VLP-exposure. However, that VLP-instillation increased $CD11c^+$ cell numbers in the lungs, enhanced migration of $CD11c^+$ cells to lymphoid tissues, and enhanced antigen processing capabilities of $CD11c^+$ cells, and that depletion of VLP-exposed $CD11c^+$ cells (followed by repopulation) annulled protection, strongly suggests that the VLP-enhanced protection is dependent on direct changes in the $CD11c^+$ cell population due to VLP-exposure.

A third population of antigen presenting cells, Ly-$6C^{hi}CD11b^+$ expressing monocytes or TNF-α/iNOS-producing DC's (TipDC's) (both have been reported to express phenotypically similar surface staining patterns[129, 130, 132]), also appeared to be important in the enhanced viral clearance in our model. While we have referred to these cells as monocytes, it is likely that the tissue resident Ly-$6C^{hi}CD11b^+$ cells are in fact TipDC's[129, 130, 139], although we did not specifically determine their production of cytokines in the current study. It has been shown previously that the lungs of mice with pre-established iBALT maintain an overall increased number of Ly-$6C^+CD11b^+$-expressing cells[201]. However, to the best of our knowledge, the functional contributions and trafficking of Ly-$6C^{hi}CD11b^+$ monocytes/TipDC's have not been determined in

relation to innate imprinting. Here we found that in the absence of Ly-6C^{hi}CD11b^{+} cells (in CCR2$^{-/-}$ mice) the protection against influenza from VLP-exposure is lost. This protection thus appeared to be partially dependent on an accelerated early contribution by these cells. Importantly, Ly-6C^{hi}CD11b^{+} cells are highly multifunctional and may situationally promote or discourage inflammation[132, 133, 136, 139, 149]. Thus Ly-6C^{hi}CD11b^{+} cells could have been important to VLP-enhanced viral clearance, through the repopulation of APC's into the effector sites, through promoting T cell activation via their APC function[136, 139], or by dampening late T cell responses to control damage through the production of nitric oxide (NO)[136, 142]. Importantly, while there is some debate about the necessity for CCR2-dependent signaling in the clearance of influenza and control of morbidity[133, 139, 149], we find that proficient CCR2-signaling is imperative to the accelerated influenza virus clearance in VLP-exposed mice and does not cause increased damage (Supplementary Figure S2). Additionally, others have similarly reported the necessity for early CCR2-dependent trafficking of Ly-6C-expressing cells in the clearance of pathogens including *Mycobacterium tuberculosis*[148], *Cryptococcus neoformans*[131], *Listeria monocytogenes*[129], and many others[132].

Proficient influenza virus clearance is dependent on both innate and adaptive immunity. Thus, while APC antigen uptake, processing, and trafficking are important in the initiation of immunity, T cell presentation and co-stimulation also represent essential APC functions. Importantly, we found that VLP-exposed DC's display a wildly divergent pattern of T cell co-stimulatory molecules in both the lungs and TBLNs as compared to controls. The very early (within 12 hours of infection) upregulation of VCAM-1 and

ICAM-1 likely facilitated the formation of immunological synapses, which allowed for a jump-start in $CD4^+$ T cell expansion. Interestingly, while some have reported that no innate immunity can be detected until after day 2 of influenza infection[47], we show here that in an educated lung (achieved here by VLP-priming), the "stealth phase[47]" of viral replication prior to innate immunity activation may be avoided. We found that indeed, in VLP-exposed mice, influenza-specific naïve $CD4^+$ T cells proliferated, upregulated activation markers, and then contracted, especially in lymphatic areas including iBALT at an accelerated rate. We and others have previously shown that $CD4^+$ T cells, and especially T follicular helper cells (T_{FH}) are essential components to iBALT, as they are capable of T cell priming directly in iBALT areas, and mediate GC reactions, including the differentiation of plasma cells, and the promotion of clearance of virus[6, 199, 200, 224]. Furthermore, recent evidence suggests that $CD4^+$ T cells are capable of antiviral functions that have been historically associated with $CD8^+$ T cells including cytolytic activity and the production of perforin, granzyme B, and IFN-γ[174-176]. Thus, we find that in our system $CD4^+$ T cells, and not $CD8^+$ T cells can be enhanced in response to innate imprinting. Furthermore, our system does not appear to be reliant on cross-reactive $CD8^+$ T cells, as has been described for other heterologous infection models[257, 280].

It has been reported that $S1P_1$ agonism (resulting in inhibition of the receptor) enhances survival, and dampens cytokine production without affecting viral load[348]. We found that viral load was similarly not affected in vehicle-exposed FTY720-treated animals. Also, although we did not measure cytokine production, we did measure indicators of damage and found that in our system damage is not dependent on $S1P_1$

agonism, but is in fact very dependent on innate imprinting. Damage and weight loss were closely associated with each other and with the viral load, as could be expected. A similar result has been demonstrated for a system in which memory lymphocytes are present, indicating iBALT as an important niche for APC-lymphocyte interactions[2].

As we[200, 224] and others[203, 250, 251, 331, 332] have suggested, iBALT may represent an important niche that could be exploited as a site for vaccine delivery to great benefit, especially considering the unique requirements of the lung. However few strategies to safely establish iBALT without the use of live viruses, harmful particulate, or bacterial products have been described to date. Here we illustrate a mechanism by which we can harness the pulmonary mucosa to provide accelerated site-specific immunity to a primary challenge with a distinct pathogen. Furthermore, we suggest that the utilization of non-infectious and non-pathogenic VLPs, sharing no cross-reactive epitopes to influenza, may provide a novel model by which we may begin to better understand the complex interplay between lung priming, heterologous immunity, innate imprinting, and memory responses. This system could be particularly advantageous in that, unlike primary viral challenge models, no damage to the epithelium or pulmonary function occurs by VLP-priming.

Taken together, we have shown that the exposure of VLPs to the lungs of naïve mice provides exquisite resistance to high-dose pathogen challenge. The mechanisms by which resistance is achieved include accelerated alternative trafficking patterns and antigen processing of conventional respiratory DC's, alveolar macrophages, and Ly-$6C^{hi}CD11b^{+}$ monocytes/TipDC's which required direct exposure to VLPs. These responses further relied on proficient CCR2-dependent signaling, and the rapid and

transient upregulation of T-cell co-stimulatory molecules. These initial innate events led to an accelerated opportunity for naïve effector $CD4^+$ T cell expansion and subsequent contraction, indicating regulation and control of damage. Finally innate imprinting was sufficient to provide a local immune response in the lung without TBLN aid, or homologous memory responses, as indicated by $S1P_1$ inhibition. Thus we propose that VLP-priming poses an important tool for our evolving understanding of pulmonary immunity in our non-sterile world.

Methods

Virus-Like Particle Production and Purification.

Virus-like particles (small heat-shock protein cage nanoparticles G41C) were produced, purified, and characterized as previously described[200, 304].

Influenza Viruses.

The influenza virus A/PR8/8/34 was produced at the Trudeau Institute (Saranac Lake, NY). Briefly, 10 day old embryonated chicken eggs were infected for 55 hours, and resultant allantoic fluid was recovered and stored at -80° C until used. The NS1-GFP PR8 virus was a kind gift from Dr. Adolfo García-Sastre and was engineered as reported previously[349].

Animals and *in vivo* Procedures.

Female or male BALB/c, Thy1.1, C57BL/6, $CCR2^{-/-}$, HNT [1], or CD11c-DTR [336, 337] mice were bred in-house at Montana State University, maintained in SPF conditions in

HEPA-filtered cages, and fed sterile food and water *ad libitum.* All animal procedures were performed in accordance with protocols pre-approved by the Montana State University Institutional Animal Care and Use Committee (IACUC). Experimental results were confirmed by at least two independent repetitions of similar design with 5 animals per group. Virus-like particles and subsequent challenges were delivered intranasally in 50 μl volumes to mice lightly anesthetized with 5% inhaled isoflurane. VLP-treatment was delivered in five doses of 100 μg given either daily, or spaced 3 days apart (both schedules produced equivalent results). Mice were then rested for 72 hours before challenge or further manipulation. In most experiments mice were challenged with influenza. We utilized two strains of influenza with intrinsically varying degrees of pathogenicity. 1.5 X 10^3 plaque-forming units (pfu) PR8 or $1X10^6$ pfu NS1-GFP PR8[349] were delivered in 50 μl volumes i.n. In some experiments mice were challenged with 100 μg Ovalbumin-DQ (Molecular Probes; Carlsbad, CA) or regular "cold" OVA (Sigma-Aldrich; St. Louis, MO) in 50 μl i.n. For experiments using CD11c-DTR-facilitated depletion, anesthetized mice received an intratracheal (i.t.) instillation of 100 ng diphtheria toxin (DT) (Sigma-Aldrich) in 100 μl sterile DPBS. For antibody depletion experiments VLP-treated or vehicle control mice received 250 μg anti-mouse CD11c-depleting antibody (BioXCell; West Lebanon, NH) in 500 μl sterile DPBS, or vehicle intraperitoneally (i.p.).

In lymphocyte sequestration studies, VLP-treated or control mice were administered with FTY720 (Cayman Chemical; Ann Arbor, Michigan) $(4\ mg/kg)^2$ in sterile DPBS or vehicle i.p., 6 hours prior to infection with influenza. Mice then received

daily doses of 4 mg/kg FTY720 or DPBS i.p. over the course of the experiment. The magnitude of peripheral blood lymphocyte depletion was determined by Unopette reservoir (BD biosciences; San Jose, CA) hemocytometer counts. In all experiments involving infection, mice were weighed over the experimental time course to evaluate morbidity. At indicated timepoints per experiment, mice were sacrificed by an i.p. injection of sodium pentobarbital (90 mg/kg) and exsanguinated after no pedal response could be elicited.

Bronchoalveolar lavage (BAL) samples were collected by instilling the lung with 2 mL DPBS with 3 mM EDTA. Resultant cells were spun at 209 x g for 10 minutes at 4°C and supernatants were collected for antibody ELISA or lung damage assays. Pellets were then resuspended in FcR block (clone 93) prior to staining for FACS. Lungs were excised and either snap frozen in 2 mL DMEM for plaque assay to determine viral load, or digested in 0.2% collagenase (Worthington Biochemical Corporation; Lakewood, NJ) with 0.1% DNase (Sigma-Aldrich) in RPMI with agitation at 37° C for 1 hr. Red blood cells were lysed from the lung homogenates using ACK lysis buffer. Remaining cells were washed, resuspended in FcR block, and stained for flow cytometry. Tracheobronchial lymph nodes (TBLNs) and spleens were either homogenized through a wire mesh screen to collect lymphocytes or digested to collect macrophages and DCs. Total cells from each tissue were counted by hemocytometer to allow for total quantification by FACS.

For adoptive transfer studies, the spleens of naïve HNT mice[1] (Thy1.2) were sterilely collected and homogenized. Red blood cells were lysed, and remaining cells

were labeled with 5 μM CFSE (eBioscience; San Diego, CA). $CD4^+$ T cells were then positively selected by $CD4^+$ T cell columns (R and D Systems; Minneapolis, MN), washed, and resuspended in sterile DPBS. 1.2 $X10^7$ $CD4^+$ T cells were then adoptively transferred into VLP-treated or control mice (Thy1.1) in 200 μl intravenously (i.v.). Mice were rested for 24 hrs. prior to infection with 1.5 X 10^3 pfu PR8.

iBALT Microdissection.

To specifically obtain areas of iBALT which were not contaminated with additional cellular components of the lung, whole lungs were instilled with 1% warm low-melt agarose (Fluka Analytical; St. Louis, MO) in DPBS and excised en bloc into ice-cold DPBS. 300 μM sections were then cut by vibratome (Leica Microsystems; Wetzlar, Germany) and resultant sections were floated in cold RPMI with 5% FBS (Atlas Biologicals; Fort Collins, CO). Each section was then gently arranged on a microscope slide and flooded with media. Areas of iBALT were identified by dissecting microscopy according to the characteristic density and location, and excised with a scalpel. Areas of excised iBALT were placed in cold RPMI with FBS and remaining parenchymal areas of the lung section were discarded. Combined iBALT areas per animal were then either digested in collagenase/DNase, or homogenized through a wire mesh screen. Single-cell suspensions were then filtered through 100 μM mesh, resuspended in FcR block (clone 93), and subsequently stained for FACS.

FACS Staining and Antibodies.

Single-cell suspensions from indicated organs were filtered through 100 μM mesh, and incubated with FcR block (clone 93) for 10 minutes on ice. Antibody cocktails were then added and the cells were incubated on ice for an additional 20-30 minutes. Tetramers were allowed to incubate for 45 minutes at room temperature. Antibodies purchased from Biolegend (San Diego, CA) included CD11c-PerCP-Cy5.5 (clone N418); CD103-APC (clone 2E7); CD11b-APC-Cy7 (clone M1/70); I-A/I-E-PE-Cy7 (M5/114.15.2); Ly-6C-FITC (clone HK1.4); ICAM-1-APC (clone YN1/1.7.4); VCAM-1-PerCP-Cy5.5 (clone 429 (MVCAM.A)); CD4-PerCP-Cy5.5 (clone GK1.5); and CD8-PE-Cy7 (clone IM7). Antibodies purchased from BD biosciences (San Jose, CA) included CD44-PE (clone 515); and Siglec-F-PE (clone E50-2440). APC-conjugated MHC I influenza tetramers H-2D^{b} NP$_{366-374}$ (NP) and H-2D^{b} PA$_{224-233}$ (PA) were purchased from the Trudeau Institute Molecular Biology Core Facility (Saranac Lake, NY). Samples were acquired on a FACSCanto (BD) and data was analyzed using FlowJo software (Treestar; Ashland, OR). Briefly, forward and side scatter plots were gated on the population of interest (lymphocytes or DC's/macrophages) as determined by size and granularity. Cells were then further analyzed for the expression of appropriate combinations of surface antigens based off negative staining controls. Total cell numbers were then calculated based off total hemocytometer cell counts for each tissue.

Histology.

For frozen section histology, lungs were instilled with OCT (SakuraFinetek; Torrance, CA), excised, and snap frozen in liquid nitrogen. Blocks were then cut into 5

μM sections by cryostat (Leica Microsystems; Buffalo Grove, IL). Slides were washed with PBS, blocked with an avidin/biotin blocking kit (Vector; Burlingame, CA) and normal goat serum (MP Biomedicals; Solon, Ohio). CD11c-biotin (BD biosciences) was then added and incubated for 30 minutes. Slides were washed and streptavidin conjugated Alexa Fluor-594 (Invitrogen; Carlsbad, CA) was added and incubated for an additional 20 minutes. Nuclei were counterstained and slides were coverslipped with prolong gold with DAPI (Invitrogen). Images were acquired on a Nikon Eclipse E800 microscope (Nikon Instruments, Melville, NY) using Nikon NIS-Elements Imaging software. Control sections were utilized to determine staining specificity.

ELISA.

BALF antibodies levels were determined by ELISA. Briefly, high-binding polystyrene plates (Corning; Corning, NY) were coated and incubated with influenza virus membrane at 37°C for 3 hrs., then moved to 4°C overnight. Plates were washed with PBS with .05% tween, and blocked with nonfat dry milk. BALF samples were plated in duplicate and in 2-fold serial dilution and were then incubated at 37°C for 2 hrs. Plates were again washed and alkaline phosphatase IgG or IgA from (Sigma-Aldrich) were added and incubated for an additional 2 hrs. at 37°C. Finally, plates were again washed, developed with 4-Nitrophenyl phosphate disodium salt hexahydrate (Sigma-Aldrich) in diethanolamine buffer, and read on a SpectraMax Plus plate reader (Molecular Devices; Sunnyvale, CA) at 450 nm.

Serum Albumin and Lactate Dehydrogenase Concentration Determination.

The concentration of serum albumin and lactate dehydrogenase were measured by commercially available colorimetric assay (Sigma-Aldrich; and CytoTox 96, Promega, respectively), as previously described[200]. Samples were plated in duplicate and read on a SpectraMax Plus plate reader (Molecular Devices).

Plaque Assay.

Plaque assay was used to determine viral titers from total lung homogenate, as previously described[200, 350]. Briefly, Madin-Darby canine kidney (MDCK) cells were grown to confluence. Next, 10-fold serial dilutions of total lung homogenate were plated onto the monolayer, and the assay was overlayed with 1.2% agarose with DEAE. The assay was incubated at 35° C in the presence of CO_2 for 3-5 days. It was then fixed with 20% acetic acid and stained with 0.2% crystal violet.

Statistics.

Statistical significance was determined by One-way ANOVA with a Bonferroni post-test of multiple comparisons, or in some cases an unpaired t-test using GraphPad Prism (La Jolla, CA). Significance was indicated by * $P<.05$, ** $P<.01$, *** $P<.001$, or **** $P<.0001$.

Supplementary Material

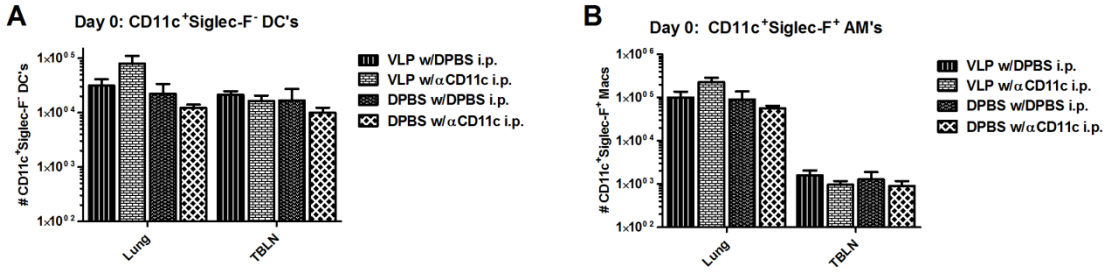


Figure S1 VLP-exposure alters the activity of $CD11c^{+}$ cells. Mice were exposed to VLPs or vehicle i.n., rested for 72 hours, and then treated with 250 µg CD11c-depleting mAb, or DPBS i.p. Next, all groups were rested for 9 days to allow for $CD11c^{+}$ cell reconstitution from the bone marrow, and finally challenged with 1.5 X 10^3 pfu PR8 influenza. (a-b) At day 0, uninfected, reconstituted mice were sacrificed and (a) total DC's and (b) AM's were quantified from the multilobe of the lungs and whole TBLNs.

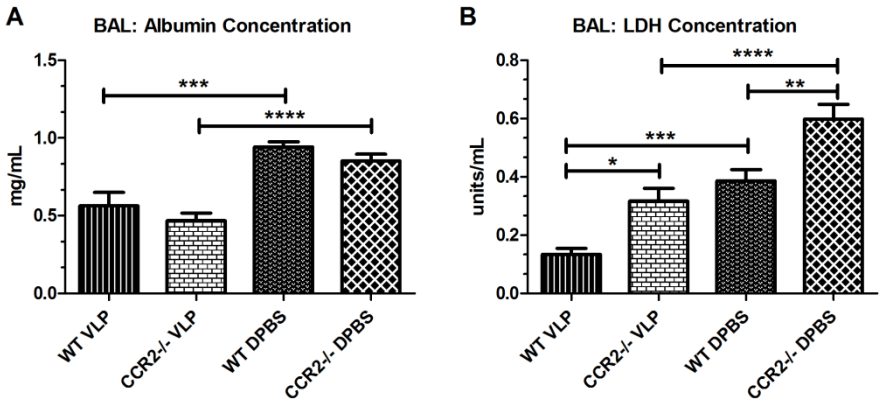


Figure S2 VLP-exposure reduces collateral damage in the lungs of both WT and $CCR2^{-/-}$ mice. WT or CCR2-/- mice were exposed to VLPs or vehicle i.n., rested for 72 hours, and then challenged with 1.5 X 10^3 pfu PR8 influenza. At day 7 post-infection, mice were lavaged, and the concentration of damage indicators (a) serum albumin and (b) lactate dehydrogenase (LDH) were determined by colorimetric assay. * $P<.05$, ** $P<.01$, *** $P<.001$, **** $P<.0001$.

Acknowledgements

This work was supported by NIH/NIAID R56AI089458; the Rocky Mountain Research Center of Excellence (RMRCE) U54AI065357; NIH/NIAID R21AI083520; the IDeA Network for Biomedical Research Excellence (INBRE) P20GM103474; the Center for Zoonotic and Emerging Infectious Diseases (COBRE) P20GM103500; the M.J. Murdock Charitable Trust, and the Montana State University Agricultural Experimental Station. We thank Dr. Adolfo García-Sastre for his kind and generous gift of the NS1-GFP virus, all Harmsen lab staff for technical assistance in experiments, Amy Servid for producing and purifying the VLPs, and the staff of Montana State University's Animal Resource Center for animal care and technical aid.

CHAPTER FOUR

A VIRUS-LIKE PARTICLE VACCINE PLATFORM ELICITS HEIGHTENED AND HASTENED LOCAL LUNG MUCOSAL ANTIBODY PRODUCTION AFTER A SINGLE DOSE

Contributions of Authors and Co-Authors

Manuscript in Chapter 4

Author: Laura E. Richert

Contributions: Contributed to designing studies, collected and analyzed data, and wrote the manuscript.

Author: Amy E. Servid

Contributions: Created, purified, and characterized the biochemical identity of the vaccine constructs, and contributed to writing the manuscript.

Co-author: Ann L. Harmsen

Contributions: Performed experiments, collected and analyzed data, and critically read the manuscript.

Co-author: Soo Han

Contributions: Collected and analyzed data, and critically read the manuscript.

Co-author: James A. Wiley

Contributions: Contributed to funding the studies, designing studies, and critically read the manuscript.

Senior Co-author: Trevor Douglas

Contributions: Obtained funding for the biochemical aspects of the studies, designed studies, and critically read and edited the manuscript.

Senior Co-author: Allen G. Harmsen

Contributions: Obtained funding for all immunology studies, designed the studies, and critically read and edited the manuscript.

Manuscript Information Page

Laura E. Richert, Amy E. Servid, Ann L. Harmsen, Soo Han, James A. Wiley, Trevor Douglas, Allen G. Harmsen
Journal Name: *Vaccine*

Status of Manuscript:
__ Prepared for submission to a peer-reviewed journal
__ Officially submitted to a peer-reviewed journal
__ Accepted by a peer-reviewed journal
_X_ Published in a peer-reviewed journal
Published by Elsevier
Appeared in print: May 21, 2012.
Published in: Volume 30, Issue 24, Pages 3653-3665

The following chapter has been published in the journal *Vaccine* and appears in this dissertation with the permission of Elsevier (license number 2911000875328).

Abstract

We show that a model antigen, ovalbumin (OVA), can be chemically conjugated to the exterior of a small heat shock protein (sHsp) cage that has structural similarities to virus-like particles (VLPs). OVA-sHsp conjugation efficiency was dependent upon the stoichiometry and the length of the small molecule linker utilized, and the attachment position on the sHsp cage. When conjugated OVA-sHsp was delivered intranasally to naïve mice, the resulting immune response to OVA was accelerated and intensified, and OVA-specific IgG1 responses were apparent within 5 days after a single immunizing dose, illustrating its utility for vaccine development. If animals were pretreated with a disparate VLP, P22 (a non-replicative bacteriophage capsid), before OVA-sHsp conjugate immunization, OVA-specific IgG1 responses were apparent already by 4 days after a single immunizing dose of conjugate in OVA-naïve mice. Additionally, the mice pretreated with P22 produced high titer mucosal IgA, and isotype-switched OVA-specific serum IgG. Similarly, sHsp pretreatment enhanced the accumulation of lung germinal center B cells, T follicular helper cells, and increased polymeric Ig receptor expression, priming the lungs for subsequent IgG and IgA responses to influenza virus challenge. Thus, sHsp nanoparticles elicited quick and intense antibody responses and these accelerated responses could similarly be induced to antigen chemically conjugated to the sHsp. Pretreatment of mice with P22 further accelerated the onset of the antibody response to OVA-sHsp, demonstrating the utility of conjugating antigens to VLPs for pre-, or possibly post-exposure prophylaxis of lung, all without the need for adjuvant.

Introduction

Respiratory infections are one of the most prominent afflictions in individuals of all ages and immune statuses, signifying a significant global health concern. Unfortunately, we are currently unable to provide vaccines against many clinically relevant lower respiratory tract pathogens, nor are we able to fully predict the identity of future outbreaks. This global vulnerability has been clearly illustrated by several epidemics in recent memory, including the newly emerged coronavirus, SARS-CoV outbreak of 2002, various influenza strain reassortments (H5N1 "bird flu" and H1N1pandemic), and bioterrorism events involving pathogen aerosolization. Thus, there is an urgent and crucial need for the development of broad-spectrum, rapidly acting vaccination strategies.

Unlike most other mucosal sites in the body, which are protected and immunologically shaped by their commensal microbial communities, the lung is more or less sterile. Therefore, the lung relies on an intricate network of sentinel dendritic cells, antimicrobial secretions, and resident macrophages for defense. Importantly, immune responses in the lung must be tightly regulated to promote immunity, while avoiding tissue damage associated with either the pathogen or the host response. As such, pulmonary immune responses are quite unique, and as suggested by others, the individual history of specific pathogen exposures to the lungs may contribute to shaping the appropriate ensuing immune responses to subsequent challenges [7, 255, 256, 273]. Here, (and elsewhere [200]) we further demonstrate that virus-like particles (VLPs), which are unrelated to the antigen of subsequent challenge, can similarly impact the lung

microenvironment, without the associated pathology, thereby shaping future immune responses. Many groups have previously suggested that the lung may provide an important route of delivery for mucosal vaccination [249, 250, 331]. However, the potential for utilizing localized mucosal vaccination strategies in the lower respiratory tract have historically been overlooked, and approaches which elicit tissue-specific immune responses are just beginning to be developed. An FDA-approved tribute to the realization of this strategy is the highly effective Flumist vaccine, which is delivered intranasally, and provides better comprehensive local immunity than injectable versions [351-353].

Additionally, the application of nanomaterials to biomedicine is one of the most exciting and potentially revolutionary applications of nanotechnology. Here, we describe a mechanism by which we can enhance primary local immune responses to antigens without the necessity of specific antigen priming. We achieved this result by intranasally delivering empty virus-like particles (VLPs), which act to modulate the lung microenvironment, and harness and focus immune responses. Recent exploration in the utilization of nanoparticles [354-356], virus-like particles [292, 357-362], and viruses which have no mammalian cell tropism, has shown that these platforms are naturally immunostimulatory, and likely utilize evolutionarily-conserved cell surface receptors, thereby safely engaging immune signaling pathways without replicating [300, 301, 363-365]. Furthermore, many of these strategies are currently on the market or undergoing clinical trials, and have already had broad global impact in safely preventing disease [289-292]. Importantly, virus-like particles can be produced in large quantities, provide a stable

product, often are amenable to lyophilization or freeze-drying, and are fiscally economical. These features are especially important for less industrialized nations.

In the following studies we utilize two empty, non-pathogenic virus-like particles-- a small heat shock protein cage nanoparticle (sHsp) and the P22 phage-derived virus-like particle (P22) as immunomodulatory antigens in both a non-specific pre-priming scenario, and as a platform for the delivery of specific antigen to the lung. The small heat shock protein 16.5 (sHsp) from *Methanocaldococcus jannaschii* (a hyperthermophilic archaeon) is comprised of 24 repeating subunits [302, 327]. These subunits self-assemble to produce an empty cage-like structure, comparable to that of a virus capsid by virtue of the high symmetry and quaternary structure [200, 303, 304, 306]. We have previously shown that sHsp can be genetically engineered to incorporate cysteine residues, thereby providing attachment sites for bioconjugation [303, 366, 367], which we exploit here for the display of a foreign protein, similarly to described strategies [368, 369]. P22 is a bacteriophage capsid which infects *Salmonella typhimurium* (when intact tail fibers are present) [307, 309]. The P22 used here is devoid of both genetic material and tail fibers, and is therefore composed of only the non-infectious empty viral capsid. We would like to note here that previously we have referred to the sHsp nanoparticles as “protein cage nanoparticles” or PCN [200]. However, we now find it to be more descriptive to classify both the sHsp and P22 as virus-like particles, given their structural architecture and immunological parallels to other particles described in the literature. Importantly, neither sHsp nor P22 target known mammalian pattern-recognition receptors, nor do they infect mammalian cells.

And while the immunomodulatory potential in exploiting non-pathogenic viruses is still in its infancy, others have begun to describe similar successful strategies [300, 301, 365].

P22 and sHsp are herein used as immunomodulatory agents alone in a lung priming strategy to achieve heightened heterologous immunity to distinct antigens, such as OVA and influenza virus; or, in the case of sHsp, as a vaccine delivery platform for a model antigen, OVA, which we have conjugated (in its entirety) to the exterior surface of the sHsp cage. This immunization strategy is advantageous because it accelerates and intensifies the primary immune response, after only a single dose. We further show that conjugating a model antigen (OVA) to sHsp elicits an immune response to OVA which mirrors the response to the sHsp itself. sHsp conjugation also acts to adjuvant OVA, and the local delivery of sHsp and antigen complexes induce potent local IgA secretion in sHsp pretreated mice. Therefore, we show that VLPs (sHsp and P22) can be used as both immunomodulatory agents by pretreating the lung and/or as a carrier of antigens, allowing local immunization of the lower respiratory tract against a pathogen of interest, with a single dose. This platform could be useful for both pre- and post-exposure prophylaxis.

Materials and Methods

Production of Small Heat-Shock Protein Cage Nanoparticle (sHsp)

The small heat-shock protein (sHsp 16.5) was initially purified as described previously [303]. In a slight modification of the previously described protocol, the supernatants from 2 L of cell culture were combined and concentrated to 10 mL with a

100k MWCO amicon filter (Millipore, Billerica, MA) prior to size exclusion chromatography on a Superose 6 column (GE Healthcare, Piscataway, NJ) so that purification of large amounts of sHsp could be accomplished efficiently. In order to remove residual protein contaminants, additional steps were added to the previous protocol. The fractions containing sHsp from size exclusion chromatography were re-concentrated to 10 mL and purified by anion exchange on a Sepharose Q column (GE Healthcare) using a linear gradient from 300 mM to 800 mM NaCl in 25 mM HEPES Buffer at pH 7.3. Following this, the fractions containing sHsp were dialyzed overnight into 50 mM phosphate, 100 mM NaCl, and 5 mM EDTA, at pH 7.3, concentrated a third time to 10 mL, and re-subjected to size exclusion chromatography using a Superose 6 column (GE Healthcare) with the same buffer. For the S121C sHsp variant protein, tris(2-carboxyethyl)phosphine (Pierce, Rockford, IL) was added to a final concentration of 2 mM during each amicon concentration step prior to the FPLC runs to inhibit disulfide formation between external thiols on these cages. The sHsp protein concentration was determined via UV-visible spectroscopy using an extinction coefficient of A280 = 0.565 $(mg/mL)^{-1}$ as previously documented [303].

OVA Preparation

Larger aggregates from commercially available ovalbumin (OVA) (Sigma-Aldrich, Saint Louis, MO, A5503) were removed by size exclusion chromatography using a Superose 6 column (GE Healthcare). Fifty millimolar phosphate, 100 mM NaCl, and 5 mM EDTA at pH 7.3 was used as an elution buffer. Protein concentrations were

determined by UV-visible spectroscopy using a previously documented extinction coefficient of A280 = 0.789 $(mg/mL)^{-1}$ for OVA [370].

P22 Preparation

The P22 K118C coat and scaffold protein were expressed in *E.coli*, purified, and assembled *in vitro* as described previously [307]. The purified P22 particles were heated for 20 minutes at 75ºC to remove the scaffold protein, purified on a sephacryl 500 column (Amersham, Piscataway, NJ), and concentrated to 2 mg/mL, and dialyzed extensively into 50 mM phosphate, 100 mM NaCl, and at pH 7.2.

Optimization of OVA-sHsp Conjugation

To determine the initial conditions for conjugation, a matrix of linking conditions were tested. All reactions were carried out in 50 mM phosphate, 100 mM NaCL, 5 mM EDTA, pH 7.3. OVA (80 µL, 7.72 mg/mL) was labeled with a 2-fold molar excess of each $SM(PEG)_n$ linker ($SM(PEG)_2$, $SM(PEG)_6$, or $SM(PEG)_{12}$) using a stock solution of 25 mM linker in DMSO respectively. These samples were incubated at room temperature for 50 min, and un-conjugated linker was immediately removed using Micro Bio-Spin Columns P30 (Biorad). The labeled OVA samples were combined with either sHsp S121C or sHsp E102C cages using a 5:1 molar ratio. The proteins were combined, vortexed, and reacted 1 hour at room temperature and overnight at 4°C. The final sHsp concentration was 2.34 mg/mL and the OVA concentration was 11.72 mg/mL in a total volume of 45 µL for each reaction. These reactions were repeated using a 20-fold excess

of each $SM(PEG)_n$ linker ($SM(PEG)_2$, $SM(PEG)_6$, or $SM(PEG)_{12}$) from a stock solution of 250 mM to label the OVA.

Prior to conjugation, lysines on sHsp G41C were reacted with 50-fold molar excess of SPDP (Thermo Scientific) per sHsp subunit by the addition of 500 mM SPDP in DMSO to 2 mL of protein at 2.61 mg/mL. This reaction was stirred for 90 min at room temperature, and the labeled sHsp was purified by Superose 6, and stored at 4°C overnight. For these reactions, a seven-fold molar excess of TCEP (Invitrogen) was added to the sHsp-SPDP (above) to reduce the SPDP, and this reaction was left for 30 minutes at room temperature to reduce the disulfides on the linker. UV-visible spectroscopy was used to monitor the completeness of the reaction as indicated by increasing absorbance at 324 nm corresponding to the thiopyridone product [371]. This sulfhydryl functionalized sHsp was reacted with OVA (80 µL, 7.72 mg/mL) samples labeled with a 2-fold or 20-fold molar excess of each $SM(PEG)_n$ linker ($SM(PEG)_2$, $SM(PEG)_6$, or $SM(PEG)_{12}$) using the protocol described above for the S121C and E102C reactions. The linking conditions for the sHsp G41C mutant combined with the OVA contained a final concentration of 30 mM TCEP. The final sHsp G41C and OVA concentrations were normalized to the conditions used with the other mutants: 2.34 mg/mL and 11.72 mg/mL respectively, in a total volume of 45 µL.

Synthesis and Purification of the
OVA-sHsp Conjugate

A 250 mM stock solution of the commercially labeled cross-linking reagent $SM(PEG)_6$ (Thermo Scientific, Waltham, MA) was made in DMSO. The OVA was

concentrated to 9.75 mg/mL, and 2.0 mL was reacted with a 2-fold molar excess of the linker, added dropwise to a vigorously stirring solution. The reaction was stirred for 40 min at room temperature, followed by immediate purification of the maleimide functionalized OVA from un-conjugated small molecule linker by Superose 6 size exclusion chromatography (GE Healthcare). Immediately after elution, the maleimide functionalized OVA was concentrated to approximately 13.4 mg/mL (using E =0.789 $mL^{-1}mg^{-1}cm^{-1}$) with a 10k MWCO Microcon filter (Millipore), and was mixed with sHsp S121C (2.62 mg/mL) for one hour at room temperature followed by overnight at 4ºC.

A molar ratio of 5:1 OVA to sHsp was used to give final concentrations of 1.34 mg/mL OVA and 2.4 mg/mL sHsp within the linking reactions. Control reactions containing identical concentrations of sHsp or linker-labeled OVA alone were run in parallel. Free sulfhydryls on the proteins were then capped by reaction with 20-fold excess N-ethyl maleimide (Pierce) per sHsp subunit for 2 hours at room temperature. The above procedure was repeated six times to obtain sufficient yield of the conjugated construct. Similar samples from these reactions were combined, spun down (5 min x 17,000g) to remove precipitate, and dialyzed into 25 mM triethanolamine (USB Corp, Santa Clara, CA) at pH 7.3.

The samples were purified by anion exchange chromatography on a MonoQ column (Amersham Pharmacia) using a linear gradient of 0 M to 500 mM NaCl in 25 mM triethanolamine at pH 7.3. (Fig. S1) Fractions corresponding to conjugated sample, sHsp and maleimide functionalized OVA were combined based on SDS-PAGE analysis of the fractions. The sHsp and maleimide functionalized OVA were mixed in a 5:1 molar

ratio to obtain the mixed sample used for the *in vivo* experiments. All the samples were extensively dialyzed into 50 mM phosphate, 100 mM NaCl, and at pH 7.2 prior to *in vivo* experiments. The admixture of OVA and sHsp was comprised of equal microgram amounts of both sHsp (100 µg) and OVA (57 µg) (Sigma-Aldrich) as the conjugated form, and was suspended in sterile PBS.

Limulus Amebocyte Lysate Assay

Prior to administration *in vivo* the endotoxin contamination for each protein preparation was determined using a limulus amebocyte lysate (LAL) assay (Associates of Cape Cod, Inc.; East Falmouth, MA). We determined that sHsp alone contained 1.3 µg LPS per dose, the OVA-sHsp conjugate contained 2.4 ng LPS per dose, the admixture of sHsp and OVA contained 3.4 ng LPS per dose, the P22 preparation contained 3 ng LPS per dose, and OVA alone contained 619 ng LPS per dose. A second batch of P22 was used for only Fig. 3B, with the following LAL results: The "LPS-high" P22 contained 8 µg LPS per dose, while the "LPS-low" P22 contained 14 ng per dose.

Confirmatory Analysis

The size distribution of the VLPs was determined using dynamic light scattering (Brookhaven 90Plus particle size analyzer). For the Bradford assay, a series of protein standards was made using BSA (Sigma, A7906). One hundred microliters of Bradford Reagent (Amresco) was combined with 5 µL of each protein solution, and samples were incubated for 20 minutes, and the absorbance was measured at 315 and 605 nm. Samples were also run on one millimeter SDS-PAGE reducing gels (15% acrylamide for the

running gel, 4% acrylamide for the stacking gel). The AlphaEaseFC software (Alpha Innotech) was used to identify bands and calculate the migration distances of species on the gels.

Western Blots

Proteins were transferred from the SDS-PAGE gels to Hybond C nitrocellulose membranes for 2 hours at 200 mAmps. Membranes were blocked overnight with 5% milk and 0.01% Tween-20 in Tris-buffered saline, incubated with a 1:10,000 dilution of rabbit anti-OVA polyclonal antibody or rabbit anti-sHsp antibody (Millipore) for 3 hours. The anti-sHsp antibody was purified from rabbit serum by ammonium sulfate precipitation. The membranes were incubated with a ratio of 1:5,000 anti-rabbit antibody HRPO conjugate to blocking solution for 30 minutes, and blots were detected using an Opti-4CN kit (Biorad). Densitometry analysis was done using AlphaEaseFC software (Alpha Innotech).

Influenza Virus

The influenza virus A/PR8/8/34 was produced at the Trudeau Institute, Saranac Lake, NY. Briefly, 10 day old embryonated chicken eggs were infected for 72 hours, and resultant allantoic fluid was recovered and stored at -80° C until used.

Mice, Pretreatment, and Challenges

BALB/c, C57BL/6 or TLR4-/- mice were bred in-house at Montana State University, Bozeman, MT. At 6-8 weeks of age, male or female mice were enrolled in described experiments (n=5 per group). In experiments utilizing intranasal pretreatments,

100 µg of sHsp (sHspG41C), or P22 were delivered in 50 µl volumes while the mice were lightly anesthetized under inhaled 5% isoflurane. Five pretreatment doses were delivered either daily for five days, or spaced evenly over the course of 2 weeks (both schedules produced equivalent results). Importantly, we have extensively explored potential adverse side-effects on pulmonary function due to repeated sHsp administration, and have found none [200, 306]. Pretreated mice were rested for 72 hours, then challenged. In some experiments mice were challenged with the OVA-sHsp conjugate (sHspS121C), the OVA and sHsp (sHspS121C) admixture, OVA alone, or sHsp alone (sHspS121C), delivered i.n. in 100 µl volumes, again under light anesthesia. The OVA concentration (.57 mg/ml), as determined by UV-visible spectroscopy, was held constant throughout groups, regardless of conjugation. For subcutaneous (s.c.) studies, no pretreatment was utilized. Instead, one s.c. dose of 100 µl OVA-sHsp, OVA with sHsp admixture, OVA with alum (10% $AlkSO_4$) admixture, alum alone (10% $AlkSO_4$), or OVA alone (.57 mg/ml) were injected and antibody titers were measured over time. For influenza challenge studies, 1500 plaque forming units (pfu) A/PR8/8/34 influenza virus were delivered in 50 µl i.n. In experiments to determine the impacts of residual LPS, mice were similarly pretreated with "LPS-high" P22, "LPS-low" P22, an equal amount of LPS as in the "LPS-high" P22, or sterile pyrogen-free PBS in 50 µl i.n. All mice were then rested, and subsequently challenged with 100 µg sHspG41C in 50 µl i.n.

Mice were bled at relevant timepoints, and serum was separated from whole blood by centrifugation in separation tubes (Sarstedt; Germany). At indicated timepoints per experiment, mice were euthanized by intraperitoneal injection of sodium

pentobarbital (90 mg/kg) and exsanguinated after no pedal response could be elicited. Mice were then lavaged with sterile PBS with 3 mM EDTA. BALF and sera were used to determine antibody titers by ELISA. In some experiments, lungs and tracheobronchial lymph nodes (TBLNs) were additionally collected and either homogenized through a wire mesh screen, or digested with agitation in 0.2% collagenase (Worthington Biochemical Corporation; Lakewood, NJ) with DNase (Sigma) at 37° C for 1 hr. Red blood cells were lysed from the lung homogenates using ACK lysis buffer, washed, resuspended in FcR block (clone 93), and stained for flow cytometry. Total cells from each tissue (BAL, lungs and TBLNs) were counted by hemocytometer. In some cases, whole lungs were instilled with OCT (SakuraFinetek; Torrance, CA), excised, and snap frozen in liquid nitrogen for histology. All animal procedures were pre-approved by Montana State University's IACUC. Experimental results were confirmed by at least two independent repetitions of similar design.

Immunostaining and Flow Cytometry

Frozen blocks were cut into 5 μM sections by cryostat (Leica Microsystems; Buffalo Grove, IL) and resultant lung sections were stained for expression of the polymeric Ig receptor (pIgR) with biotinylated goat anti-mouse pIgR (R&D Systems, Minneapolis, MN) followed by AF488-streptavidin (Invitrogen, Carlsbad, CA). Control sections were utilized to determine staining specificity. Images were acquired on a Nikon Eclipse E800 microscope (Nikon Instruments, Melville, NY) using Nikon NIS-Elements Imaging software.

Antibodies used for FACS staining of lung and TBLN homogenates included CD4 (GK1.5), B220 (RA3-6B2), Fas (Jo2), CXCR5 (2G8), CD138 (281-2), and streptavidin from BD Pharmingen; San Diego, CA; GL7 (GL7), and CXCR4 (2B11) from eBioscience; San Diego, CA; and ICOS (C398.4A) from Biolegend, San Diego, CA. FACS data was collected on a FACSCanto (BD) and FACS analysis was completed using FlowJo Software (Treestar, Ashland, OR). Briefly, forward and side scatter plots were gated on lymphocytes, as determined by size and granularity. Lymphocyte populations were then further analyzed for the expression of appropriate combinations of surface antigens, based off negative staining controls. Total cell numbers were then calculated based off total hemocytometer cell counts for each tissue.

ELISA

Serum and BALF antibodies levels were determined by ELISA. Briefly, high-binding polystyrene plates (Corning; Corning, NY) were coated and incubated with antigen (OVA, sHsp, or influenza virus membrane preparation) at 37°C for 3 hrs., then moved to 4°C overnight. Plates were washed with PBS with .05% tween, and blocked with nonfat dry milk. Serum samples were diluted at 1:100, and BALF samples were plated neat (from a 2 mL lavage) in duplicate. For influenza-specific ELISAs, samples were diluted in 2-fold dilutions to endpoint titer. All ELISAs were then incubated at 37°C for 2 hrs. Plates were again washed and appropriate HRP-conjugated secondary antibodies (whole IgG, IgG1, IgG2a, IgG2b, IgG2c, IgG3, and IgA from SouthernBiotech, Birmingham, AL) were added and incubated for an additional 2 hrs. at 37°C. Finally, plates were again washed, developed using TMB substrate (Sigma-

Aldrich), stopped with 1M H_3PO_4, and read on a SpectraMax Plus plate reader (Molecular Devices; Sunnyvale, CA) at 450 nm. In some results, OVA-specific IgG was quantified using the mouse monoclonal antibody to OVA (Abcam, Cambridge, MA, ab17292).

Statistics

Statistical significance was determined by One-way ANOVA with a Bonferroni post-test of multiple comparisons, or in some cases an unpaired t-test was used. Significance was indicated by *p<.05, **p<.01, ***p<.001, or ****p<.0001. In some graphs, (*) symbols are replaced by other symbols for clarity in comparison between multiple groups, but the number of symbols always corresponds to the appropriate p-value as described above for the asterisk, and explained in individual figure legends.

Results

Conjugation of OVA to sHsp

We carefully optimized conditions for the conjugation of the 45 kDa model antigen, ovalbumin (OVA), to the exterior surface of the sHsp cage. Our analysis revealed differences in conjugation efficiency dependent on the length of the small molecule linker, the stoichiometry of linker utilized, and the position of the reactive groups on the sHsp cage architecture. We chose conditions that provided the best yield of the conjugate product, while avoiding the formation of protein aggregates, to prepare the conjugated sample for *in vivo* experiments (see supplemental materials).

For preparation of the samples for administration to the lung, OVA was conjugated to the exterior of the sHsp S121C cage. A commercially available hetero-bifunctional cross-linking reagent $SM(PEG)_6$ was reacted with the lysines of OVA (Fig. 1 and S3A) to produce maleimide-functionalized OVA (Fig. 1Aii and S3B). Immediately following the labeling of OVA with $SM(PEG)_6$, unreacted small molecule linker was removed via size exclusion chromatography, and the maleimide-functionalized OVA (Fig. 1Aii) was reacted with sulfhydryl groups present on the sHsp S121C cage (Fig. 1Ai) to produce the OVA-sHsp conjugate (Fig. 1Aiii). Subsequent to conjugation, unreacted sulfhydryls on the sHsp S121C were capped by reaction with N-ethyl maleimide to inhibit disulfide formation, and the samples were further purified by anion exchange chromatography, which effectively separated free OVA from the sHsp S121C cage and OVA-sHsp conjugate (Fig. S1).

Characterization of the
OVA-sHsp Conjugate

The protein conjugates (OVA-sHsp) were detected on SDS-PAGE gels. As a comparison to the OVA-sHsp conjugate, samples containing sHsp, maleimide functionalized OVA, and an admixture of sHsp and OVA were prepared. The admixture was prepared in a ratio of 5 OVA per 1 sHsp cage, and the OVA concentration within each sample was normalized to 0.57 mg/mL by UV-visible spectroscopy. The sHsp oligomeric complex dissociates into subunits under SDS-PAGE conditions, and a corresponding protein band (16.5 kDa) migrated close to the bottom of the gel (Fig. 1Bi). Also OVA appeared as two bands-- whole OVA (45 kDa), and cleaved OVA (40.1 kDa)

(Fig. 1Bii), as previously described [372]. Protein bands at higher molecular weights (>62 kDa) in Fig. 1Biii represented a polydisperse species of conjugated OVA-sHsp, and were later combined in total for use as the OVA-sHsp conjugate *in vivo* (further described below).

To determine if both OVA and sHsp were present in the upper bands of the sample in Fig. 1Biii, we performed Western Blot analysis using anti-sHsp (Fig. 1C) and anti-OVA (Fig. 1D) antibodies. Reactivity to both sHsp and OVA antibodies within the upper bands of the conjugated sample alone (Fig. 1Ciii and 1Diii) indicated the conjugation of OVA to sHsp. A semi-quantitative Western Blot (Fig. S4) suggested an average ratio of 2.6 OVA per sHsp cage within the conjugated sample. The total protein concentration of the conjugated (0.99 mg/mL), admixed (0.82 mg/mL), sHsp (0.61 mg/mL), and OVA (0.66 mg/mL) samples used for *in vivo* experiments were confirmed via Bradford assay.

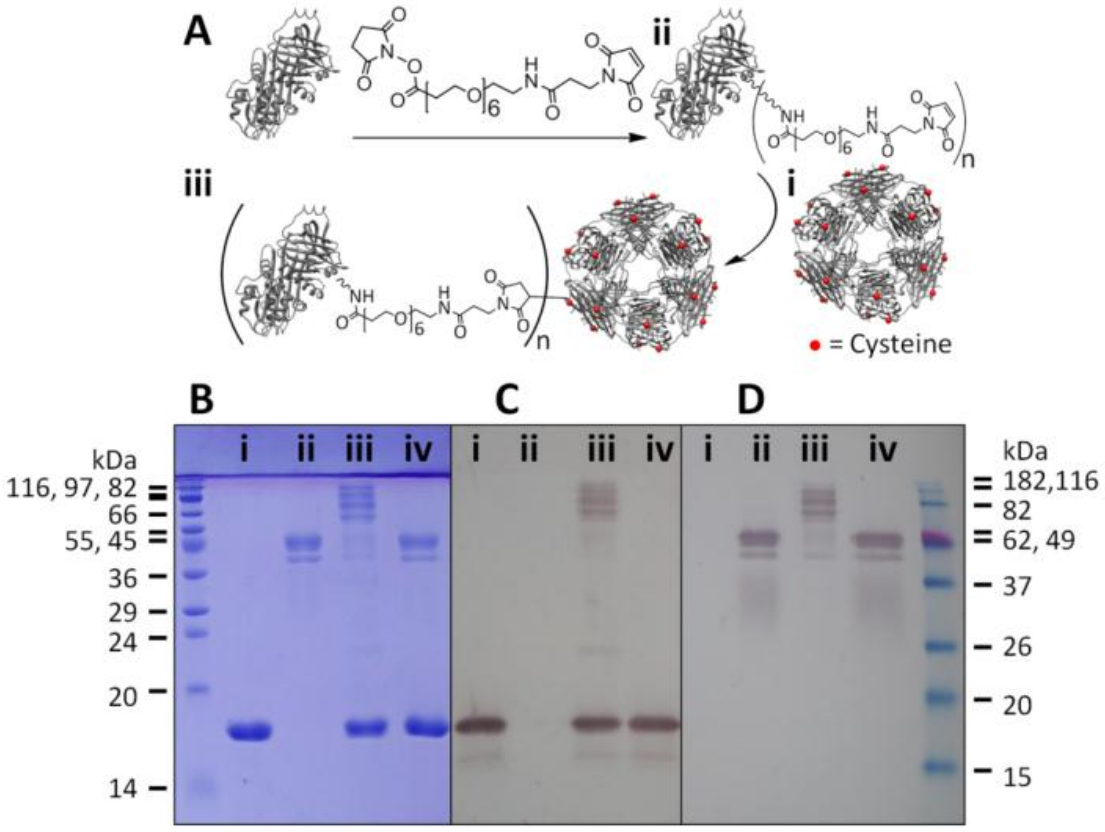


Fig. 1. OVA was conjugated to the sHsp S121C platform. The cross-linking methodology utilized to create the OVA-sHsp conjugate is shown (A). Ovalbumin was initially reacted with a commercially available crosslinking reagent, $SM(PEG)_6$, to produce a maleimide functionalized OVA (Aii) with n number of linkers attached. The functionalized OVA was reacted with sufhydryls on the sHsp S121C cage (Ai) to yield an OVA-sHsp conjugate (Aiii). The samples used for *in vivo* administration were analyzed by SDS-PAGE (B), and Western Blots with detection for either sHsp (C) or OVA (D). The lanes for each panel correspond to: sHsp S121C (i), OVA (ii), OVA-sHsp conjugate (iii), and an unlinked admixture (iv) of sHsp S121C (i) and OVA (ii).

The molecular weights of the bands corresponding to the OVA-sHsp conjugates were determined based upon their migration distance on SDS-PAGE gels (Fig. 1B and S5), and densitometry analysis (not shown). We detected bands with calculated molecular weights of 58 and 62 kDa that corresponded to the conjugation of a single sHsp subunit (16.5 kDa) to one cleaved OVA (40.1 kDa) or full length OVA (45 kDa), respectively.

The upper bands detected between 67 and 84 kDa likely resulted from various forms of conjugation of OVA to sHsp (Fig. S5), and the smear of sample corresponding to molecular weights 85-150 kDa likely represented the conjugation of OVA to multiple sHsp subunits, as this entire smear reacted to both anti-OVA and anti-sHsp antibodies on a Western Blot. Thus, the resultant conjugated OVA-sHsp sample used for immunization was the culmination of a polydisperse species of OVA-sHsp, with varying degrees of multivalent array architecture.

We utilized size exclusion chromatography and dynamic light scattering measurements to probe the native state and size distribution of the particles within the samples used for immunization. The OVA-sHsp conjugate contained particles that were larger in size than those in the admixture, sHsp, or OVA. Size exclusion chromatography indicated that a distribution of larger species was present within the OVA-sHsp sample (Fig. S6) and by dynamic light scattering, the OVA-sHsp conjugate showed a larger average diameter than the maleimide functionalized OVA, sHsp S121C, or the admixture. The range of average diameters based on the intensity measurements on the samples repeated seven times were 6.0-9.9 nm for OVA, 15.1-17.3 nm for the admixture, 15.6-18.1 nm for sHsp S121C, and 29.9-41.0 nm for the OVA-sHsp conjugated sample (Fig. S7).

The Immune Response to OVA-sHsp is Quick and Intense After Only a Single Intranasal Dose

In our first *in vivo* studies we determined the potential of sHsp to serve as a novel vaccine delivery platform by its ability to facilitate the generation of antigen-specific immunity to OVA. Simultaneously, we determined how pretreatment of the lung with a heterologous VLP, P22, affects the subsequent response to antigen challenge. BALB/c mice were pretreated with either P22 or vehicle (PBS) intranasally (i.n.) in five doses and then allowed to rest for 72 hours. Mice were then challenged with OVA conjugated to sHsp (OVA-sHsp), OVA and sHsp separately in solution (OVA-sHsp admixture), OVA alone, or sHsp alone. Serum was then collected at a range of timepoints post-antigen challenge for kinetic analysis. We found that mice which had received the P22 pretreatment, followed by a single dose of the OVA-sHsp conjugate, produced high amounts of OVA-specific serum IgG as early as 4 days post-challenge (Fig. 2A). This combination far outperformed any of the other treatment scenarios in both rapidity of antibody production and amount. Interestingly, the next highest antibody producing group, at early timepoints, was those mice that had also been challenged with the single dose OVA-sHsp conjugate, but had been pretreated with vehicle (PBS) only. This group also produced significantly higher antibody titers than the remaining combinations, although the response was delayed by about one day, as compared to those mice which had received P22 pretreatment (P22/OVA-sHsp conjugate). The remaining groups however, did not achieve the same peak titers until day 14 post-challenge, if at all, and equal early responses were delayed by 3-4 days (P22/OVA-sHsp admixture) or more

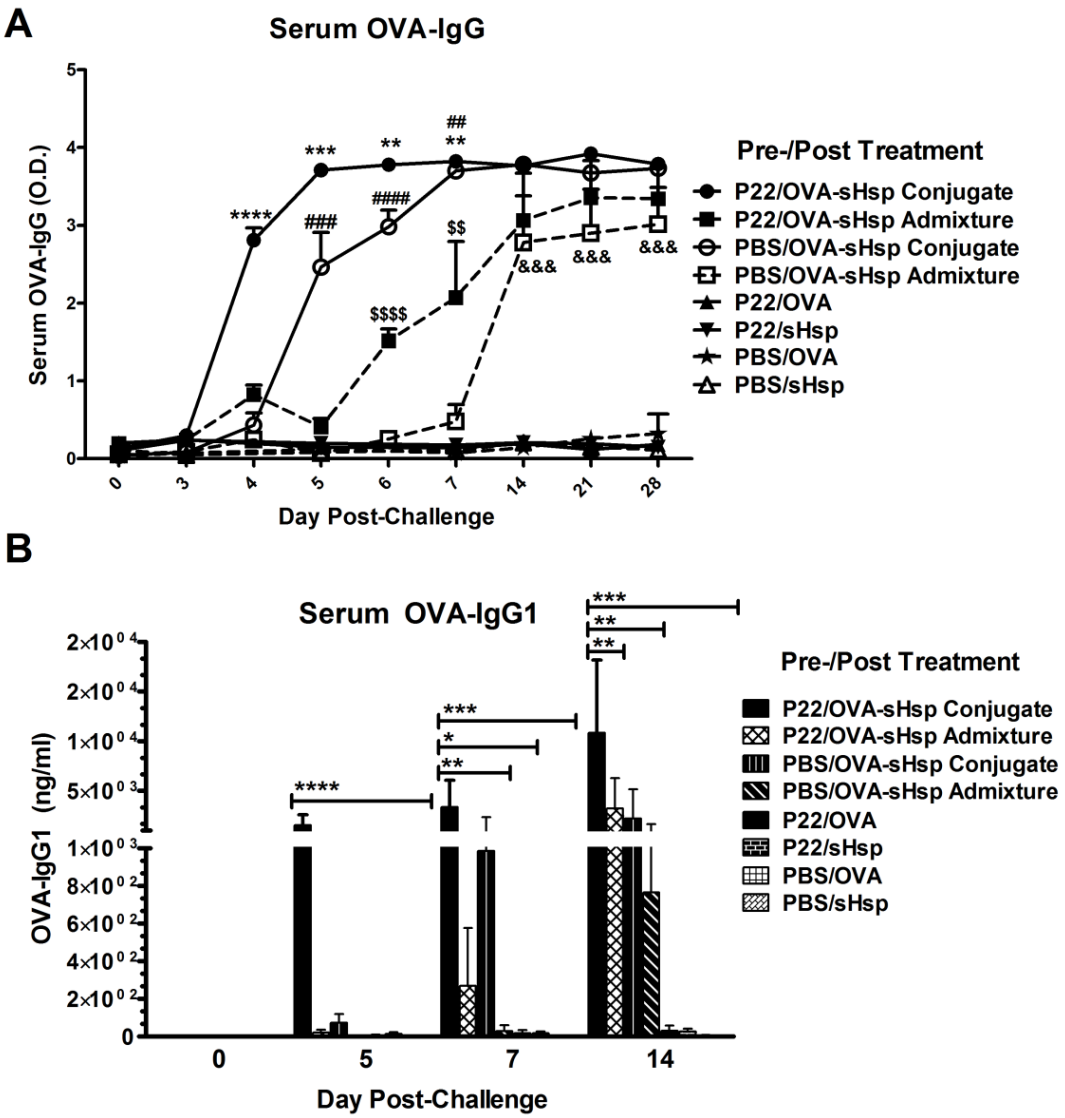


Fig. 2. The immune response to sHsp is accelerated and intensified after only a single intranasal dose. Mice were pretreated with P22 or vehicle (PBS), then challenged with the OVA-sHsp conjugate, the OVA and sHsp admixture, OVA alone, or sHsp alone. At indicated timepoints post-challenge, serum was collected and total OVA-specific IgG (A) or IgG1 (B) were determined by ELISA, and expressed as either O.D., or concentration (ng/ml). Results in this figure were compiled from two independent experiments with alternate days of serum collection. Statistics: In 2A (*) corresponds to the P22/OVA-sHsp conjugate group, (#) corresponds to the PBS/OVA-sHsp conjugate group, ($) corresponds to the P22/OVA-sHsp admixture group, and (&) corresponds to the top 4 traces as compared to the bottom four traces. In 2B the P22/OVA-sHsp conjugate group was evaluated against each other group and significance is indicated by (*).

(PBS/OVA-sHsp admixture), as compared to the P22/OVA-sHsp conjugate group. This indicated that the OVA-sHsp conjugate is immunologically recognized differently than is the admixture, and further that this resulted in accelerated antibody production.

We also determined the absolute concentration of the OVA-specific IgG1 response to the same pre- and post-treatment combinations (Fig. 2B). Consistent with our other results, mice that were pretreated with P22, then challenged with the OVA-sHsp conjugate, produced OVA-specific serum IgG1 in significant levels by day 5, and the quantities increased over the next nine days. Second best at producing high quantities of antibodies were both those mice which had received the control (PBS) pretreatment, but had been challenged with the OVA-sHsp conjugate, and those mice which had been pretreated with P22, then challenged with the sHsp and OVA admixture, which were measurable by day 7 post-challenge. Again, by day 14 post-challenge, the amounts of OVA-specific IgG1 were converging in only those groups in which the sHsp was delivered with OVA. Importantly, two additional conditions further heightened and accelerated the initiation of antibody production—heterologous VLP pretreatment with P22, and the physical conjugation of OVA to sHsp. While we will further discuss the impacts of pretreatment on subsequent challenge, we have demonstrated here that we can elicit an accelerated and intensified immune response to a weak antigen, in a single dose, by covalently conjugating it to sHsp.

The Conjugation of an Antigen to sHsp
Results in the Generation of the Same
Immune Response to that Antigen as sHsp Itself

We have previously demonstrated that the priming of the lung with sHsp elicits an enhanced immune response to a subsequent pathogen challenge [200]. However, we had yet to define the immune response to sHsp itself. Therefore to determine the rate and intensity of the sHsp-specific antibody response we again pretreated mice intranasally with P22, or vehicle. Mice were then rested for 72 hours, and challenged with the OVA-sHsp conjugate, the OVA and sHsp admixture, OVA alone, or sHsp alone. We then evaluated the sHsp-specific serum antibody response over 14 days post-challenge (Fig. 3A). We found that after only one challenge dose, all mice exposed to sHsp generated strong sHsp-specific IgG1 responses, which peaked as early as day 5 post-challenge in mice which had been pretreated with P22. Mice that did not receive P22 pretreatment were again two days delayed in the production of similar amounts of sHsp-specific antibody. However by day 7 post-challenge, all groups (except control OVA-only challenged mice) had generated similar levels of systemic sHsp-specific IgG1 in response to a single intranasal dose of sHsp antigen. Thus, the above-described OVA-specific response (Fig. 2) mirrors the accelerated kinetics of the sHsp-specific response, indicating that sHsp facilitates a carrier effect that results in an immune response to OVA that is similar to the response to the sHsp in both onset of antibody production and quantities produced.

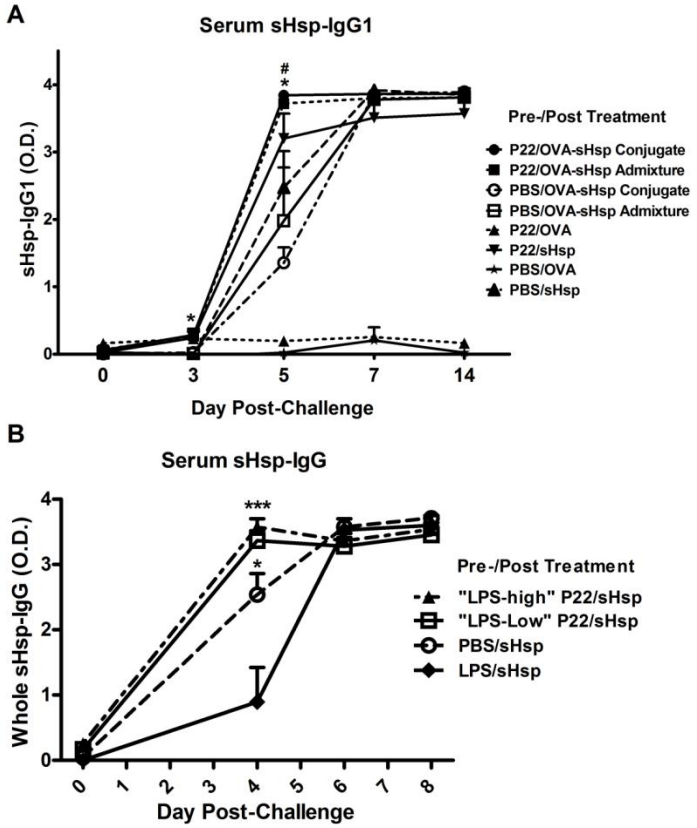


Fig. 3. The conjugation of an antigen to sHsp results in the generation of the same immune response to that antigen as sHsp itself. In 3A mice were pretreated with P22 or vehicle (PBS) i.n. All mice were then challenged with either the OVA-sHsp conjugate, OVA and sHsp admixture, sHsp alone, or OVA alone. At indicated times, serum was collected and sHsp-specific IgG1 was measured by ELISA (A). In 3B Mice were pretreated with "LPS-high" P22 (8 μg LPS per dose), "LPS-low" P22 (14 ng LPS per dose), an equivalent amount of LPS alone (8 μg per dose), or sterile pyrogen-free PBS in five doses i.n. All mice were then challenged with 100 μg sHsp and whole serum IgG to sHsp was determined over 8 days (B). Statistics: In 3A, at day 3, the P22/OVA-sHsp conjugate group (*) had significantly higher levels of antibody than the PBS/sHsp group only. At day 5, the P22/OVA-sHsp conjugate group had significantly higher levels of antibody than both the PBS/OVA-sHsp conjugate (**) and PBS/OVA-sHsp admixture (*) groups. Additionally, the P22/OVA-sHsp admixture and P22/sHsp groups had significantly higher levels of antibody than the PBS/OVA-sHsp conjugate group (## and #, respectively). In 3B at day 4 all groups had produced significantly more antibody than the LPS pretreated group where both P22 groups ("LPS-high" and "LPS-low") were *** $p<.001$, and PBS was *$p<.05$ comparatively to the LPS group.

Because our samples were purified from an *E. coli* expression system, we examined whether or not the heightened antibody responses observed were amplified by the residual LPS contained in our VLPs. We pretreated mice with either "LPS-low" P22, "LPS-high" P22, an equivalent amount of LPS as contained in the "LPS-high" P22 preparation, or sterile pyrogen-free PBS in five daily intranasal doses, as above. Mice were then challenged with sHsp alone, and serum was collected over 8 days to evaluate total anti-sHsp IgG. Importantly, we found that both "LPS-low" and "LPS-high" P22 elicited an equally enhanced early antibody response to the heterologous VLP challenge, while mice which were pretreated with LPS did not (Fig 3B). In addition, we pretreated TRL4-/- or C57BL/6 mice with sHsp or PBS and challenged all mice with high-dose influenza virus. Importantly, only those mice that had been pretreated with sHsp were protected from influenza-induced body weight loss, regardless of their ability to respond to LPS (Fig. S2). These results indicated that the observed heightened immunity in VLP pretreated mice was not dependent on contaminating LPS.

sHsp Can Act as an Adjuvant in the Lungs

Next, to determine how the addition of sHsp, either delivered as a conjugate or an admixture with OVA, could act as an adjuvant for the immune response in the lungs, we pretreated mice with PBS only, and subsequently challenged them with the OVA-sHsp conjugate, admixture, or OVA alone, as described above. At day 7 post-challenge, we determined the level of OVA-specific serum IgG subclasses, and found that both the conjugated and admixture preparations of OVA elicited high-titer serum antibody O.Ds., while no such response to OVA alone was seen (Fig. 4A). Interestingly however, the

OVA-sHsp conjugate promoted accelerated class-switching to IgG2a, IgG2b and IgG3 while only IgG1 was significantly detected for the admixture. To further determine the early events of isotype switching, we pretreated mice with either sHsp or vehicle, and challenged with the OVA-sHsp conjugate, or admixture. At days 0, 4, and 6, serum was collected and the OVA-specific IgG subclasses were determined by ELISA. We found that OVA-specific total IgG and IgG1 production was quicker by about two days in mice that had been pretreated with sHsp and challenged with the conjugated OVA-sHsp (Fig. 4B-C) as compared to the other treatments. The early IgG1 response in this group then translated into an enhanced production of class-switched IgG2a and IgG2b at day 6 post-challenge (Fig. 4D and E). This extent of isotype switching was not fully realized in any other group. Interestingly however, the enhanced class-switching capacity appeared to be more dependent upon the structure of the challenge antigen (OVA-sHsp conjugate vs. admixture) than the pretreatment with sHsp. Mice which had received only PBS pretreatment and had been challenged with the OVA-sHsp conjugate generated significantly higher IgG1, 2a, 2b, and IgG3 titers at day 6 post-challenge than those which were challenged with the admixture of sHsp and OVA (Fig. 4C-E, and G). Very little IgG2c was produced at any timepoint (Fig. 4F). Thus, sHsp acts as an adjuvant when mixed with OVA and acts as a carrier when conjugated to OVA, resulting in unexpectedly potent antibody titers as early as 4 days after a single immunization in naïve mice.

Figure 4

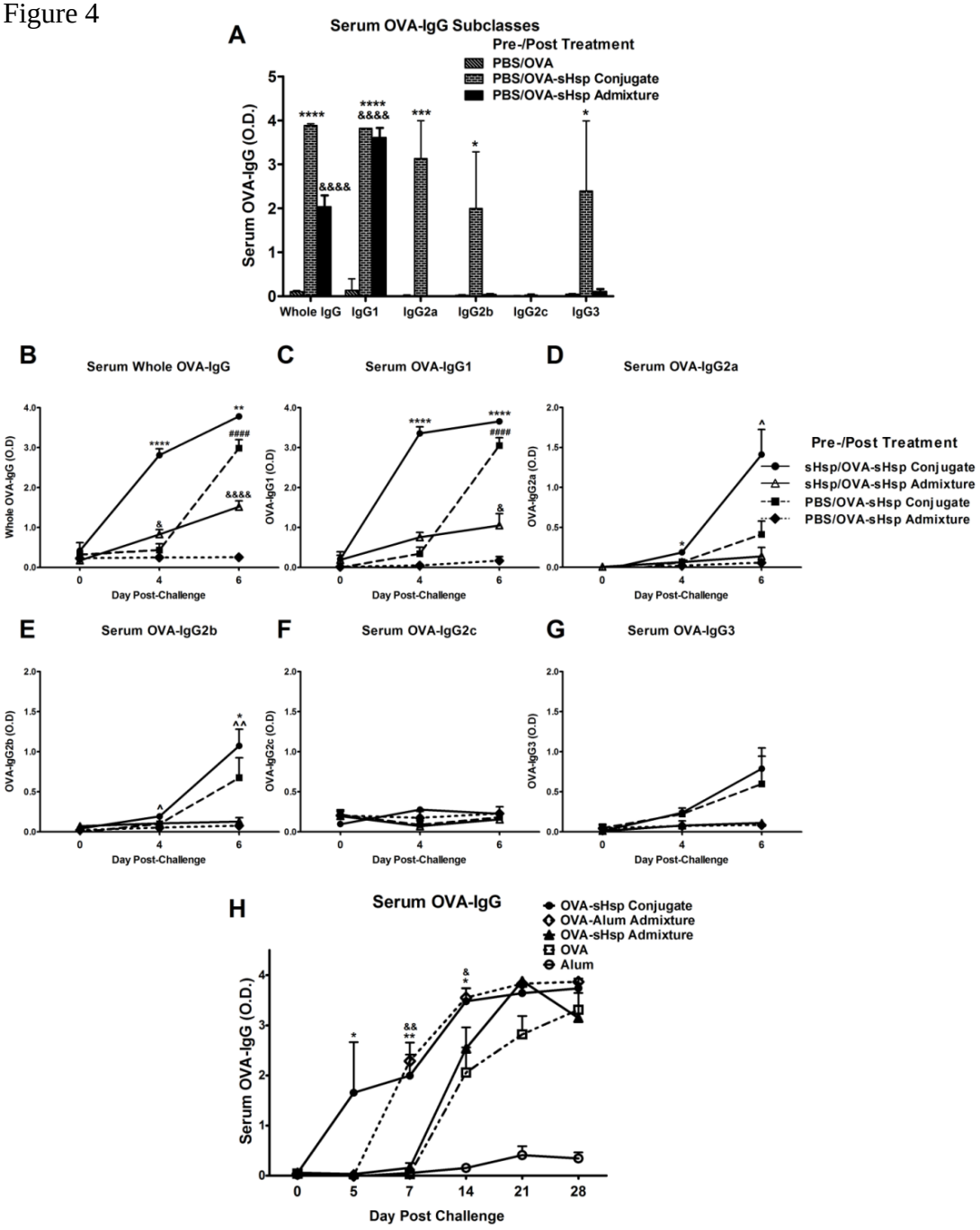

A
Serum OVA-IgG Subclasses
Pre-/Post Treatment
PBS/OVA
PBS/OVA-sHsp Conjugate
PBS/OVA-sHsp Admixture
Serum OVA-IgG (O.D.)
Whole IgG
IgG1
IgG2a
IgG2b
IgG2c
IgG3
B
Serum Whole OVA-IgG
C
Serum OVA-IgG1
D
Serum OVA-IgG2a
Day Post-Challenge
Pre-/Post Treatment
sHsp/OVA-sHsp Conjugate
sHsp/OVA-sHsp Admixture
PBS/OVA-sHsp Conjugate
PBS/OVA-sHsp Admixture
E
Serum OVA-IgG2b
F
Serum OVA-IgG2c
G
Serum OVA-IgG3
H
Serum OVA-IgG
OVA-sHsp Conjugate
OVA-Alum Admixture
OVA-sHsp Admixture
OVA
Alum
Day Post Challenge

Fig. 4 Continued. sHsp can act as an adjuvant in the lungs. In Fig. 4A, all mice were pretreated with PBS i.n., and then challenged with the OVA-sHsp conjugate, OVA and sHsp admixture, or OVA alone. Serum IgG subclass titers were then determined by ELISA at day 7 post-challenge. In 4B-G, mice were pretreated with either sHsp or vehicle (PBS) i.n., then challenged with the OVA-sHsp conjugate, or the OVA and sHsp admixture. At days 0, 4, and 6 serum was collected and total OVA-specific IgG subclasses were determined by ELISA. In 4H, mice were not pretreated, but were challenged s.c. with the OVA-sHsp conjugate, OVA and sHsp admixture, OVA and alum, OVA alone, or alum alone. Serum was then collected over 28 days, and OVA-specific serum IgG was determined by ELISA. Statistics: For Fig. 4A (*) denote the PBS/OVA-sHsp conjugate group as compared to the PBS/OVA-sHsp admixture group and OVA alone and (&) denotes the PBS/OVA-sHsp admixture group as compared to OVA alone. For Fig. 4B-C symbols are used per line to indicate significance over all other groups. In Fig. 4D (^) represents that the sHsp/OVA-sHsp conjugate group is significant as compared to the PBS/OVA-sHsp admixture group, but not the PBS/OVA-sHsp conjugate group at day 6. And in Fig. 4E, at day 4 and 6 (^) indicates that the sHsp/OVA-sHsp conjugate group was significant over the PBS/OVA-sHsp admixture group, and was also significant over the PBS/OVA-sHsp conjugate group (*) at day 6 only. For Fig. 4H at day 5 (*) denotes that the OVA-sHsp conjugate group was significant as compared to the OVA-alum admixture. At day 7, both the OVA-sHsp conjugate group (*) and the OVA-alum admixture group (&) were significant as compared to the remaining groups. At day 14 both the OVA-sHsp conjugate group (*) and the OVA-alum admixture group (&) were significant as compared to the OVA alone group. Significance was not denoted for differences against alum alone.

Because we found that sHsp is a strong mucosal adjuvant, we next determined if sHsp would elicit a similar response when delivered to a non-mucosal site. We subcutaneously (s.c.) injected naïve mice with either the OVA-sHsp conjugate, the OVA and sHsp admixture, OVA alone, or OVA with its classical adjuvant—alum. We then determined the resultant serum antibody responses and found that when conjugated to antigen, sHsp acts as a strong adjuvant to OVA to produce an accelerated OVA-specific antibody response as early as day 5 post-challenge, while OVA-alum responses are delayed by two days comparatively (Fig. 4H). Again, the OVA and sHsp admixture elicited high titer antibody responses, as did the OVA and alum admixture, however,

these combinations required more time to produce similar results. Taken together, sHsp conjugated to antigen acts as a carrier and elicits an accelerated antibody response to that antigen when delivered to several immunologically distinct sites.

sHsp-Treatment Induces Local IgA Responses

Growing recognition of the importance of site-specific immunity at mucosal surfaces [250], as well as tailoring immune responses per tissue [2, 6, 373, 374] led us to determine whether pretreatment with sHsp or the conjugation of sHsp to OVA affects local IgA production. After pre-treatment with sHsp or PBS, and challenge with either the OVA-sHsp conjugate or the admixture, lung lavage fluids contained high levels of mucosal IgA and IgG in only those mice pretreated with sHsp (Fig. 5A and B). Local IgG production was further enhanced by the conjugation of sHsp to OVA (Fig. 5B). Notably, while many of our results demonstrate that the admixed OVA and sHsp preparation does not elicit the same enhancement as the conjugate, here, the admixture is equally potent in initiating mucosal IgA responses (Fig. 5A). sHsp thus serves a dual role—first as an immunomodulatory agent during pretreatment, and second, as an adjuvant for specific antigens. Furthermore, we found that the pretreatment of the lung with sHsp caused an upregulation of the polymeric Ig receptor (pIgR) on lung epithelial cell surfaces prior to antigen challenge (Fig. 5C). Thus, the capacity for the release of local secretory IgA into the airway lumen is enhanced by sHsp pretreatment.

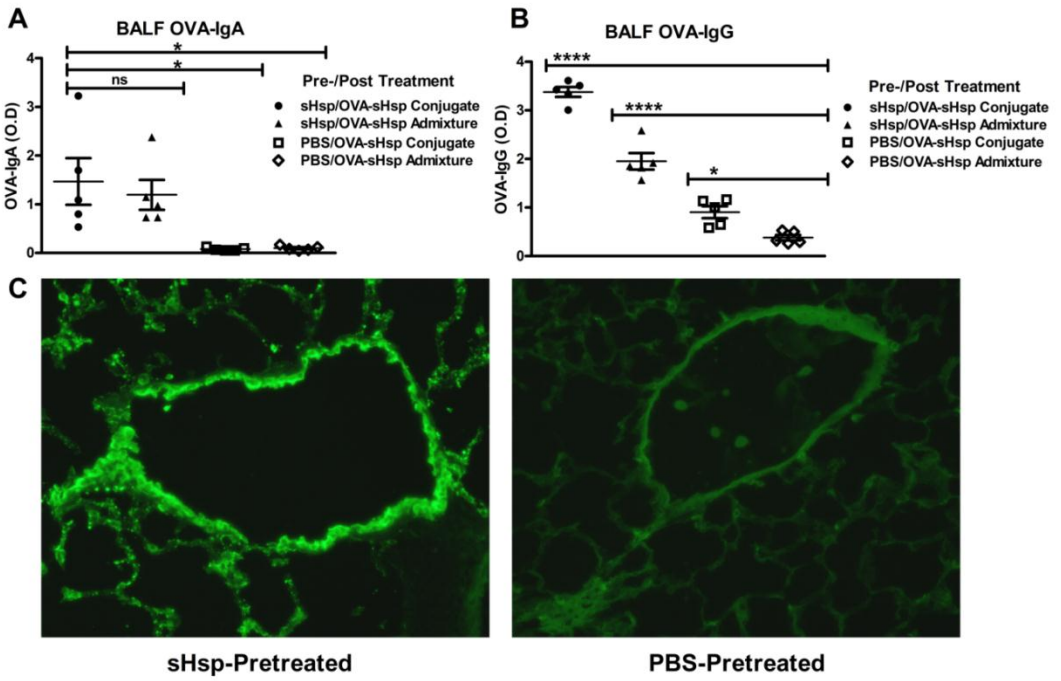


Fig. 5. sHsp treatment induces local IgA responses. Mice were pretreated with sHsp or vehicle control (PBS) i.n., then challenged with the OVA-sHsp conjugate, or the OVA and sHsp admixture. In 5A and B, BALF OVA-specific IgA and IgG were measured at day 7 post-challenge by ELISA. In 5C, frozen lungs were sectioned and stained for the presence of the polymeric Ig receptor in either sHsp- (Left) or vehicle-primed (Right) mice. Statistics: For Fig. 5A the sHsp/OVA-sHsp conjugate was significant as compared to both PBS pretreated groups. In Fig 5B the sHsp/OVA-sHsp conjugate was significant as compared to all the below groups, as was the sHsp/OVA-sHsp admixture, and the PBS/OVA-sHsp conjugate.

sHsp Pretreatment of the Lungs Enhances Influenza-Specific Antibody Responses and Changes the Lung Environment, Making it More Conducive to Local Antibody Responses

We have previously shown that sHsp pretreatment of mice subsequently infected with influenza, accelerates the onset and intensity of an influenza-specific IgG response similar to how sHsp pretreatment enhances the antibody response to OVA-sHsp [200]. We then determined whether sHsp pretreatment also affected the kinetics of antibody class

switching after influenza infection as it does with OVA-sHsp. In mice pretreated with sHsp or control, then challenged with 1500 pfu mouse-adapted PR8 (H1N1) influenza virus, we determined the corresponding endpoint-dilution titer of influenza-specific IgG subclasses in the local BALF, and found that, as had been expected due to the OVA results, influenza-specific BALF IgG was enhanced both in titer and in the rate of class-switching in mice which had been exposed to sHsp prior to infection (Fig. 6A-F). Thus, sHsp pretreatment similarly affects antibody responses to a model antigen and a pathogen-associated antigen.

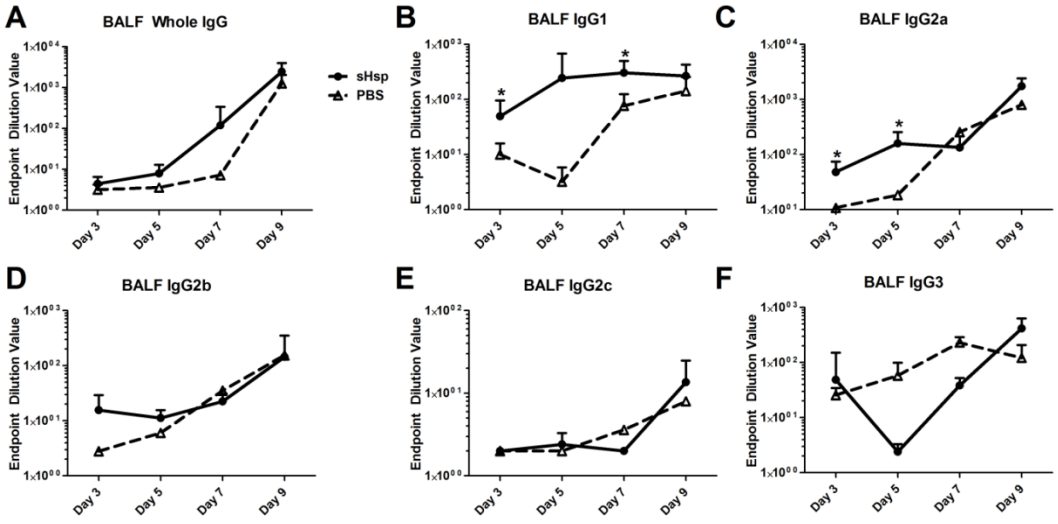


Fig. 6. sHsp pretreatment accelerates the onset of influenza-specific IgG in BALF. Mice were pretreated with either sHsp or vehicle (PBS), and challenged with 1500 pfu PR8 influenza i.n. At indicated times post-challenge, mice were sacrificed and lavaged. Influenza-specific whole IgG (A), IgG1 (B), IgG2a (C), IgG2b (D), IgG2c (E), and IgG3 (F) in the BALF were determined to endpoint titer in 2-fold dilutions by ELISA.

We next determined how sHsp pretreatment modulates the lung environment. We pretreated mice with sHsp, then challenged with influenza. We found that sHsp pretreatment stimulated the formation of germinal centers (GC) in the lung and enlarged GC B cell areas in the tracheobronchial lymph node (TBLN) (Fig. 7A and B). In both tissues, GC B cells were more prevalent by at least one log in sHsp-primed mice before infection, indicating that the microenvironment within the lung and local lymph node had been stimulated to adjust to the current antigenic exposure. We also found that T follicular helper (T_{FH}) cells were more abundant in both the lungs and TBLNs of sHsp-primed mice (Fig. 7C and D). Thus, germinal center reactions were more easily facilitated within the lungs and local lymph nodes of sHsp-primed mice. Over the course of infection, a clear advantage in GC organization and establishment was observed as both GC B cells and T_{FH} cells retained significantly higher numbers in sHsp-primed mice as opposed to controls. Thus, highly active GC reactions, complete with T_{FH} cell help, were likely facilitating the enhanced antibody isotype switching and elevated antibody production.

Given that GC's are enhanced, we also stained for the presence of plasma cells, as defined by their lymphocyte size and morphology, loss of B220 and CD19, with or without CD138 (syndecan) expression, and the upregulation of CXCR4 (Fig. 7E and F). Interestingly, we found that in the lung, plasma cells at day 0, assumedly secreting antibody against sHsp, were markedly more abundant in primed mice. However, the number of cells present rapidly declined over the course of the influenza infection, which may represent profound plasticity in the specificity of the inhabitants of GC areas of the

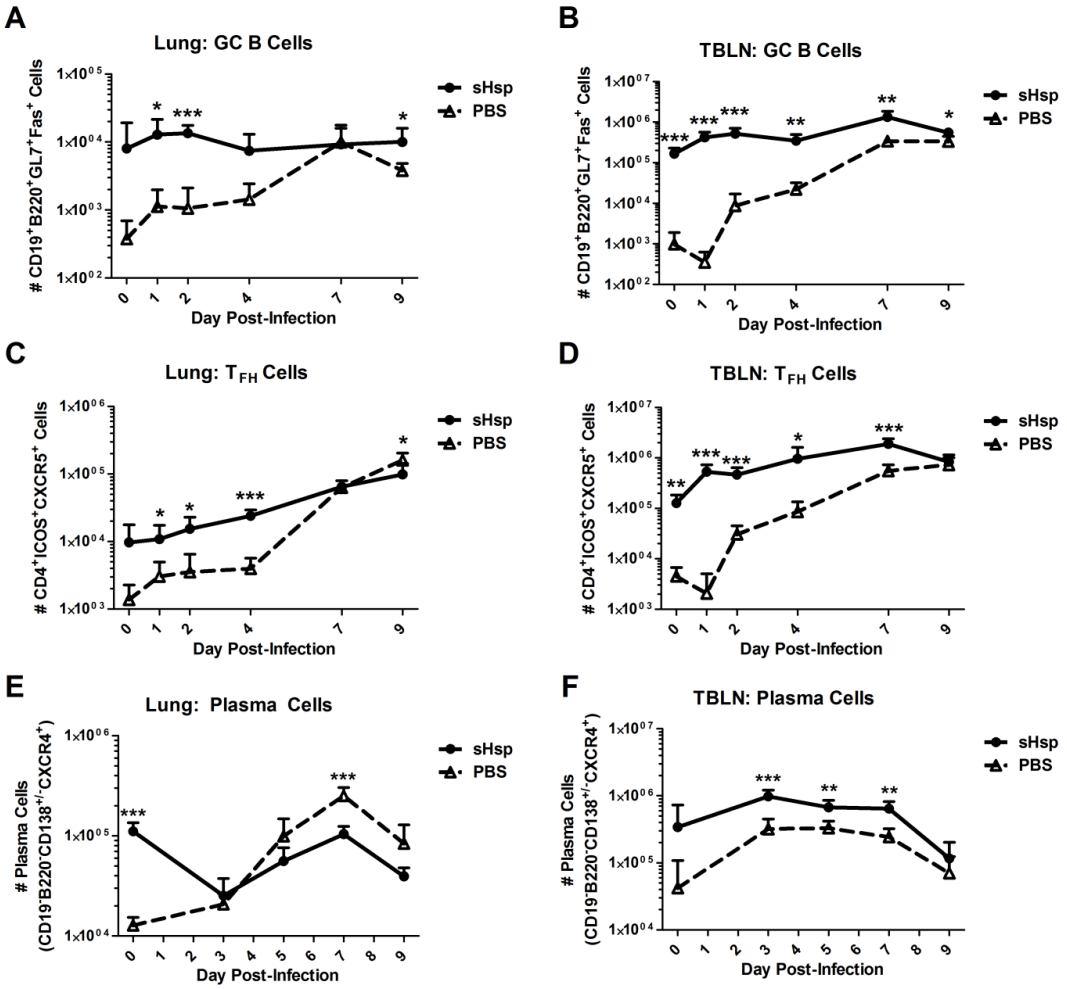


Fig. 7. sHsp pretreatment of the lungs leads to an even faster response to subsequent antigens. Mice were pretreated with sHsp or vehicle (PBS) i.n., infected with 1500 pfu PR8, and then sacrificed at indicated times post-infection. Lungs and tracheobronchial lymph nodes (TBLNs) were homogenized and stained for germinal center (GC) B cells (A and B), T follicular helper cells (TFH) (C and D), or plasma cells (E and F) and total cell numbers were quantified by FACS and cell counts.

lung (as has been described by others)[375]. In the TBLN, plasma cells were again more numerous before infection in the sHsp-primed mice. However, here, they remained elevated as compared to control mice until the resolution of infection, at which point the plasma cell numbers in the TBLNs of both groups converged. Unlike the lung however, similar trends were followed by both groups in the TBLN. We surmise from this data that sHsp-specific plasma cells in the lung are decreasing, while simultaneously, influenza-specific plasma cells are increasing. Therefore, due to the likely variable rates of influx and efflux, we may not have exclusively quantified the rate of increase in influenza-specific plasma cells due to sHsp priming. What remains puzzling however is how sHsp-specific germinal centers and plasma cells become influenza- or OVA-specific at an accelerated rate when compared to control mice. Given our experimental data, we surmise, as have others [7], that the pulmonary microenvironment adjusts in the context of innate, humoral, and cellular immune responses in reaction to the menagerie of antigenic exposures encountered, which are unique to that individual. Thus, sHsp pretreatment significantly enhances the efficiency of future immune responses.

Discussion

We have shown previously that sHsp pretreatment induces pulmonary changes that protect against a subsequent challenge with a variety of pathogens, and additionally sHsp pretreatment decreases tissue damage, while accelerating viral clearance [200]. We demonstrate here that both sHsp pretreatment, and the conjugation of sHsp to an antigen of interest, provided enhanced immunity, by likely distinct immunological mechanisms.

Pretreatment with sHsp elicited the organization of GCs in the lungs and TBLNs, which then functioned to accelerate and intensify the onset of antibody production. Most importantly, pre-priming of the lung with sHsp elicited an enhanced mucosal IgA response, and the upregulation of epithelial pIgR. This response is not dependent upon the physical conjugation of OVA to sHsp, as the OVA and sHsp admixture elicited IgA production equally well. For local BALF IgG production, however while sHsp pretreatment seemed to be the factor majorly responsible for the enhanced antibody titers, the conjugation of sHsp to OVA also contributed. Finally, heterologous VLP pretreatment was equally efficient at eliciting heightened immunity, as demonstrated with P22 pretreatment followed by OVA-sHsp challenge, and sHsp pretreatment followed by influenza challenge. While heterologous immunity has been extensively described in both the context of cross-protective immunity, and inappropriate or harmful skewing, the underlying mechanisms are still incompletely defined [7, 254, 255, 272, 273, 375, 376]. We demonstrate here that pretreatment of mice with non-pathogenic VLPs stimulated immunity through some type of priming, which resulted in a subsequent enhanced response to OVA, and furthermore, facilitated pathogen clearance and decreased damage in response to viral challenge (Figs. 5 and 6, and ref. [200]).

In addition to pretreatment, we also demonstrate the utility of sHsp as a novel vaccine platform through the direct conjugation to an antigen of interest. In contrast to the conjugation of antigenic peptides to a multivalent scaffold, we present the conjugation of an entire protein antigen to the protein cage surface for *in vivo* application. Through this approach, it is possible for the conjugated antigen to be seen by the immune

system as part of the VLP, and elicits a response similar to that the VLP elicits. As previous work has demonstrated that chemical conjugation efficiency of large unrelated proteins to a viral capsid is inhibited as the size of the protein is increased [369], conditions for the chemical conjugation of the 45 kDa OVA to the sHsp cage were optimized for these proteins. We observed that the attachment position on the sHsp cage, the length of the chemical linker, and the stoichiometry of linker labeling affected the conjugation efficiency.

When delivered as an OVA-sHsp conjugate, sHsp acted to enhance OVA-specific early antibody production. Thus, sHsp acted as a carrier, causing the OVA-specific response to mirror the sHsp-specific response in onset of antibody production and quantity produced. Interestingly, while we have utilized sHsp in two scenarios, as a pretreatment, or a vaccine delivery platform, and these scenarios likely are working through distinct immunostimulatory mechanisms, the activities of each are not mutually exclusive, and can in fact, synergize—as the antibody responses to the conjugated OVA-sHsp are enhanced by the pretreatment with either sHsp or P22.

While we have yet to define the exact cellular receptors responsible for signal transduction to initiate the immune response to the VLPs, we hypothesize that the repeating subunits of sHsp or P22 allow for the ability to crosslink or otherwise engage single or multiple cellular receptor domains. And as it has been suggested by others, cell surface integrins on antigen-presenting cells likely play a role in recognizing viral capsids [300, 363, 364]. Targeting evolutionarily conserved domains therefore facilitates plasticity in this delivery system, allowing for the utilization of sHsp conjugation with other

antigens—especially those which have complicated or precluded the design and manufacture of potent vaccines. Additionally, the complex geometry of the OVA-sHsp conjugate may be impacting the resultant immune responses observed. It has been well demonstrated that the specific geometric display of multivalent antigens significantly heightens immune responses [295, 362, 377], and especially B cell recognition [295-298], and further, that such displays may even provide enough co-stimulation to break tolerance to self-antigens without the need for adjuvants [297, 378]. Thus the arrangement of the OVA-sHsp conjugate may explain the enhanced class-switching which we observed only in those mice which received the conjugated form of OVA-sHsp (Fig. 4A-G). We therefore demonstrate the utility in displaying a poorly immunogenic antigen as a multivalent array through the conjugation to a VLP platform to elicit enhanced specific immunity.

Furthermore, the implications for a single-dose vaccine that accelerates the antibody response to antigens, producing high titer antibody within 4-7 days of primary immunization holds significant clinical potential. In this regard, new strategies which employ post-exposure prophylaxis represent an arguably greater demand than pretreatment, as we continually lose antibiotic options due to the emergence of resistant strains of bacteria, and are no better at predicting future viral outbreaks. Thus, we may be able to exploit sHsp, conjugated to an antigen of choice, to elicit early IgA responses. Importantly, few adjuvants currently on the market can be safely delivered to the lung, nor do they produce high titer, site-specific mucosal IgA [379].

We have presented a novel vaccine platform that is amenable to easy manipulation, facilitating flexibility and broad implications for vaccination strategies

against many types of pathogens. This type of platform is especially noteworthy, as it may be utilized as an immunomodulatory agent alone (as in the case of pretreatments), for modifying the current state of immune homeostasis, or as a carrier and adjuvant for a defined antigen of interest. This phenomenon of immune homeostasis and skewing has been extensively described in terms of an individual's history of pathogen and allergen exposure [254, 255]. However, to date few attempts to harness the potential of immune priming, with or without involving pathogen-specific epitopes or proteins, have been described [256]. Thus, we propose that we have identified an approach which utilizes strategies for priming against undefined broad-spectrum antigens, and also for delivering a highly efficacious single-dose vaccine against a defined antigen.

Importantly, we have additionally shown that the route of delivery (directly to the lung by intranasal instillation) results in the creation of an immune response that is specifically tailored to that tissue, and its individual requirements. While concern in purposely eliciting an immune response in the lung is justified, we and others[295] indicate here (and elsewhere[200]) that by doing so with VLPs, the power of tissue-specific immunity can be harnessed to provide a safe and appropriate response in the context of both the pathogen (sterilizing immunity), and the protection of lung function. Furthermore, the onset of immunity when the lung is pre-exposed to sHsp is accelerated, again indicating that the pretreatment with sHsp impacts the future, unpredictable pathogen challenge. In addition, we have previously shown that the deposition of VLPs in mouse lungs has no adverse effects and even attenuates lung hypersensitivity[200].

Virus-like particle and nanoparticle vaccination strategies are gaining recognition as the next class of safe and effective platforms. Notably, while many vaccines are expensive to produce, and require refrigeration, many types of VLPs and nanoparticles are stable, and easily preserved through freeze-drying, creating opportunities for distribution that may be otherwise precluded due to cost or logistics. Therefore, we have herein described a novel mucosal vaccination strategy that accounts for tissue-specificity, and exploits natural immunity to provide accelerated and enhanced antibody and cellular immune responses to primary antigen challenge.

Acknowledgements

We thank the Harmsen lab staff for technical assistance in experiments, Erin Dobrinen for LAL assay results, Abby Leary for immunostaining and microscopy, Ben Johnson and Suzanne Wilson for producing and purifying the sHsp and P22, Peter Previlege (University of Alabama, Birmingham) for providing the P22 expression vectors, and the staff of Montana State University's Animal Resource Center for animal care and technical aid. This work was made possible by funding from NIH/NIAID R56AI089458; the Rocky Mountain Research Center of Excellence (RMRCE) U54AI065357; NIH/NIAID R21AI083520; the IDeA Network for Biomedical Research Excellence (INBRE) P20GM103474; the Center for Zoonotic and Emerging Infectious Diseases (COBRE) P20GM103500; the M.J. Murdock Charitable Trust, and the Montana State University Agricultural Experimental Station.

Supplementary Material

Optimization of OVA-sHsp Conjugation.

SDS-PAGE was utilized to screen for the formation of protein conjugates (OVA-sHsp) between maleimide functionalized OVA samples and sHsp. A matrix of reaction conditions comprised of three sHsp mutants, 3 different SM(PEG)n linker lengths, and 2 stoichiometric ratios of SM(PEG)n to OVA were tested to determine relative linking efficiency (Fig. S8). Fig. S8 shows the result of reactions in which three sHsp cage mutants with free sulfhydryls (S121C, E102C, and G41C-SPDP, shown in Fig. S8: Ai, Bi, and Ci, respectively) were reacted with OVA samples labeled with a 2-fold molar excess of either SM(PEG)2, SM(PEG)6, or SM(PEG)12 (Fig. S8: Dii, Diii, and Div, respectively). The sHsp subunit (16.5 kDa) appeared close to the bottom of the gels, the OVA appeared as two major bands (45 kDa and 40.1 kDa), and protein bands at higher molecular weights (>62 kDa) corresponded to the conjugated species (Fig. S8).

The efficiency of conjugation differed based upon the length of cross-linker, the molar excess of linker utilized for OVA labeling, and the location of the reactive sulfhydryl on the sHsp cage. A comparison of the panels of Fig. S8A-C revealed that the reaction of labeled OVA with sHsp S121C (Fig. S8A) produced more linked conjugate than the reaction of the same OVA samples with sHsp E102C (Fig. S8Bii-iv) or sHsp G41C (Fig. S8Cii-iv). A comparison of lanes B-D within each panel revealed no significant trends in linking efficiency with respect to linker length for S121C or G41C sHsp (Fig. S8A and S8C). For the sHsp E102C mutant (Fig. S8B), the amount of conjugated species increased as the linker length increased from left to right on the gel

(Fig. S8Bii-iv). Similar trends in linking efficiency were observed when this matrix of conditions was repeated using a 20-fold molar excess of linker per OVA (Fig. S8E-H). These relative conjugation efficiencies for S121C and E102C correlated well with the observed positions of the residues on the sHsp crystal structure [380]. The S121C location was exposed on the surface of the protein shell, whereas the E102C was around the three-fold pores and appeared less accessible to the cage surface (Fig. S9).

Reaction conditions that provided the best yield of conjugated products and avoided the formation of protein aggregates were chosen for in vivo experiments. Because it provided the highest linking efficiency, the sHsp S121C mutant was selected for the generation of the OVA-sHsp conjugate. We observed that a longer linker provided more efficient conjugation between OVA and sHsp E102C. However, the appearance of a band at the running gel-stacking gel interface (Fig. S8Div, and S8Aiv) for the OVA labeled with SM(PEG)12, indicated OVA-OVA crosslinking within this sample. As protein was not visible at the stacking and running gel interface for the maleimide functionalized OVA samples labeled with the SM(PEG)2 or SM(PEG)6 linkers (Fig. S8Dii and S8Diii), the SM(PEG)6 linker was chosen for the conjugation experiments. Finally, to determine if both sHsp S121C and OVA were present in the higher molecular weight bands observed on an SDS-PAGE gel (Fig. S8A), Western Blots of the same samples were run using antibody to detect either OVA (Fig. S10A) or sHsp (Fig. S10B).

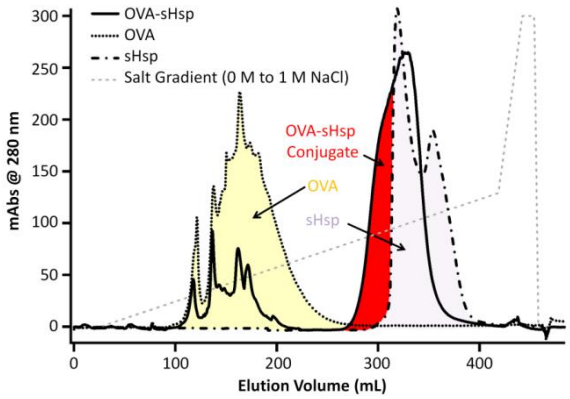


Fig. S1. Anion exchange chromatography was utilized to separate sHsp, OVA, and the conjugated species. The samples were eluted from a MonoQ anion exchange column with a salt gradient from 0-1 M NaCl. The OVA-sHsp conjugate elutes at higher salt concentration than the OVA, and appears as a shoulder to the left side of the sHsp elution.

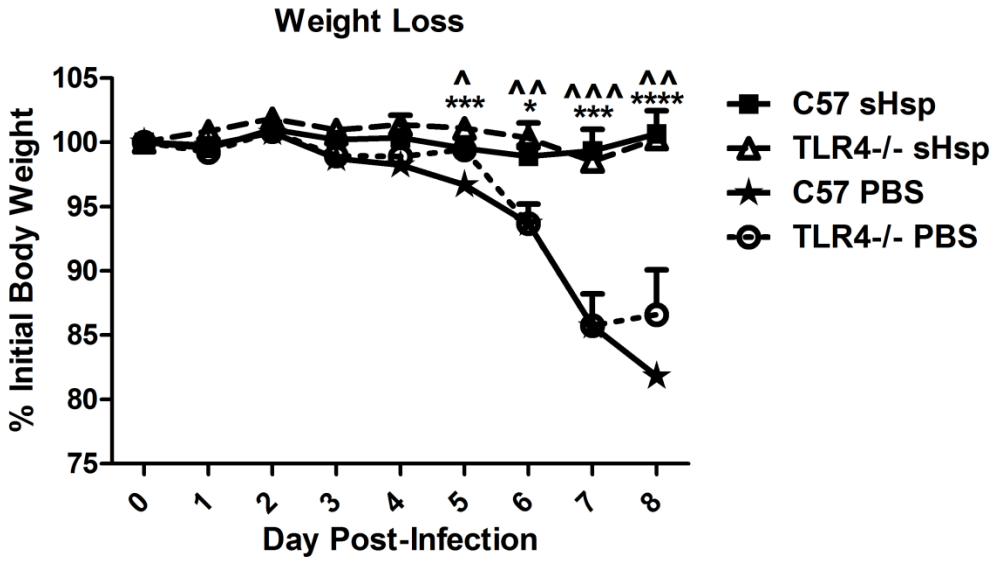


Fig. S2. sHsp pretreated TLR4-/- mice are protected from influenza-associated weight loss. LPS-irresponsive TLR4-/- or C57BL/6 wild-type control mice were pretreated with sHsp or PBS in five doses i.n., rested for 72 hours, and then challenged with 1500 pfu PR8 influenza. Body weights were measured daily to determine disease severity. Statistics: At days 5 through 8 of influenza infection, the C57BL/6 sHsp pretreated group maintained significantly more body weight as compared to the C57BL/6 PBS group, as indicated by (*'s), while the TLR4-/- sHsp pretreated group also retained significantly more body weight as compared to the TLR4-/- PBS pretreated group, as indicated by (^'s).

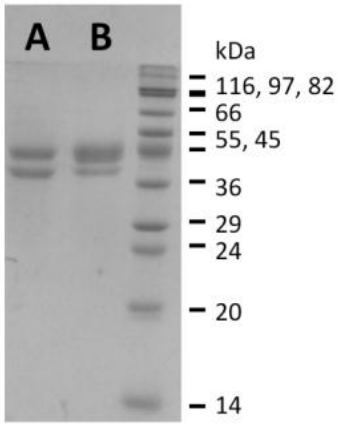


Fig. S3. This SDS-PAGE gel shows the ovalbumin sample prior to conjugation with $SM(PEG)_n$ linkers (A), and OVA labeled with $SM(PEG)_6$ (B).

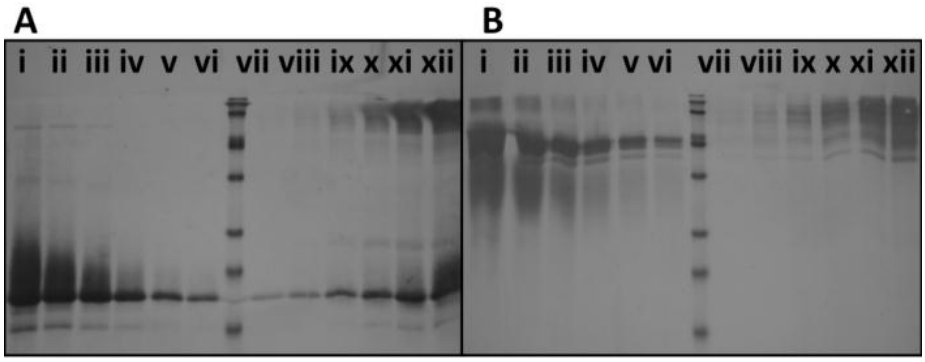


Fig. S4. The ratio of OVA to sHsp cage within the mixed sample was determined by densitometry analysis of Western Blots. A dilution series of the linked sample appears on both blots (lanes vii-xii). The blots show detection for sHsp (A) with an sHsp dilution series (Ai-Avi) and detection for OVA (B) with an OVA dilution series (Bi-Bvi).

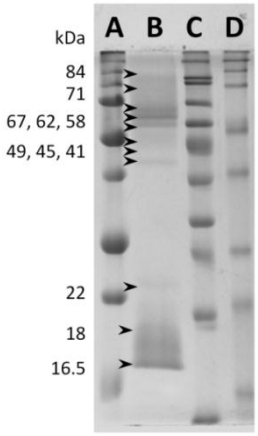


Fig. S5. The molecular weights of cross-linked proteins within the linked sample were determined by SDS-PAGE. This gel displays the Precision Plus Dual Color Std (A), OVA-sHsp conjugate (B), Sigma Wide Range Marker (C), and Invitrogen Benchmark PreStained Ladder (D). Arrows and numbers indicate predicted molecular weights of the bands within the conjugated sample.

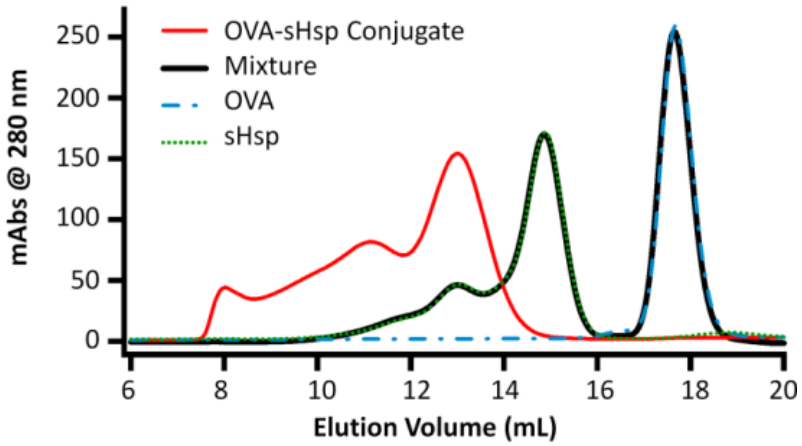


Fig. S6. Size exclusion chromatography was utilized to compare the sizes of particles within the samples used for *in vivo* experiments. Chromatograms show that the OVA-sHsp conjugate contains a distribution of molecular species that elute at earlier times than those in the other samples.

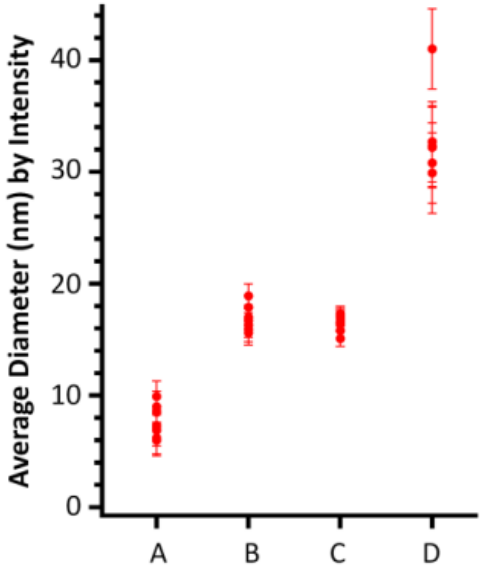


Fig. S7. Dynamic light scattering measurements show the average diameter of the particles within the solutions used for *in vivo* experiments. Points on the graph correspond to seven measurements of the average diameter in the sample, and the error bars to represent the standard deviation of the average measurements. The samples shown are malemide functionalized OVA (A), sHsp S121C (B), OVA + sHsp admixture (C) and the OVA-sHsp conjugate (D). The range of average diameters based on the intensity measurements on the samples repeated 6X are 6-9.9 nm for OVA, 15.1-17.3 nm for the admixture 15.6-18.1 nm for sHsp S121C, and 29.9-41.0 nm for the OVA-sHsp conjugated sample.

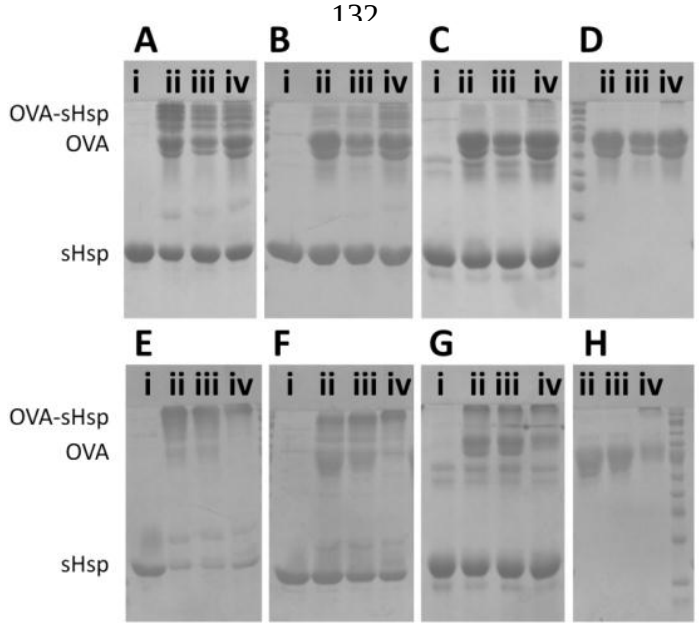


Fig. S8. The relative conjugation efficiency of OVA to sHsp for a matrix of reaction conditions was analyzed via SDS-PAGE. These gels show the reaction of maleimide functionalized OVA with sHsp S121C (A and E), sHsp E102C (B and F), or sulfhydryl functionalized sHsp G41C (C and G). The maleimide functionalized OVA was reacted with either a 2 fold (A-D) or 20 fold molar excess (E-H) of $SM(PEG)_n$ linker, where n= 2, 6, or 12, prior to reaction with sHsp. Lanes on the gels show the reactions utilizing linkers of increasing length and correspond to sHsp only (i), OVA + sHsp labeled with $SM(PEG)_2$ (ii), OVA + sHsp labeled with $SM(PEG)_6$ (iii), and OVA + sHsp labeled with $SM(PEG)_{12}$ (iv). Panels D and H show controls of the OVA labeled with $SM(PEG)_2$ (ii), $SM(PEG)_6$ (iii), or $SM(PEG)_{12}$ (iv).

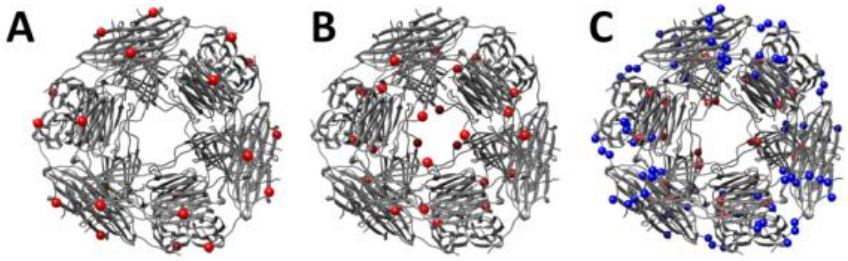


Fig. S9. The positions of the reactive cysteines (red spheres) on the sHsp crystal structure for S121C (A), E102C (B), and G41C (C). The lysines on the sHsp G41C that were successfully labeled with N-hydroxy succinimide are shown as blue spheres, which represent SPDP labeling of the amines to create sulfhydryl moieties at these locations. These images were produced using the UCSF Chimera package from the Resource for Biocomputing, Visualization, and Informatics at the University of California, San Francisco (supported by NIH P41 RR001081).

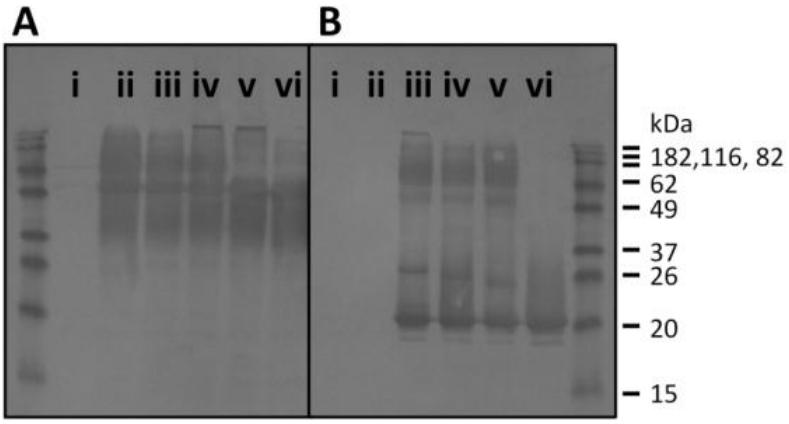


Fig. S10. Western Blots were utilized to identify OVA and sHsp within the protein bands at higher molecular weights. OVA was labeled with a 2-fold molar excess of either $SM(PEG)_2$, $SM(PEG)_6$, $SM(PEG)_{12}$ linker and reacted with sHsp S121C. The panels correspond to detection of the blots with either OVA (A) or sHsp (B). The lanes in panel A are sHsp (i), OVA + sHsp labeled with $SM(PEG)_2$ (ii), OVA + sHsp labeled with $SM(PEG)_6$ (iii), OVA + sHsp labeled with $SM(PEG)_{12}$ (iv), OVA labeled with $SM(PEG)_{12}$ (v), and OVA (vi). The lanes in panel B correspond to OVA (i), OVA labeled with $SM(PEG)_{12}$ (ii), OVA + sHsp labeled with $SM(PEG)_{12}$ (iii), OVA + sHsp labeled with $SM(PEG)_6$ (iv), OVA + sHsp labeled with $SM(PEG)_2$ (v), and sHsp (vi).

CHAPTER FIVE

CONCLUSIONS AND FUTURE STUDIES

Innate imprinting is clinically pertinent in that it may explain the variability of efficacy in vaccination and infection outcomes across individuals. These concepts can be further transferred to provide insight into potential improvements for vaccine design, as we have done here. The application of VLPs to medicine provides effective and novel methods for inspiring an immune response without risking viral replication, infection, or collateral damage. Moreover, the delivery of VLPs to a mucosal surface elicits pre-programmed immune responses and the production of local IgA. As such, the delivery of VLPs to the lung represents a safe and novel strategy by which to study the mechanisms of innate imprinting. Thus, we have delivered non-pathogenic VLPs to the lung to achieve a state of "immune education" in the lungs of mice. The exposure of the lungs to VLPs stimulated the formation of inducible bronchus-associated lymphoid tissue (iBALT), which we hypothesized to significantly impact the outcome of infection.

In chapter three, we provide evidence that mucosally-delivered VLPs provide non-pathogenic priming to elicit local, tissue-specific immune responses (including the development of iBALT) that prompt accelerated primary adaptive immune responses against a subsequent pathogen challenge. These protective responses depended on heightened DC and AM function and trafficking. Both $CD103^+$ and $CD11b^+$ DCs exhibited alternative and highly dynamic trafficking patterns as they migrated to the TBLN, and processed both a model antigen, OVA-DQ, as well as a fluorescent influenza

virus to a higher degree and with a quicker response time than what was achieved by control mice. VLP-exposed alveolar macrophages also took up and processed antigen and migrated to the TBLNs in both antigen and viral challenge scenarios. Thus, in agreement with other lines of evidence[127], we find that the AM is an important component for antigen presentation and the initiation of innate immune responses to influenza virus infection. We additionally determined that VLP-mediated protection was dependent upon CCR2-mediated trafficking. In this regard, Ly-6C^{hi}CD11b^{+} monocytes were essential for the repopulation of APCs into the lungs, as VLP-exposed CCR2$^{-/-}$ mice were unable to clear influenza virus to the same degree as VLP-exposed wild-type mice, despite their equal capacity to recruit T and B cells. Moreover, we determined that the direct exposure of CD11c^{+} cells (both DCs and AMs) to the VLPs was necessary for VLP-mediated clearance of the influenza virus, as VLP-primed mice which lacked VLP-primed CD11c^{+} cells were not protected from influenza-associated weight loss, and were permissive to viral replication equally to controls. Finally, APCs quickly up- and downregulated surface co-stimulatory molecules via a highly regulated program which allowed for the efficient (but not exuberant) activation of T cells. Thus, the heightened immunity to IAV induced with VLPs was the result of enhanced APC function in the lungs.

These tightly regulated and heightened innate events led to enhanced and highly regulated co-stimulation for CD4^{+} T cells. Thus, local CD4^{+} T cell responses were given an advantageous jump start in fighting infection, allowing for an accelerated viral clearance. Importantly, the flu-specific CD4^{+} T cell responses in areas of iBALT mirrored the responses in other lymphatic tissues such as the TBLN and spleen.

Furthermore, the $CD4^+$ T cell accumulation in the iBALT and BALF may be partially occurring independently from TBLN egress and trafficking, as was indicated in studies using a lymphocyte sequestration strategy. Finally, in neither the iBALT nor the BAL are $CD8^+$ T cell responses noticeably altered by VLP-exposure. Therefore, $CD8^+$ T cell responses may depend on the TBLN and not on locally-mediated immunity. Taken together, the VLP-derived enhancements in both the innate and adaptive immune responses to influenza during a primary viral challenge skew the resultant response to more closely represent a secondary response. Importantly, it is well documented that secondary (memory) responses to viral infection are much more rapid, efficient, and evoke less damage than primary responses. Thus, the ability for a primary immune response to mimic a secondary immune response to influenza by pre-priming the lungs could provide great benefit.

Others have reported that highly variant responses to a pathogen challenge occur if the host has been previously exposed to a distinct virus, and it is now thought that innate cells primarily mediate these discrepant responses. Whereas our system does not include two live viruses, we argue that we have harnessed similar immunological mechanisms, and moreover that we have done so without the need for natural infection. Thus by utilizing VLPs, we have herein reported some of the underlying immunological mechanisms which govern the concept of innate imprinting.

In chapter four we described how VLPs can be used both in a heterologous or homologous priming strategy to achieve heightened immunity to a subsequent antigen challenge, as well as a vaccine delivery platform to elicit heightened and accelerated

antibody responses after only a single dose. In these studies we utilized both an sHsp VLP as well as a P22 phage VLP to prime the lungs. The sHsp was also conjugated to, or admixed with OVA, in which case the antibody responses to both sHsp and OVA were measured. We found that when we conjugated OVA to sHsp, the sHsp-specific antibody responses after sHsp challenge were accelerated and intensified and that the linkage of an exogenous antigen to the sHsp elicited the same fast and intense response against the antigen as would be expected for sHsp itself. Interestingly, the sHsp in an admixture with OVA also acted as an adjuvant to elicit the same response to OVA as to sHsp itself. In this regard, we detected high-titer OVA-specific IgG in the serum as early as four days (with P22-priming) or 5 days (without P22-priming) after a single immunizing dose. The rapidity of these responses represent profound implications for vaccine development, and notably, whereas OVA is a normally poor immunogen, the conjugation of soluble OVA to our sHsp resulted in a potent antibody response, thus providing a potential avenue by which a poorly immunogenic vaccine may be improved.

Further characterization of the mechanism of heightened antibody responses in a pathogenic model revealed that non-specific VLP-treatment induced the formation of germinal centers in the lung, complete with T_{FH} cells and plasma cells, thus facilitating the production of high-titer isotype switched antibody days before controls.

Taken together, our work has revealed some of the underlying mechanisms of innate imprinting which include the development of iBALT in the lungs, alternative innate and adaptive immune responses, and an amelioration of damage during influenza infection. Significantly, these results impact our understanding of observed alternative

outcomes to respiratory infections on an individual basis, and also offer a highly manipulable platform for vaccine design.

Future Studies

Receptor Recognition of VLPs

We have observed that the intranasal delivery of several distinct VLPs elicits the formation of iBALT; however the cell surface receptors and downstream signaling pathways required for these events to occur remain to be defined. TLR recognition of viruses occurs via viral utilization of "foreign" genomic packaging strategies, such as unmethylated DNA (TLR9), ssRNA (TLR7), or dsRNA (TLR3), as well as by membrane lipoproteins (TLR2 and TLR4). Our VLPs lack genomic material and host plasma membrane components, but do contain LPS. Thus, some of the obvious contributing mechanisms of host cell recognition are dependent upon TLR2 and TLR4. We surmise, however that additional recognition mechanisms must be in play due to several lines of evidence. First, mice which received either an LPS-high or LPS-low formulation of VLPs were protected against high-dose influenza (not published). Furthermore, the delivery of LPS alone cannot substitute for the effects of the VLPs, as mice which had been pretreated with LPS did not achieve the same degree of antibody production in response to a subsequent challenge as did VLP-treated mice[224]. Using various knock-out strains of mice including C3H, TLR4$^{-/-}$, and MyD88$^{-/-}$ we have further observed that iBALT may still be elicited in response to VLPs, that lymphocyte responses in VLP-treated KO mice best mirror those of VLP-treated WT mice, and that upon influenza virus challenge, these

mice are protected from morbidity[200] (and data not shown). Interestingly, the P22 VLP appears to be immunologically recognized differently than is the sHsp VLP. Whereas the intranasal instillation of LPS-high P22 formulations protect mice from influenza-associated morbidity and reduce the viral load, LPS-free P22 formulations do not. Conversely, additional work with this LPS-free P22 highly indicates that the P22 is not immunologically inert, and in fact it may elicit antiviral responses in the lung regardless of its absent genome and inability to replicate. Taken together, we conclude that TLR2 and TLR4 are contributing to the above-described responses while additional signaling receptors must be involved. Candidate receptors may include CLEC9A (DNGR-1), which is known to recognize the damage-associated molecular pattern (DAMP), filamentous actin[381, 382], or cell surface integrins expressed on APCs, which are known to play a role in recognizing viral capsids[300, 363, 364]. In this regard, in chapter four we have proposed that the highly repetitive surfaces of VLPs may engage B cell receptors[295-298], which has been extensively described for other particles[295, 362, 377], and furthermore such engagement is known to be highly potent—possessing the ability to break self-tolerance without co-stimulation or adjuvant[297, 378].

Differential Functions of iBALT?

As described in chapter two, numerous inhaled exacerbants may incite the organization and formation of iBALT. It remains unclear however, how the formation, existence, and maintenance of iBALT may differentially contribute to the resolution of infection and the promotion of disease in autoimmunity and cancer. Whereas in influenza virus infection local iBALT-resident B cells produce flu-specific antibodies and provide a

less damaging response than is observed in mice lacking iBALT, in Rheumatoid arthritis (RA) patients local B cells produce anti–cyclic citrullinated peptide (anti-CCP) antibodies, contributing to pulmonary pathology[209]. In both cases however, similar architecture, cellular constituents, and organizational patterns are observed. Furthermore, it appears that the formation and homeostasis of tertiary lymphoid organs (including those found in sites other than the lung) equally rely on the expression CXCL13, CCL19, CCL21, and LT-α[6, 235-240]. Thus, the function of iBALT in different disease states must be differentially governed, and apparently, this is independent of the expression and functions of organizational/homeostatic chemokines. Understanding these mechanisms may provide clinical insight.

Governance of Trafficking

The mechanisms that govern the trafficking to DC's and AM's from peripheral sites (the lung) to the local lymph nodes are well established and include the upregulation of CCR7 on APC's which thus allow for the homing towards CCL19 and CCL21. It remains unknown whether DC's and AM's which have taken up antigen in the airways may migrate to areas of iBALT instead of to the TBLN. Moreover, the signaling mechanisms required for these cells to preferentially pick one homing location over the other also remain elusive. It is known that areas of iBALT in both humans and mice have an increased expression of CCL19 and CCL21[6, 209, 240]. Thus, it could be hypothesized that APC's may equally migrate from the lung to the lymph node as well as from the lung airways into areas of iBALT. It could also be hypothesized that these two sites compete for APC entry, and that perhaps the concentration of the chemokine gradients established

by the iBALT and the lymph node dictate the migration patterns. In this regard, it remains unknown whether the lymphatic vessels found in the areas of iBALT are afferent or efferent. Thus, the factors controlling the differential trafficking of APC's must be determined to understand how iBALT impacts an immune response in the presence of intact secondary lymphoid tissues.

Regulatory Mechanisms

Pulmonary immunity requires that tightly regulated responses occur to achieve the clearance of the pathogen while maintaining pulmonary function. In our above-described studies we have detailed how VLP-exposure of the lungs elicits a more controlled immune response to a subsequent influenza challenge. We find that both innate and adaptive immune responses are heightened at very early timepoints after viral challenge, and furthermore that these responses are turned off quickly thereafter. Thus, we assume that regulatory mechanisms must be mitigating collateral damage and the timing of the responses. In preliminary studies we have begun to evaluate the contributions of both $CD4^+CD25^+Foxp3^+$ and $CD8^+CD122^+$ Treg cells (results not shown). We have found that VLP-exposed mice have a higher prevalence of both $CD4^+$ and $CD8^+$ Treg populations in both their lungs and TBLNs. Importantly, when we purified the $CD4^+CD25^+Foxp3^+$ Tregs from the lungs of VLP-exposed mice, adoptively transferred them to naïve mice, and infected these mice with high-dose influenza virus, we found that these mice were protected from influenza-associated weight loss, whereas an adoptive transfer of Tregs isolated from control mice did not exert similar effects (results not shown). Thus, we hypothesize that $CD4^+CD25^+FoxP3^+$ Treg function represents an important component of

the observed regulation in VLP-exposed mice. Tellingly, Tsuji *et al.* have shown that $CD4^+Foxp3^+$ Tregs can become T_{FH} cells in Peyer's patches[243], and Kocks *et al.* have shown Tregs regulate the formation of iBALT[210]. Future avenues for this work will include the evaluation of cell-to-cell interactions that provide regulatory functions, as well as a determination of the important cytokines produced in each scenario.

We have also begun to evaluate the role for innate lymphoid cells (ILCs) in the lungs and TBLNs of VLP-exposed mice and find that whereas ILCs are more prevalent in the TBLNs of VLP-exposed mice, we detect a higher concentration of the damage repair protein, amphiregulin, in the lavage fluid of control mice (results not shown). This result may be dependent upon the viral load, and as we have established that VLP-exposed mice intrinsically show a reduced level of collateral damage, the contributions of ILCs may be more significant during early timpoints of infection when the viral load is similar between groups.

iBALT-Independent Immune Mechanisms

Whereas the work detailed here focuses on the iBALT-dependent immune responses to the influenza virus after the exposure of the lungs to VLPs, other evidence from our lab indicates that upon pulmonary challenge with methicillin-resistant *Staphylococcus aureus* (MRSA) VLP-elicited immunity is not reliant on iBALT[265]. Similarly to the influenza work, however $CD11c^+$ cells were necessary for bacterial clearance (as well as Ly-$6G^+$ cells). Thus, common threads of innate immune enhancements significantly impact pulmonary immunity regardless of the pathogen's identity. It has been suggested by others that the exposure to a respiratory pathogen

impacts the pulmonary epithelium[7], endothelium[383, 384], and lymphatics to provide lasting alterations in future responsiveness[7], but it remains unknown whether a newly remodeled pulmonary mucosa can "remember". Finally, Lukacs-Kornek *et al.* have reported that pulmonary stromal cells may provide suppression of T cell proliferation via cytokine secretion[385], and such mechanisms may be very important in regulating tertiary lymphoid tissues[386].

Illustrative Mechanism

The culmination of these results and conclusions are illustrated in the below diagram (Figure 5.1) in which our studies have filled in the gaps in the literature related to innate imprinting in the lung. While many of the items indicated here have been experimentally determined, we have also conservatively speculated about the players involved in our observed results, as indicated in the text.

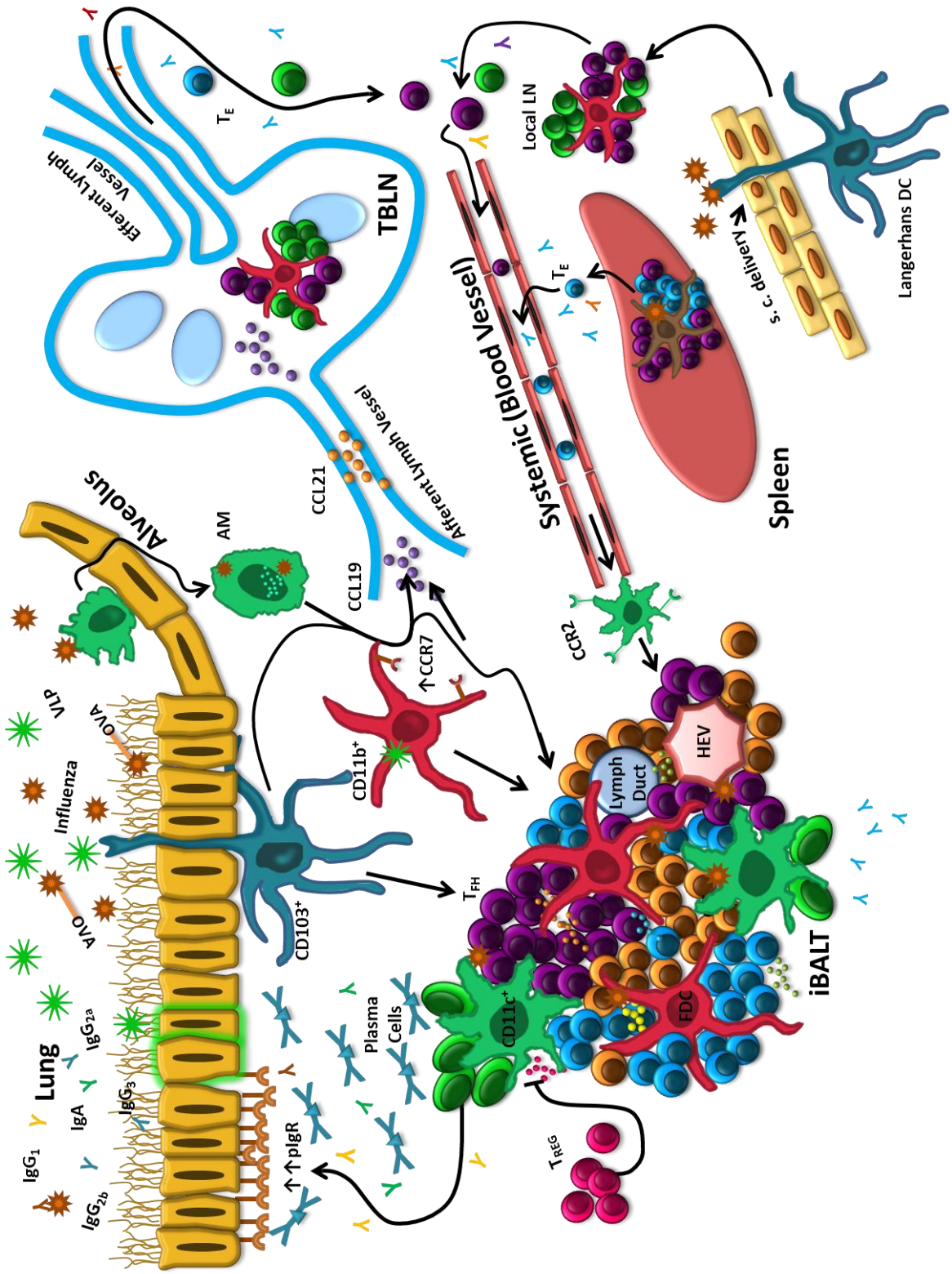

Lung
Alveolus
AM
CCL21
CCL19
Afferent Lymph Vessel
Efferent Lymph Vessel
TBLN
Systemic (Blood Vessel)
Local LN
Spleen
s. c. delivery
Langerhans DC
CCR2
CCR7
CD11b+
CD103+
CD11c+
Lymph Duct
HEV
FDC
iBALT
Plasma Cells
pIgR
IgG1
IgG2b
IgA
IgG3
IgG2a
Influenza
OVA
OVA
VLP
TE
TFH
TREG

Figure 5.1-Continued. Mechanism of dissertation. In the lung, antigen (shown here as virus, VLPs, or OVA-conjugated to VLPs) is inhaled and is taken up by epithelial cells, dendritic cells (either $CD103^+$ or $CD11b^+$), and alveolar macrophages. Both dendritic cells and macrophages will upregulate CCR7 and thus react to a chemokine gradient of CCL19 and CCL21 which percolates from the lymph node to the lung via lymph vessels. Alternatively, we conjecture that DC's and AM's may equally migrate into areas of iBALT, although the signaling governing these events are unknown.

Within the TBLN, antigen-bearing DC's and AM's present antigen to naïve T cells, which initiate adaptive immune responses including the generation of $T_{effector}$ (T_e) cells as well as antibody. These cells will traffick back to the lung via the blood stream, entering iBALT areas via high endothelial venules (HEV's). For those APC's that migrated directly from the airways into iBALT areas, much of the following interactions are still undefined. We hypothesize that these $CD11c^+$ cells establish themselves in the iBALT similarly as they would in the TBLN. Thus, they may interact with naïve T cells and further facilitate germinal center reactions. In this regard, we have shown that iBALT does in fact contain T_{FH} cells[224]. Such local reactions require much less trafficking, and therefore adaptive immune responses such as activated T cells and the production of antibody are detectable days ahead of those cells which traveled to the lymph node.

iBALT areas appear to be regulated by T regulatory cells (T_{reg}) of both $CD4^+$ and $CD8^+$ subtypes. As plasma cells are generated in iBALT areas, their antibodies can be detected in the serum and lavage fluid much earlier than the lymph node counterparts.

Polymeric IgA receptors (pIgR) are highly upregulated on the basolateral surface of the airway epithelium, which facilitates the transport of dimeric IgA to the luminal surface of the lung. The reason for pIgR upregulation remains unknown.

During an immune response in the lung, macrophage/dendritic cell progenitors migrate from the bone marrow through the blood stream to the site of infection in order to repopulate dead and dying APCs. One common progenitor, which expresses Ly-6C and CCR2, may equally differentiate into AM's and pulmonary DC's. As such, CCR2-dependent trafficking is essential to viral clearance, and is especially important in the enhancements of VLP-exposed lungs.

When an antigen is delivered subcutaneously (s.c.), Langerhans cells (LC's) serve similar functions as is observed for lung DC's. LC's which have taken up the delivered antigen will migrate to the local lymph node in which it will present antigen to naïve T cells, and elicit the production of antibody. Activated T cells and secreted antibody will then migrate to the site of infection via the bloodstream, as described for the TBLN.

Finally, the spleen is also involved in immunity both with and without prior VLP-exposure. We do know that the VLPs have some effects on the spleen, as the spleens of mice which had been previously exposed to VLPs better supported the proliferation and activation of influenza-specific $CD4^+$ T cells experimentally. Taken together, iBALT provides an additional avenue for pulmonary immunity, and thus immune responses in a primed lung are privy to additional options for trafficking, thus providing an accelerated rate of pathogen clearance without eliciting collateral damage.

REFERENCES

1. Roman, E. et al. CD4 effector T cell subsets in the response to influenza: heterogeneity, migration, and function. *J Exp Med* **196**, 957-68 (2002).

2. Moyron-Quiroz, J.E. et al. Persistence and responsiveness of immunologic memory in the absence of secondary lymphoid organs. *Immunity* **25**, 643-54 (2006).

3. Young, F. & Marra, F. A systematic review of intradermal influenza vaccines. *Vaccine* **29**, 8788-801 (2011).

4. Tosh, P.K., Boyce, T.G. & Poland, G.A. Flu myths: dispelling the myths associated with live attenuated influenza vaccine. *Mayo Clin Proc* **83**, 77-84 (2008).

5. Carter, N.J. & Curran, M.P. Live attenuated influenza vaccine (FluMist(R); Fluenz): a review of its use in the prevention of seasonal influenza in children and adults. *Drugs* **71**, 1591-622 (2011).

6. Moyron-Quiroz, J.E. et al. Role of inducible bronchus associated lymphoid tissue (iBALT) in respiratory immunity. *Nat Med* **10**, 927-34 (2004).

7. Goulding, J. et al. Respiratory infections: do we ever recover? *Proc Am Thorac Soc* **4**, 618-25 (2007).

8. Clark, N.M. & Lynch, J.P., 3rd. Influenza: epidemiology, clinical features, therapy, and prevention. *Semin Respir Crit Care Med* **32**, 373-92 (2011).

9. Kobasa, D. et al. Enhanced virulence of influenza A viruses with the haemagglutinin of the 1918 pandemic virus. *Nature* **431**, 703-7 (2004).

10. Muller, K.H. et al. Emerging cellular targets for influenza antiviral agents. *Trends Pharmacol Sci* **33**, 89-99 (2011).

11. Jagger, B.W. et al. An overlapping protein-coding region in influenza A virus segment 3 modulates the host response. *Science* **337**, 199-204 (2012).

12. Fields, B.N., Knipe, D.M. & Howley, P.M. Fields virology (Wolters Kluwer Health/Lippincott Williams & Wilkins, Philadelphia, 2007).

13. Fouchier, R.A. et al. Characterization of a novel influenza A virus hemagglutinin subtype (H16) obtained from black-headed gulls. *J Virol* **79**, 2814-22 (2005).

14. Petric, M., Comanor, L. & Petti, C.A. Role of the laboratory in diagnosis of influenza during seasonal epidemics and potential pandemics. *J Infect Dis* **194 Suppl 2**, S98-110 (2006).

15. Fukuyama, S. & Kawaoka, Y. The pathogenesis of influenza virus infections: the contributions of virus and host factors. *Curr Opin Immunol* **23**, 481-6 (2011).

16. Tumpey, T.M. et al. Pathogenicity of influenza viruses with genes from the 1918 pandemic virus: functional roles of alveolar macrophages and neutrophils in limiting virus replication and mortality in mice. *J Virol* **79**, 14933-44 (2005).

17. Rossman, J.S. & Lamb, R.A. Influenza virus assembly and budding. *Virology* **411**, 229-36 (2011).

18. Keawcharoen, J. et al. Avian influenza H5N1 in tigers and leopards. *Emerg Infect Dis* **10**, 2189-91 (2004).

19. Webster, R.G., Bean, W.J., Gorman, O.T., Chambers, T.M. & Kawaoka, Y. Evolution and ecology of influenza A viruses. *Microbiol Rev* **56**, 152-79 (1992).

20. Watanabe, Y., Ibrahim, M.S., Suzuki, Y. & Ikuta, K. The changing nature of avian influenza A virus (H5N1). *Trends Microbiol* **20**, 11-20 (2012).

21. Ito, T. & Kawaoka, Y. Host-range barrier of influenza A viruses. *Vet Microbiol* **74**, 71-5 (2000).

22. Rogers, G.N. & Paulson, J.C. Receptor determinants of human and animal influenza virus isolates: differences in receptor specificity of the H3 hemagglutinin based on species of origin. *Virology* **127**, 361-73 (1983).

23. Medina, R.A. & Garcia-Sastre, A. Influenza A viruses: new research developments. *Nat Rev Microbiol* **9**, 590-603 (2011).

24. Matrosovich, M.N., Matrosovich, T.Y., Gray, T., Roberts, N.A. & Klenk, H.D. Human and avian influenza viruses target different cell types in cultures of human airway epithelium. *Proc Natl Acad Sci U S A* **101**, 4620-4 (2004).

25. Ito, T. et al. Molecular basis for the generation in pigs of influenza A viruses with pandemic potential. *J Virol* **72**, 7367-73 (1998).

26. Murphy, B.R. et al. Reassortant virus derived from avian and human influenza A viruses is attenuated and immunogenic in monkeys. *Science* **218**, 1330-2 (1982).

27. Beare, A.S. & Webster, R.G. Replication of avian influenza viruses in humans. *Arch Virol* **119**, 37-42 (1991).

28. Hinshaw, V.S., Webster, R.G., Naeve, C.W. & Murphy, B.R. Altered tissue tropism of human-avian reassortant influenza viruses. *Virology* **128**, 260-3 (1983).

29. Kida, H. et al. Potential for transmission of avian influenza viruses to pigs. *J Gen Virol* **75 (Pt 9)**, 2183-8 (1994).

30. Hinshaw, V.S., Webster, R.G., Easterday, B.C. & Bean, W.J., Jr. Replication of avian influenza A viruses in mammals. *Infect Immun* **34**, 354-61 (1981).

31. Sriwilaijaroen, N. et al. N-glycans from porcine trachea and lung: predominant NeuAcalpha2-6Gal could be a selective pressure for influenza variants in favor of human-type receptor. *PLoS One* **6**, e16302 (2011).

32. Suzuki, Y. Sialobiology of influenza: molecular mechanism of host range variation of influenza viruses. *Biol Pharm Bull* **28**, 399-408 (2005).

33. Holland, J. et al. Rapid evolution of RNA genomes. *Science* **215**, 1577-85 (1982).

34. Steinhauer, D.A. & Holland, J.J. Rapid evolution of RNA viruses. *Annu Rev Microbiol* **41**, 409-33 (1987).

35. Han, T. & Marasco, W.A. Structural basis of influenza virus neutralization. *Ann N Y Acad Sci* **1217**, 178-90 (2011).

36. Scholtissek, C., Burger, H., Kistner, O. & Shortridge, K.F. The nucleoprotein as a possible major factor in determining host specificity of influenza H3N2 viruses. *Virology* **147**, 287-94 (1985).

37. Castrucci, M.R. et al. Genetic reassortment between avian and human influenza A viruses in Italian pigs. *Virology* **193**, 503-6 (1993).

38. Claas, E.C., Kawaoka, Y., de Jong, J.C., Masurel, N. & Webster, R.G. Infection of children with avian-human reassortant influenza virus from pigs in Europe. *Virology* **204**, 453-7 (1994).

39. Thompson, W.W. et al. Mortality associated with influenza and respiratory syncytial virus in the United States. *JAMA* **289**, 179-86 (2003).

40. Hancock, K. et al. Cross-reactive antibody responses to the 2009 pandemic H1N1 influenza virus. *N Engl J Med* **361**, 1945-52 (2009).

41. Cooper, C.L. Pandemic H1N12009 influenza and HIV: a review of natural history, management and vaccine immunogenicity. *Curr Opin Infect Dis* **25**, 26-35 (2012).

42. Cox, N.J. & Subbarao, K. Influenza. *Lancet* **354**, 1277-82 (1999).

43. (CDC), C.f.D.C.a.P. Deaths related to 2009 pandemic influenza A (H1N1) among American Indian/Alaska Natives - 12 states, 2009. *MMWR Morb Mortal Wkly Rep* **58**, 1341-4 (2009).

44. Jain, S. et al. Hospitalized Patients with 2009 H1N1 Influenza in the United States, April-June 2009. *New England Journal of Medicine* **361**, 1935-1944 (2009).

45. Fiore, A.E. et al. Antiviral agents for the treatment and chemoprophylaxis of influenza --- recommendations of the Advisory Committee on Immunization Practices (ACIP). *MMWR Recomm Rep* **60**, 1-24 (2011).

46. Brankston, G., Gitterman, L., Hirji, Z., Lemieux, C. & Gardam, M. Transmission of influenza A in human beings. *Lancet Infect Dis* **7**, 257-65 (2007).

47. Moltedo, B. et al. Cutting edge: stealth influenza virus replication precedes the initiation of adaptive immunity. *J Immunol* **183**, 3569-73 (2009).

48. O'Brien, K.L. et al. Severe pneumococcal pneumonia in previously healthy children: the role of preceding influenza infection. *Clin Infect Dis* **30**, 784-9 (2000).

49. Mandell, G.L., Bennett, J.E. & Dolin, R. Mandell, Douglas, and Bennett's principles and practice of infectious diseases (Churchill Livingstone/Elsevier, Philadelphia, PA).

50. Fainstein, V., Musher, D.M. & Cate, T.R. Bacterial adherence to pharyngeal cells during viral infection. *J Infect Dis* **141**, 172-6 (1980).

51. Reid, A.H., Fanning, T.G., Hultin, J.V. & Taubenberger, J.K. Origin and evolution of the 1918 "Spanish" influenza virus hemagglutinin gene. *Proc Natl Acad Sci U S A* **96**, 1651-6 (1999).

52. Watanabe, T. & Kawaoka, Y. Pathogenesis of the 1918 pandemic influenza virus. *PLoS Pathog* **7**, e1001218.

53. Murray, C.J., Lopez, A.D., Chin, B., Feehan, D. & Hill, K.H. Estimation of potential global pandemic influenza mortality on the basis of vital registry data from the 1918-20 pandemic: a quantitative analysis. *Lancet* **368**, 2211-8 (2006).

54. Basler, C.F. et al. Sequence of the 1918 pandemic influenza virus nonstructural gene (NS) segment and characterization of recombinant viruses bearing the 1918 NS genes. *Proc Natl Acad Sci U S A* **98**, 2746-51 (2001).

55. Reid, A.H., Fanning, T.G., Janczewski, T.A., Lourens, R.M. & Taubenberger, J.K. Novel origin of the 1918 pandemic influenza virus nucleoprotein gene. *J Virol* **78**, 12462-70 (2004).

56. Reid, A.H., Fanning, T.G., Janczewski, T.A., McCall, S. & Taubenberger, J.K. Characterization of the 1918 "Spanish" influenza virus matrix gene segment. *J Virol* **76**, 10717-23 (2002).

57. Taubenberger, J.K., Reid, A.H., Krafft, A.E., Bijwaard, K.E. & Fanning, T.G. Initial genetic characterization of the 1918 "Spanish" influenza virus. *Science* **275**, 1793-6 (1997).

58. Taubenberger, J.K. et al. Characterization of the 1918 influenza virus polymerase genes. *Nature* **437**, 889-93 (2005).

59. Taubenberger, J.K., Reid, A.H., Janczewski, T.A. & Fanning, T.G. Integrating historical, clinical and molecular genetic data in order to explain the origin and virulence of the 1918 Spanish influenza virus. *Philos Trans R Soc Lond B Biol Sci* **356**, 1829-39 (2001).

60. Kobasa, D. et al. Aberrant innate immune response in lethal infection of macaques with the 1918 influenza virus. *Nature* **445**, 319-23 (2007).

61. Smith, G.J. et al. Origins and evolutionary genomics of the 2009 swine-origin H1N1 influenza A epidemic. *Nature* **459**, 1122-5 (2009).

62. Xu, X., Subbarao, Cox, N.J. & Guo, Y. Genetic characterization of the pathogenic influenza A/Goose/Guangdong/1/96 (H5N1) virus: similarity of its hemagglutinin gene to those of H5N1 viruses from the 1997 outbreaks in Hong Kong. *Virology* **261**, 15-9 (1999).

63. Steel, J., Lowen, A.C., Mubareka, S. & Palese, P. Transmission of influenza virus in a mammalian host is increased by PB2 amino acids 627K or 627E/701N. *PLoS Pathog* **5**, e1000252 (2009).

64. Maines, T.R. et al. Lack of transmission of H5N1 avian-human reassortant influenza viruses in a ferret model. *Proc Natl Acad Sci U S A* **103**, 12121-6 (2006).

65. Peiris, J.S., de Jong, M.D. & Guan, Y. Avian influenza virus (H5N1): a threat to human health. *Clin Microbiol Rev* **20**, 243-67 (2007).

66. Swayne, D.E. & Kapczynski, D. Strategies and challenges for eliciting immunity against avian influenza virus in birds. *Immunol Rev* **225**, 314-31 (2008).

67. Gerdil, C. The annual production cycle for influenza vaccine. *Vaccine* **21**, 1776-9 (2003).

68. CDC. General recommendations on immunization --- recommendations of the Advisory Committee on Immunization Practices (ACIP). *MMWR Recomm Rep* **60**, 1-64 (2011).

69. Buonagurio, D.A. et al. Genetic stability of live, cold-adapted influenza virus components of the FluMist/CAIV-T vaccine throughout the manufacturing process. *Vaccine* **24**, 2151-60 (2006).

70. Boyce, T.G. et al. Mucosal immune response to trivalent live attenuated intranasal influenza vaccine in children. *Vaccine* **18**, 82-8 (1999).

71. He, X.S. et al. Cellular immune responses in children and adults receiving inactivated or live attenuated influenza vaccines. *J Virol* **80**, 11756-66 (2006).

72. Forrest, B.D. et al. Correlation of cellular immune responses with protection against culture-confirmed influenza virus in young children. *Clin Vaccine Immunol* **15**, 1042-53 (2008).

73. Monto, A.S. et al. Comparative efficacy of inactivated and live attenuated influenza vaccines. *N Engl J Med* **361**, 1260-7 (2009).

74. Moscona, A. Neuraminidase inhibitors for influenza. *N Engl J Med* **353**, 1363-73 (2005).

75. Couch, R.B. Prevention and treatment of influenza. *N Engl J Med* **343**, 1778-87 (2000).

76. Wang, C., Takeuchi, K., Pinto, L.H. & Lamb, R.A. Ion channel activity of influenza A virus M2 protein: characterization of the amantadine block. *J Virol* **67**, 5585-94 (1993).

77. CDC. Update: influenza activity - United States, 2009-10 season. *MMWR Morb Mortal Wkly Rep* **59**, 901-8 (2010).

78. McGeer, A. et al. Antiviral therapy and outcomes of influenza requiring hospitalization in Ontario, Canada. *Clinical Infectious Diseases* **45**, 1568-1575 (2007).

79. Yen, H.L. et al. Neuraminidase inhibitor-resistant influenza viruses may differ substantially in fitness and transmissibility. *Antimicrob Agents Chemother* **49**, 4075-84 (2005).

80. Ujike, M. et al. Oseltamivir-resistant influenza viruses A (H1N1) during 2007-2009 influenza seasons, Japan. *Emerg Infect Dis* **16**, 926-35 (2010).

81. Baz, M. et al. Emergence of oseltamivir-resistant pandemic H1N1 virus during prophylaxis. *N Engl J Med* **361**, 2296-7 (2009).

82. Le, Q.M. et al. A community cluster of oseltamivir-resistant cases of 2009 H1N1 influenza. *N Engl J Med* **362**, 86-7 (2010).

83. van der Vries, E., Schutten, M. & Boucher, C.A. The potential for multidrug-resistant influenza. *Curr Opin Infect Dis* **24**, 599-604 (2011).

84. Hurt, A.C. et al. Antiviral resistance during the 2009 influenza A H1N1 pandemic: public health, laboratory, and clinical perspectives. *Lancet Infect Dis* **12**, 240-8 (2012).

85. Ariki, S., Nishitani, C. & Kuroki, Y. Diverse functions of pulmonary collectins in host defense of the lung. *J Biomed Biotechnol* **2012**, 532071 (2012).

86. Hicks, J.T., Ennis, F.A., Kim, E. & Verbonitz, M. The importance of an intact complement pathway in recovery from a primary viral infection: influenza in decomplemented and in C5-deficient mice. *J Immunol* **121**, 1437-45 (1978).

87. Kopf, M., Abel, B., Gallimore, A., Carroll, M. & Bachmann, M.F. Complement component C3 promotes T-cell priming and lung migration to control acute influenza virus infection. *Nat Med* **8**, 373-8 (2002).

88. GeurtsvanKessel, C.H. & Lambrecht, B.N. Division of labor between dendritic cell subsets of the lung. *Mucosal Immunol* **1**, 442-50 (2008).

89. GeurtsvanKessel, C.H. et al. Clearance of influenza virus from the lung depends on migratory langerin+CD11b- but not plasmacytoid dendritic cells. *J Exp Med* **205**, 1621-34 (2008).

90. Moltedo, B., Li, W., Yount, J.S. & Moran, T.M. Unique type I interferon responses determine the functional fate of migratory lung dendritic cells during influenza virus infection. *PLoS Pathog* **7**, e1002345 (2011).

91. Chandran, S.S., Verhoeven, D., Teijaro, J.R., Fenton, M.J. & Farber, D.L. TLR2 engagement on dendritic cells promotes high frequency effector and memory CD4 T cell responses. *J Immunol* **183**, 7832-41 (2009).

92. Mogensen, T.H. Pathogen recognition and inflammatory signaling in innate immune defenses. *Clin Microbiol Rev* **22**, 240-73, Table of Contents (2009).

93. Ichinohe, T., Lee, H.K., Ogura, Y., Flavell, R. & Iwasaki, A. Inflammasome recognition of influenza virus is essential for adaptive immune responses. *J Exp Med* **206**, 79-87 (2009).

94. Diebold, S.S., Kaisho, T., Hemmi, H., Akira, S. & Reis e Sousa, C. Innate antiviral responses by means of TLR7-mediated recognition of single-stranded RNA. *Science* **303**, 1529-31 (2004).

95. Pichlmair, A. et al. RIG-I-mediated antiviral responses to single-stranded RNA bearing 5'-phosphates. *Science* **314**, 997-1001 (2006).

96. Kawai, T. & Akira, S. Toll-like receptor and RIG-I-like receptor signaling. *Ann N Y Acad Sci* **1143**, 1-20 (2008).

97. Takeuchi, O. & Akira, S. Innate immunity to virus infection. *Immunol Rev* **227**, 75-86 (2009).

98. Perrone, L.A., Plowden, J.K., Garcia-Sastre, A., Katz, J.M. & Tumpey, T.M. H5N1 and 1918 pandemic influenza virus infection results in early and excessive infiltration of macrophages and neutrophils in the lungs of mice. *PLoS Pathog* **4**, e1000115 (2008).

99. Kato, H. et al. Cell type-specific involvement of RIG-I in antiviral response. *Immunity* **23**, 19-28 (2005).

100. Kato, H. et al. Differential roles of MDA5 and RIG-I helicases in the recognition of RNA viruses. *Nature* **441**, 101-5 (2006).

101. Akira, S., Uematsu, S. & Takeuchi, O. Pathogen recognition and innate immunity. *Cell* **124**, 783-801 (2006).

102. Mogensen, T.H. & Paludan, S.R. Reading the viral signature by Toll-like receptors and other pattern recognition receptors. *J Mol Med (Berl)* **83**, 180-92 (2005).

103. Martinon, F., Mayor, A. & Tschopp, J. The inflammasomes: guardians of the body. *Annu Rev Immunol* **27**, 229-65 (2009).

104. Kanneganti, T.D. et al. Critical role for Cryopyrin/Nalp3 in activation of caspase-1 in response to viral infection and double-stranded RNA. *J Biol Chem* **281**, 36560-8 (2006).

105. Allen, I.C. et al. The NLRP3 inflammasome mediates in vivo innate immunity to influenza A virus through recognition of viral RNA. *Immunity* **30**, 556-65 (2009).

106. Thomas, P.G. et al. The intracellular sensor NLRP3 mediates key innate and healing responses to influenza A virus via the regulation of caspase-1. *Immunity* **30**, 566-75 (2009).

107. Ichinohe, T., Pang, I.K. & Iwasaki, A. Influenza virus activates inflammasomes via its intracellular M2 ion channel. *Nat Immunol* **11**, 404-10 (2010).

108. Colonna, M., Trinchieri, G. & Liu, Y.J. Plasmacytoid dendritic cells in immunity. *Nat Immunol* **5**, 1219-26 (2004).

109. Ballesteros-Tato, A., Leon, B., Lund, F.E. & Randall, T.D. Temporal changes in dendritic cell subsets, cross-priming and costimulation via CD70 control CD8(+) T cell responses to influenza. *Nat Immunol* **11**, 216-24 (2010).

110. Hao, X., Kim, T.S. & Braciale, T.J. Differential response of respiratory dendritic cell subsets to influenza virus infection. *J Virol* **82**, 4908-19 (2008).

111. Sung, S.S. et al. A major lung CD103 (alphaE)-beta7 integrin-positive epithelial dendritic cell population expressing Langerin and tight junction proteins. *J Immunol* **176**, 2161-72 (2006).

112. Stevens, W.W., Kim, T.S., Pujanauski, L.M., Hao, X. & Braciale, T.J. Detection and quantitation of eosinophils in the murine respiratory tract by flow cytometry. *J Immunol Methods* **327**, 63-74 (2007).

113. Beaty, S.R., Rose, C.E., Jr. & Sung, S.S. Diverse and potent chemokine production by lung CD11bhigh dendritic cells in homeostasis and in allergic lung inflammation. *J Immunol* **178**, 1882-95 (2007).

114. Vermaelen, K.Y., Carro-Muino, I., Lambrecht, B.N. & Pauwels, R.A. Specific migratory dendritic cells rapidly transport antigen from the airways to the thoracic lymph nodes. *J Exp Med* **193**, 51-60 (2001).

115. Kim, T.S. & Braciale, T.J. Respiratory dendritic cell subsets differ in their capacity to support the induction of virus-specific cytotoxic CD8+ T cell responses. *PLoS One* **4**, e4204 (2009).

116. Randolph, G.J., Sanchez-Schmitz, G. & Angeli, V. Factors and signals that govern the migration of dendritic cells via lymphatics: recent advances. *Springer Semin Immunopathol* **26**, 273-87 (2005).

117. MartIn-Fontecha, A. et al. Regulation of dendritic cell migration to the draining lymph node: impact on T lymphocyte traffic and priming. *J Exp Med* **198**, 615-21 (2003).

118. Randolph, G.J., Angeli, V. & Swartz, M.A. Dendritic-cell trafficking to lymph nodes through lymphatic vessels. *Nat Rev Immunol* **5**, 617-28 (2005).

119. McGill, J., Van Rooijen, N. & Legge, K.L. Protective influenza-specific CD8 T cell responses require interactions with dendritic cells in the lungs. *J Exp Med* **205**, 1635-46 (2008).

120. del Rio, M.L., Rodriguez-Barbosa, J.I., Kremmer, E. & Forster, R. CD103- and CD103+ bronchial lymph node dendritic cells are specialized in presenting and cross-presenting innocuous antigen to CD4+ and CD8+ T cells. *J Immunol* **178**, 6861-6 (2007).

121. Lawrence, C.W. & Braciale, T.J. Activation, differentiation, and migration of naive virus-specific CD8+ T cells during pulmonary influenza virus infection. *J Immunol* **173**, 1209-18 (2004).

122. Lambrecht, B.N. & Hammad, H. Lung dendritic cells in respiratory viral infection and asthma: from protection to immunopathology. *Annu Rev Immunol* **30**, 243-70 (2012).

123. Furuhashi, K. et al. Mouse lung CD103+ and CD11bhigh dendritic cells preferentially induce distinct CD4+ T-cell responses. *Am J Respir Cell Mol Biol* **46**, 165-72 (2012).

124. Desch, A.N. et al. CD103+ pulmonary dendritic cells preferentially acquire and present apoptotic cell-associated antigen. *J Exp Med* **208**, 1789-97 (2011).

125. Ho, A.W. et al. Lung CD103+ dendritic cells efficiently transport influenza virus to the lymph node and load viral antigen onto MHC class I for presentation to CD8 T cells. *J Immunol* **187**, 6011-21 (2011).

126. McGill, J., Heusel, J.W. & Legge, K.L. Innate immune control and regulation of influenza virus infections. *J Leukoc Biol* **86**, 803-12 (2009).

127. Kirby, A.C., Coles, M.C. & Kaye, P.M. Alveolar macrophages transport pathogens to lung draining lymph nodes. *J Immunol* **183**, 1983-9 (2009).

128. Harmsen, A.G., Muggenburg, B.A., Snipes, M.B. & Bice, D.E. The role of macrophages in particle translocation from lungs to lymph nodes. *Science* **230**, 1277-80 (1985).

129. Serbina, N.V., Salazar-Mather, T.P., Biron, C.A., Kuziel, W.A. & Pamer, E.G. TNF/iNOS-producing dendritic cells mediate innate immune defense against bacterial infection. *Immunity* **19**, 59-70 (2003).

130. Serbina, N.V. & Pamer, E.G. Monocyte emigration from bone marrow during bacterial infection requires signals mediated by chemokine receptor CCR2. *Nat Immunol* **7**, 311-7 (2006).

131. Osterholzer, J.J. et al. Accumulation of CD11b+ lung dendritic cells in response to fungal infection results from the CCR2-mediated recruitment and differentiation of Ly-6Chigh monocytes. *J Immunol* **183**, 8044-53 (2009).

132. Dominguez, P.M. & Ardavin, C. Differentiation and function of mouse monocyte-derived dendritic cells in steady state and inflammation. *Immunol Rev* **234**, 90-104 (2010).

133. Lin, K.L., Suzuki, Y., Nakano, H., Ramsburg, E. & Gunn, M.D. CCR2+ monocyte-derived dendritic cells and exudate macrophages produce influenza-induced pulmonary immune pathology and mortality. *J Immunol* **180**, 2562-72 (2008).

134. Nakano, H. et al. Blood-derived inflammatory dendritic cells in lymph nodes stimulate acute T helper type 1 immune responses. *Nat Immunol* **10**, 394-402 (2009).

135. Herold, S. et al. Lung epithelial apoptosis in influenza virus pneumonia: the role of macrophage-expressed TNF-related apoptosis-inducing ligand. *J Exp Med* **205**, 3065-77 (2008).

136. Zhu, B. et al. Plasticity of Ly-6C(hi) myeloid cells in T cell regulation. *J Immunol* **187**, 2418-32 (2011).

137. Fei, M. et al. TNF-alpha from inflammatory dendritic cells (DCs) regulates lung IL-17A/IL-5 levels and neutrophilia versus eosinophilia during persistent fungal infection. *Proc Natl Acad Sci U S A* **108**, 5360-5 (2011).

138. Iijima, N., Mattei, L.M. & Iwasaki, A. Recruited inflammatory monocytes stimulate antiviral Th1 immunity in infected tissue. *Proc Natl Acad Sci U S A* **108**, 284-9 (2011).

139. Aldridge, J.R., Jr. et al. TNF/iNOS-producing dendritic cells are the necessary evil of lethal influenza virus infection. *Proc Natl Acad Sci U S A* **106**, 5306-11 (2009).

140. De Santo, C. et al. Invariant NKT cells reduce the immunosuppressive activity of influenza A virus-induced myeloid-derived suppressor cells in mice and humans. *J Clin Invest* **118**, 4036-48 (2008).

141. Gabrilovich, D.I. et al. The terminology issue for myeloid-derived suppressor cells. *Cancer Res* **67**, 425; author reply 426 (2007).

142. Deshane, J. et al. Free radical-producing myeloid-derived regulatory cells: potent activators and suppressors of lung inflammation and airway hyperresponsiveness. *Mucosal Immunol* **4**, 503-18 (2011).

143. Landsman, L. & Jung, S. Lung macrophages serve as obligatory intermediate between blood monocytes and alveolar macrophages. *J Immunol* **179**, 3488-94 (2007).

144. Landsman, L., Varol, C. & Jung, S. Distinct differentiation potential of blood monocyte subsets in the lung. *J Immunol* **178**, 2000-7 (2007).

145. Auffray, C., Sieweke, M.H. & Geissmann, F. Blood monocytes: development, heterogeneity, and relationship with dendritic cells. *Annu Rev Immunol* **27**, 669-92 (2009).

146. Jakubzick, C. et al. Blood monocyte subsets differentially give rise to CD103+ and CD103- pulmonary dendritic cell populations. *J Immunol* **180**, 3019-27 (2008).

147. Tsou, C.L. et al. Critical roles for CCR2 and MCP-3 in monocyte mobilization from bone marrow and recruitment to inflammatory sites. *J Clin Invest* **117**, 902-9 (2007).

148. Peters, W. et al. Chemokine receptor 2 serves an early and essential role in resistance to Mycobacterium tuberculosis. *Proc Natl Acad Sci U S A* **98**, 7958-63 (2001).

149. Lin, K.L., Sweeney, S., Kang, B.D., Ramsburg, E. & Gunn, M.D. CCR2-antagonist prophylaxis reduces pulmonary immune pathology and markedly improves survival during influenza infection. *J Immunol* **186**, 508-15 (2011).

150. Sozzani, S. et al. Differential regulation of chemokine receptors during dendritic cell maturation: a model for their trafficking properties. *J Immunol* **161**, 1083-6 (1998).

151. Sallusto, F. & Lanzavecchia, A. Understanding dendritic cell and T-lymphocyte traffic through the analysis of chemokine receptor expression. *Immunol Rev* **177**, 134-40 (2000).

152. Pooley, J.L., Heath, W.R. & Shortman, K. Cutting edge: intravenous soluble antigen is presented to CD4 T cells by CD8- dendritic cells, but cross-presented to CD8 T cells by CD8+ dendritic cells. *J Immunol* **166**, 5327-30 (2001).

153. den Haan, J.M., Lehar, S.M. & Bevan, M.J. CD8(+) but not CD8(-) dendritic cells cross-prime cytotoxic T cells in vivo. *J Exp Med* **192**, 1685-96 (2000).

154. GeurtsvanKessel, C.H. et al. Both conventional and interferon killer dendritic cells have antigen-presenting capacity during influenza virus infection. *PLoS One* **4**, e7187 (2009).

155. Hargadon, K.M. et al. Major histocompatibility complex class II expression and hemagglutinin subtype influence the infectivity of type A influenza virus for respiratory dendritic cells. *J Virol* **85**, 11955-63 (2011).

156. von Andrian, U.H. & Mempel, T.R. Homing and cellular traffic in lymph nodes. *Nat Rev Immunol* **3**, 867-78 (2003).

157. von Andrian, U.H. & Mackay, C.R. T-cell function and migration. Two sides of the same coin. *N Engl J Med* **343**, 1020-34 (2000).

158. Butcher, E.C. & Picker, L.J. Lymphocyte homing and homeostasis. *Science* **272**, 60-6 (1996).

159. Heer, A.K., Harris, N.L., Kopf, M. & Marsland, B.J. CD4+ and CD8+ T cells exhibit differential requirements for CCR7-mediated antigen transport during influenza infection. *J Immunol* **181**, 6984-94 (2008).

160. Eichelberger, M., Allan, W., Zijlstra, M., Jaenisch, R. & Doherty, P.C. Clearance of influenza virus respiratory infection in mice lacking class I major histocompatibility complex-restricted CD8+ T cells. *J Exp Med* **174**, 875-80 (1991).

161. Allan, W., Tabi, Z., Cleary, A. & Doherty, P.C. Cellular events in the lymph node and lung of mice with influenza. Consequences of depleting CD4+ T cells. *J Immunol* **144**, 3980-6 (1990).

162. Graham, M.B. & Braciale, T.J. Resistance to and recovery from lethal influenza virus infection in B lymphocyte-deficient mice. *J Exp Med* **186**, 2063-8 (1997).

163. Kopf, M., Brombacher, F. & Bachmann, M.F. Role of IgM antibodies versus B cells in influenza virus-specific immunity. *Eur J Immunol* **32**, 2229-36 (2002).

164. Brincks, E.L., Katewa, A., Kucaba, T.A., Griffith, T.S. & Legge, K.L. CD8 T cells utilize TRAIL to control influenza virus infection. *J Immunol* **181**, 4918-25 (2008).

165. Hufford, M.M., Kim, T.S., Sun, J. & Braciale, T.J. Antiviral CD8+ T cell effector activities in situ are regulated by target cell type. *J Exp Med* **208**, 167-80 (2011).

166. Topham, D.J., Tripp, R.A. & Doherty, P.C. CD8+ T cells clear influenza virus by perforin or Fas-dependent processes. *J Immunol* **159**, 5197-200 (1997).

167. Braciale, T.J., Sun, J. & Kim, T.S. Regulating the adaptive immune response to respiratory virus infection. *Nat Rev Immunol* **12**, 295-305 (2012).

168. Sun, J., Madan, R., Karp, C.L. & Braciale, T.J. Effector T cells control lung inflammation during acute influenza virus infection by producing IL-10. *Nat Med* **15**, 277-84 (2009).

169. Sun, J., Dodd, H., Moser, E.K., Sharma, R. & Braciale, T.J. CD4+ T cell help and innate-derived IL-27 induce Blimp-1-dependent IL-10 production by antiviral CTLs. *Nat Immunol* **12**, 327-34 (2011).

170. Mozdzanowska, K., Furchner, M., Maiese, K. & Gerhard, W. CD4+ T cells are ineffective in clearing a pulmonary infection with influenza type A virus in the absence of B cells. *Virology* **239**, 217-25 (1997).

171. Mayer, K.D. et al. The functional heterogeneity of type 1 effector T cells in response to infection is related to the potential for IFN-gamma production. *J Immunol* **174**, 7732-9 (2005).

172. Coutelier, J.P., van der Logt, J.T., Heessen, F.W., Warnier, G. & Van Snick, J. IgG2a restriction of murine antibodies elicited by viral infections. *J Exp Med* **165**, 64-9 (1987).

173. Cousens, L.P. et al. Two roads diverged: interferon alpha/beta- and interleukin 12-mediated pathways in promoting T cell interferon gamma responses during viral infection. *J Exp Med* **189**, 1315-28 (1999).

174. Swain, S.L., McKinstry, K.K. & Strutt, T.M. Expanding roles for CD4(+) T cells in immunity to viruses. *Nat Rev Immunol* **12**, 136-48 (2012).

175. Brown, D.M., Dilzer, A.M., Meents, D.L. & Swain, S.L. CD4 T cell-mediated protection from lethal influenza: perforin and antibody-mediated mechanisms give a one-two punch. *J Immunol* **177**, 2888-98 (2006).

176. Brown, D.M., Lee, S., Garcia-Hernandez, M.D. & Swain, S.L. Multi-functional CD4 cells expressing IFN-gamma and perforin mediate protection against lethal influenza infection. *J Virol* (2012).

177. Brown, D.M., Kamperschroer, C., Dilzer, A.M., Roberts, D.M. & Swain, S.L. IL-2 and antigen dose differentially regulate perforin- and FasL-mediated cytolytic activity in antigen specific CD4+ T cells. *Cell Immunol* **257**, 69-79 (2009).

178. Bot, A. et al. Cellular mechanisms involved in protection and recovery from influenza virus infection in immunodeficient mice. *J Virol* **70**, 5668-72 (1996).

179. McKinstry, K.K. et al. IL-10 deficiency unleashes an influenza-specific Th17 response and enhances survival against high-dose challenge. *J Immunol* **182**, 7353-63 (2009).

180. MacLennan, I.C., Liu, Y.J. & Johnson, G.D. Maturation and dispersal of B-cell clones during T cell-dependent antibody responses. *Immunol Rev* **126**, 143-61 (1992).

181. Schaerli, P. et al. CXC chemokine receptor 5 expression defines follicular homing T cells with B cell helper function. *J Exp Med* **192**, 1553-62 (2000).

182. Breitfeld, D. et al. Follicular B helper T cells express CXC chemokine receptor 5, localize to B cell follicles, and support immunoglobulin production. *J Exp Med* **192**, 1545-52 (2000).

183. King, C. New insights into the differentiation and function of T follicular helper cells. *Nat Rev Immunol* **9**, 757-66 (2009).

184. Kaur, K., Sullivan, M. & Wilson, P.C. Targeting B cell responses in universal influenza vaccine design. *Trends Immunol* **32**, 524-31 (2011).

185. Corti, D. et al. Heterosubtypic neutralizing antibodies are produced by individuals immunized with a seasonal influenza vaccine. *J Clin Invest* **120**, 1663-73 (2010).

186. Wrammert, J. et al. Broadly cross-reactive antibodies dominate the human B cell response against 2009 pandemic H1N1 influenza virus infection. *J Exp Med* **208**, 181-93 (2011).

187. Wrammert, J. et al. Rapid cloning of high-affinity human monoclonal antibodies against influenza virus. *Nature* **453**, 667-71 (2008).

188. Monto, A.S. & Kendal, A.P. Effect of neuraminidase antibody on Hong Kong influenza. *Lancet* **1**, 623-5 (1973).

189. Corti, D. et al. A neutralizing antibody selected from plasma cells that binds to group 1 and group 2 influenza A hemagglutinins. *Science* **333**, 850-6 (2011).

190. Antunes, I. & Kassiotis, G. Suppression of innate immune pathology by regulatory T cells during Influenza A virus infection of immunodeficient mice. *J Virol* **84**, 12564-75 (2010).

191. Collison, L.W. et al. The inhibitory cytokine IL-35 contributes to regulatory T-cell function. *Nature* **450**, 566-9 (2007).

192. Neill, D.R. et al. Nuocytes represent a new innate effector leukocyte that mediates type-2 immunity. *Nature* **464**, 1367-70 (2010).

193. Spits, H. & Di Santo, J.P. The expanding family of innate lymphoid cells: regulators and effectors of immunity and tissue remodeling. *Nat Immunol* **12**, 21-7 (2011).

194. Monticelli, L.A., Sonnenberg, G.F. & Artis, D. Innate lymphoid cells: critical regulators of allergic inflammation and tissue repair in the lung. *Curr Opin Immunol* (2012).

195. Sonnenberg, G.F. et al. Innate lymphoid cells promote anatomical containment of lymphoid-resident commensal bacteria. *Science* **336**, 1321-5 (2012).

196. Monticelli, L.A. et al. Innate lymphoid cells promote lung-tissue homeostasis after infection with influenza virus. *Nat Immunol* (2011).

197. Tschernig, T. & Pabst, R. Bronchus-associated lymphoid tissue (BALT) is not present in the normal adult lung but in different diseases. *Pathobiology* **68**, 1-8 (2000).

198. GeurtsvanKessel, C.H. et al. Dendritic cells are crucial for maintenance of tertiary lymphoid structures in the lung of influenza virus-infected mice. *J Exp Med* **206**, 2339-49 (2009).

199. Halle, S. et al. Induced bronchus-associated lymphoid tissue serves as a general priming site for T cells and is maintained by dendritic cells. *J Exp Med* **206**, 2593-601 (2009).

200. Wiley, J.A. et al. Inducible Bronchus-associated lymphoid tissue elicited by a protein cage nanoparticle enhances protection in mice against diverse respiratory viruses. *PLoS One* **4**, e7142 (2009).

201. Rangel-Moreno, J. et al. The development of inducible bronchus-associated lymphoid tissue depends on IL-17. *Nat Immunol* **12**, 639-46 (2011).

202. Luhrmann, A., Tschernig, T. & Pabst, R. Stimulation of bronchus-associated lymphoid tissue in rats by repeated inhalation of aerosolized lipopeptide MALP-2. *Pathobiology* **70**, 266-9 (2002).

203. Foo, S.Y. & Phipps, S. Regulation of inducible BALT formation and contribution to immunity and pathology. *Mucosal Immunol* **3**, 537-44 (2010).

204. Hiramatsu, K. et al. Inhalation of diesel exhaust for three months affects major cytokine expression and induces bronchus-associated lymphoid tissue formation in murine lungs. *Exp Lung Res* **29**, 607-22 (2003).

205. Neyt, K., Perros, F., Geurtsvankessel, C.H., Hammad, H. & Lambrecht, B.N. Tertiary lymphoid organs in infection and autoimmunity. *Trends Immunol* **33**, 297-305 (2012).

206. Demoor, T. et al. Role of lymphotoxin-alpha in cigarette smoke-induced inflammation and lymphoid neogenesis. *Eur Respir J* **34**, 405-16 (2009).

207. van der Strate, B.W. et al. Cigarette smoke-induced emphysema: A role for the B cell? *Am J Respir Crit Care Med* **173**, 751-8 (2006).

208. Sato, A., Hayakawa, H., Uchiyama, H. & Chida, K. Cellular distribution of bronchus-associated lymphoid tissue in rheumatoid arthritis. *Am J Respir Crit Care Med* **154**, 1903-7 (1996).

209. Rangel-Moreno, J. et al. Inducible bronchus-associated lymphoid tissue (iBALT) in patients with pulmonary complications of rheumatoid arthritis. *J Clin Invest* **116**, 3183-94 (2006).

210. Kocks, J.R., Davalos-Misslitz, A.C., Hintzen, G., Ohl, L. & Forster, R. Regulatory T cells interfere with the development of bronchus-associated lymphoid tissue. *J Exp Med* **204**, 723-34 (2007).

211. Brusselle, G.G., Demoor, T., Bracke, K.R., Brandsma, C.A. & Timens, W. Lymphoid follicles in (very) severe COPD: beneficial or harmful? *Eur Respir J* **34**, 219-30 (2009).

212. Hogg, J.C. et al. The nature of small-airway obstruction in chronic obstructive pulmonary disease. *N Engl J Med* **350**, 2645-53 (2004).

213. Marchal-Somme, J. et al. Dendritic cells accumulate in human fibrotic interstitial lung disease. *Am J Respir Crit Care Med* **176**, 1007-14 (2007).

214. Perros, F. et al. Pulmonary lymphoid neogenesis in idiopathic pulmonary arterial hypertension. *Am J Respir Crit Care Med* **185**, 311-21 (2012).

215. Brodie, S.J. et al. Pediatric AIDS-associated lymphocytic interstitial pneumonia and pulmonary arterio-occlusive disease: role of VCAM-1/VLA-4 adhesion pathway and human herpesviruses. *Am J Pathol* **154**, 1453-64 (1999).

216. Wallace, W.A., Howie, S.E., Krajewski, A.S. & Lamb, D. The immunological architecture of B-lymphocyte aggregates in cryptogenic fibrosing alveolitis. *J Pathol* **178**, 323-9 (1996).

217. Suda, T. et al. Development of bronchus-associated lymphoid tissue in chronic hypersensitivity pneumonitis. *Chest* **115**, 357-63 (1999).

218. Heier, I. et al. Characterisation of bronchus-associated lymphoid tissue and antigen-presenting cells in central airway mucosa of children. *Thorax* **66**, 151-6 (2011).

219. Hiller, A.S., Tschernig, T., Kleemann, W.J. & Pabst, R. Bronchus-associated lymphoid tissue (BALT) and larynx-associated lymphoid tissue (LALT) are found at different frequencies in children, adolescents and adults. *Scand J Immunol* **47**, 159-62 (1998).

220. Gould, S.J. & Isaacson, P.G. Bronchus-associated lymphoid tissue (BALT) in human fetal and infant lung. *J Pathol* **169**, 229-34 (1993).

221. Bienenstock, J., Johnston, N. & Perey, D.Y. Bronchial lymphoid tissue. I. Morphologic characteristics. *Lab Invest* **28**, 686-92 (1973).

222. Sminia, T., van der Brugge-Gamelkoorn, G.J. & Jeurissen, S.H. Structure and function of bronchus-associated lymphoid tissue (BALT). *Crit Rev Immunol* **9**, 119-50 (1989).

223. Xu, B. et al. Lymphocyte homing to bronchus-associated lymphoid tissue (BALT) is mediated by L-selectin/PNAd, alpha4beta1 integrin/VCAM-1, and LFA-1 adhesion pathways. *J Exp Med* **197**, 1255-67 (2003).

224. Richert, L.E. et al. A virus-like particle vaccine platform elicits heightened and hastened local lung mucosal antibody production after a single dose. *Vaccine* (2012).

225. Carragher, D.M., Rangel-Moreno, J. & Randall, T.D. Ectopic lymphoid tissues and local immunity. *Semin Immunol* **20**, 26-42 (2008).

226. Randall, T.D., Carragher, D.M. & Rangel-Moreno, J. Development of secondary lymphoid organs. *Annu Rev Immunol* **26**, 627-50 (2008).

227. Mebius, R.E. Organogenesis of lymphoid tissues. *Nat Rev Immunol* **3**, 292-303 (2003).

228. Tsuji, M. et al. Requirement for lymphoid tissue-inducer cells in isolated follicle formation and T cell-independent immunoglobulin A generation in the gut. *Immunity* **29**, 261-71 (2008).

229. Yokota, Y. et al. Development of peripheral lymphoid organs and natural killer cells depends on the helix-loop-helix inhibitor Id2. *Nature* **397**, 702-6 (1999).

230. Eberl, G. & Littman, D.R. The role of the nuclear hormone receptor RORgammat in the development of lymph nodes and Peyer's patches. *Immunol Rev* **195**, 81-90 (2003).

231. Marinkovic, T. et al. Interaction of mature CD3+CD4+ T cells with dendritic cells triggers the development of tertiary lymphoid structures in the thyroid. *J Clin Invest* **116**, 2622-32 (2006).

232. Ansel, K.M. et al. A chemokine-driven positive feedback loop organizes lymphoid follicles. *Nature* **406**, 309-14 (2000).

233. Legler, D.F. et al. B cell-attracting chemokine 1, a human CXC chemokine expressed in lymphoid tissues, selectively attracts B lymphocytes via BLR1/CXCR5. *J Exp Med* **187**, 655-60 (1998).

234. Luther, S.A., Ansel, K.M. & Cyster, J.G. Overlapping roles of CXCL13, interleukin 7 receptor alpha, and CCR7 ligands in lymph node development. *J Exp Med* **197**, 1191-8 (2003).

235. Luther, S.A., Lopez, T., Bai, W., Hanahan, D. & Cyster, J.G. BLC expression in pancreatic islets causes B cell recruitment and lymphotoxin-dependent lymphoid neogenesis. *Immunity* **12**, 471-81 (2000).

236. Kratz, A., Campos-Neto, A., Hanson, M.S. & Ruddle, N.H. Chronic inflammation caused by lymphotoxin is lymphoid neogenesis. *J Exp Med* **183**, 1461-72 (1996).

237. Chen, S.C. et al. Ectopic expression of the murine chemokines CCL21a and CCL21b induces the formation of lymph node-like structures in pancreas, but not skin, of transgenic mice. *J Immunol* **168**, 1001-8 (2002).

238. Furtado, G.C. et al. Lymphotoxin beta receptor signaling is required for inflammatory lymphangiogenesis in the thyroid. *Proc Natl Acad Sci U S A* **104**, 5026-31 (2007).

239. Gatumu, M.K. et al. Blockade of lymphotoxin-beta receptor signaling reduces aspects of Sjogren's syndrome in salivary glands of non-obese diabetic mice. *Arthritis Res Ther* **11**, R24 (2009).

240. Rangel-Moreno, J., Moyron-Quiroz, J.E., Hartson, L., Kusser, K. & Randall, T.D. Pulmonary expression of CXC chemokine ligand 13, CC chemokine ligand 19, and CC chemokine ligand 21 is essential for local immunity to influenza. *Proc Natl Acad Sci U S A* **104**, 10577-82 (2007).

241. Steinman, R.M. Dendritic cells: understanding immunogenicity. *Eur J Immunol* **37 Suppl 1**, S53-60 (2007).

242. Ueha, S. et al. CCR7 mediates the migration of Foxp3+ regulatory T cells to the paracortical areas of peripheral lymph nodes through high endothelial venules. *J Leukoc Biol* **82**, 1230-8 (2007).

243. Tsuji, M. et al. Preferential generation of follicular B helper T cells from Foxp3+ T cells in gut Peyer's patches. *Science* **323**, 1488-92 (2009).

244. Kocks, J.R. et al. Chemokine receptor CCR7 contributes to a rapid and efficient clearance of lytic murine gamma-herpes virus 68 from the lung, whereas bronchus-associated lymphoid tissue harbors virus during latency. *J Immunol* **182**, 6861-9 (2009).

245. van Panhuys, N., Perret, R., Prout, M., Ronchese, F. & Le Gros, G. Effector lymphoid tissue and its crucial role in protective immunity. *Trends Immunol* **26**, 242-7 (2005).

246. Maglione, P.J., Xu, J. & Chan, J. B cells moderate inflammatory progression and enhance bacterial containment upon pulmonary challenge with Mycobacterium tuberculosis. *J Immunol* **178**, 7222-34 (2007).

247. Chiavolini, D. et al. Bronchus-associated lymphoid tissue (BALT) and survival in a vaccine mouse model of tularemia. *PLoS One* **5**, e11156 (2010).

248. Tirouvanziam, R. et al. Ex vivo development of functional human lymph node and bronchus-associated lymphoid tissue. *Blood* **99**, 2483-9 (2002).

249. Tschernig, T. & Pabst, R. What is the clinical relevance of different lung compartments? *BMC Pulm Med* **9**, 39 (2009).

250. Pabst, R. & Tschernig, T. Bronchus-associated lymphoid tissue: an entry site for antigens for successful mucosal vaccinations? *Am J Respir Cell Mol Biol* **43**, 137-41 (2010).

251. Hussell, T. & Goulding, J. Structured regulation of inflammation during respiratory viral infection. *Lancet Infect Dis* **10**, 360-6 (2010).

252. Drayton, D.L., Liao, S., Mounzer, R.H. & Ruddle, N.H. Lymphoid organ development: from ontogeny to neogenesis. *Nat Immunol* **7**, 344-53 (2006).

253. Aloisi, F. & Pujol-Borrell, R. Lymphoid neogenesis in chronic inflammatory diseases. *Nat Rev Immunol* **6**, 205-17 (2006).

254. Wissinger, E., Goulding, J. & Hussell, T. Immune homeostasis in the respiratory tract and its impact on heterologous infection. *Semin Immunol* **21**, 147-55 (2009).

255. Kamradt, T., Goggel, R. & Erb, K.J. Induction, exacerbation and inhibition of allergic and autoimmune diseases by infection. *Trends Immunol* **26**, 260-7 (2005).

256. Walzl, G., Tafuro, S., Moss, P., Openshaw, P.J. & Hussell, T. Influenza virus lung infection protects from respiratory syncytial virus-induced immunopathology. *J Exp Med* **192**, 1317-26 (2000).

257. Chen, H.D. et al. Memory CD8+ T cells in heterologous antiviral immunity and immunopathology in the lung. *Nat Immunol* **2**, 1067-76 (2001).

258. Chen, H.D., Fraire, A.E., Joris, I., Welsh, R.M. & Selin, L.K. Specific history of heterologous virus infections determines anti-viral immunity and immunopathology in the lung. *Am J Pathol* **163**, 1341-55 (2003).

259. Bach, J.F. The effect of infections on susceptibility to autoimmune and allergic diseases. *N Engl J Med* **347**, 911-20 (2002).

260. Loftus, E.V., Jr. Clinical epidemiology of inflammatory bowel disease: Incidence, prevalence, and environmental influences. *Gastroenterology* **126**, 1504-17 (2004).

261. Ponsonby, A.L. et al. Exposure to infant siblings during early life and risk of multiple sclerosis. *JAMA* **293**, 463-9 (2005).

262. Herz, U., Lacy, P., Renz, H. & Erb, K. The influence of infections on the development and severity of allergic disorders. *Curr Opin Immunol* **12**, 632-40 (2000).

263. Williams, A.E. et al. Innate imprinting by the modified heat-labile toxin of Escherichia coli (LTK63) provides generic protection against lung infectious disease. *J Immunol* **173**, 7435-43 (2004).

264. Edwards, L. et al. Stimulation via Toll-like receptor 9 reduces Cryptococcus neoformans-induced pulmonary inflammation in an IL-12-dependent manner. *Eur J Immunol* **35**, 273-81 (2005).

265. Rynda-Apple, A. et al. Virus-Like Particle-Induced Protection Against MRSA Pneumonia Is Dependent on IL-13 and Enhancement of Phagocyte Function. *Am J Pathol* (2012).

266. Alpan, O., Bachelder, E., Isil, E., Arnheiter, H. & Matzinger, P. 'Educated' dendritic cells act as messengers from memory to naive T helper cells. *Nat Immunol* **5**, 615-22 (2004).

267. Dahl, M.E., Dabbagh, K., Liggitt, D., Kim, S. & Lewis, D.B. Viral-induced T helper type 1 responses enhance allergic disease by effects on lung dendritic cells. *Nat Immunol* **5**, 337-43 (2004).

268. Abdi, K., Singh, N.J. & Matzinger, P. Lipopolysaccharide-activated dendritic cells: "exhausted" or alert and waiting? *J Immunol* **188**, 5981-9 (2012).

269. Beyer, M. et al. Sustained increases in numbers of pulmonary dendritic cells after respiratory syncytial virus infection. *J Allergy Clin Immunol* **113**, 127-33 (2004).

270. Mason, D. A very high level of crossreactivity is an essential feature of the T-cell receptor. *Immunol Today* **19**, 395-404 (1998).

271. Welsh, R.M., Selin, L.K. & Szomolanyi-Tsuda, E. Immunological memory to viral infections. *Annu Rev Immunol* **22**, 711-43 (2004).

272. Rangel-Moreno, J. et al. B cells promote resistance to heterosubtypic strains of influenza via multiple mechanisms. *J Immunol* **180**, 454-63 (2008).

273. Selin, L.K. et al. Memory of mice and men: CD8+ T-cell cross-reactivity and heterologous immunity. *Immunol Rev* **211**, 164-81 (2006).

274. Kim, S.K. et al. Private specificities of CD8 T cell responses control patterns of heterologous immunity. *J Exp Med* **201**, 523-33 (2005).

275. Wedemeyer, H., Mizukoshi, E., Davis, A.R., Bennink, J.R. & Rehermann, B. Cross-reactivity between hepatitis C virus and Influenza A virus determinant-specific cytotoxic T cells. *J Virol* **75**, 11392-400 (2001).

276. Clute, S.C. et al. Cross-reactive influenza virus-specific CD8+ T cells contribute to lymphoproliferation in Epstein-Barr virus-associated infectious mononucleosis. *J Clin Invest* **115**, 3602-12 (2005).

277. Acierno, P.M. et al. Cross-reactivity between HLA-A2-restricted FLU-M1:58-66 and HIV p17 GAG:77-85 epitopes in HIV-infected and uninfected individuals. *J Transl Med* **1**, 3 (2003).

278. Nilges, K. et al. Human papillomavirus type 16 E7 peptide-directed CD8+ T cells from patients with cervical cancer are cross-reactive with the coronavirus NS2 protein. *J Virol* **77**, 5464-74 (2003).

279. Nie, S., Lin, S.J., Kim, S.K., Welsh, R.M. & Selin, L.K. Pathological features of heterologous immunity are regulated by the private specificities of the immune repertoire. *Am J Pathol* **176**, 2107-12 (2010).

280. Welsh, R.M., Che, J.W., Brehm, M.A. & Selin, L.K. Heterologous immunity between viruses. *Immunol Rev* **235**, 244-66 (2010).

281. Larsen, J.M. et al. Divergent pro-inflammatory profile of human dendritic cells in response to commensal and pathogenic bacteria associated with the airway microbiota. *PLoS One* **7**, e31976 (2012).

282. Ichinohe, T. et al. Microbiota regulates immune defense against respiratory tract influenza A virus infection. *Proc Natl Acad Sci U S A* **108**, 5354-9 (2011).

283. Yoo, J.W., Irvine, D.J., Discher, D.E. & Mitragotri, S. Bio-inspired, bioengineered and biomimetic drug delivery carriers. *Nat Rev Drug Discov* **10**, 521-35 (2011).

284. Villa, L.L. et al. Prophylactic quadrivalent human papillomavirus (types 6, 11, 16, and 18) L1 virus-like particle vaccine in young women: a randomised double-blind placebo-controlled multicentre phase II efficacy trial. *Lancet Oncol* **6**, 271-8 (2005).

285. Garland, S.M. et al. Quadrivalent vaccine against human papillomavirus to prevent anogenital diseases. *N Engl J Med* **356**, 1928-43 (2007).

286. Steinmetz, N.F. Viral nanoparticles as platforms for next-generation therapeutics and imaging devices. *Nanomedicine* **6**, 634-41 (2010).

287. Roldao, A., Mellado, M.C., Castilho, L.R., Carrondo, M.J. & Alves, P.M. Virus-like particles in vaccine development. *Expert Rev Vaccines* **9**, 1149-76 (2010).

288. Roy, P. & Noad, R. Virus-like particles as a vaccine delivery system: myths and facts. *Adv Exp Med Biol* **655**, 145-58 (2009).

289. Landry, N. et al. Preclinical and clinical development of plant-made virus-like particle vaccine against avian H5N1 influenza. *PLoS One* **5**, e15559 (2011).

290. Roldao, A., Mellado, M.C., Castilho, L.R., Carrondo, M.J. & Alves, P.M. Virus-like particles in vaccine development. *Expert Rev Vaccines* **9**, 1149-76.

291. Huang, Z. et al. Virus-like particle expression and assembly in plants: hepatitis B and Norwalk viruses. *Vaccine* **23**, 1851-8 (2005).

292. Jennings, G.T. The coming of age of virus-like particle vaccines. *Biological chemistry* **389**, 521-536 (2008).

293. Schneider-Ohrum, K. & Ross, T.M. Virus-like particles for antigen delivery at mucosal surfaces. *Curr Top Microbiol Immunol* **354**, 53-73 (2012).

294. Deml, L., Speth, C., Dierich, M.P., Wolf, H. & Wagner, R. Recombinant HIV-1 Pr55gag virus-like particles: potent stimulators of innate and acquired immune responses. *Mol Immunol* **42**, 259-77 (2005).

295. Bachmann, M.F. & Jennings, G.T. Vaccine delivery: a matter of size, geometry, kinetics and molecular patterns. *Nat Rev Immunol* **10**, 787-96 (2010).

296. Bachmann, M.F. et al. The influence of antigen organization on B cell responsiveness. *Science* **262**, 1448-51 (1993).

297. Chackerian, B., Lenz, P., Lowy, D.R. & Schiller, J.T. Determinants of autoantibody induction by conjugated papillomavirus virus-like particles. *J Immunol* **169**, 6120-6 (2002).

298. Pinschewer, D.D. et al. Kinetics of protective antibodies are determined by the viral surface antigen. *J Clin Invest* **114**, 988-93 (2004).

299. Jegerlehner, A. et al. TLR9 signaling in B cells determines class switch recombination to IgG2a. *J Immunol* **178**, 2415-20 (2007).

300. Lacasse, P., Denis, J., Lapointe, R., Leclerc, D. & Lamarre, A. Novel plant virus-based vaccine induces protective cytotoxic T-lymphocyte-mediated antiviral immunity through dendritic cell maturation. *J Virol* **82**, 785-94 (2008).

301. Acosta-Ramirez, E. et al. Translating innate response into long-lasting antibody response by the intrinsic antigen-adjuvant properties of papaya mosaic virus. *Immunology* **124**, 186-97 (2008).

302. Kim, R., Kim, K.K., Yokota, H. & Kim, S.H. Small heat shock protein of Methanococcus jannaschii, a hyperthermophile. *Proc Natl Acad Sci U S A* **95**, 9129-33 (1998).

303. Flenniken, M.L., Willits, D.A., Brumfield, S., Young, M.J. & Douglas, T. The Small Heat Shock Protein Cage from Methanococcus jannaschii Is a Versatile Nanoscale Platform for Genetic and Chemical Modification. *Nano Letters* **3**, 1573-1576 (2003).

304. Flenniken, M.L. et al. Melanoma and lymphocyte cell-specific targeting incorporated into a heat shock protein cage architecture. *Chem Biol* **13**, 161-70 (2006).

305. Flenniken, M.L. et al. Selective attachment and release of a chemotherapeutic agent from the interior of a protein cage architecture. *Chem Commun (Camb)*, 447-9 (2005).

306. Kaiser, C.R. et al. Biodistribution studies of protein cage nanoparticles demonstrate broad tissue distribution and rapid clearance in vivo. *Int J Nanomedicine* **2**, 715-33 (2007).

307. Kang, S. et al. Implementation of p22 viral capsids as nanoplatforms. *Biomacromolecules* **11**, 2804-9 (2010).

308. Patterson, D.P., Prevelige, P.E. & Douglas, T. Nanoreactors by Programmed Enzyme Encapsulation Inside the Capsid of the Bacteriophage P22. *ACS Nano* (2012).

309. Prevelige, P.E., Jr., Thomas, D. & King, J. Scaffolding protein regulates the polymerization of P22 coat subunits into icosahedral shells in vitro. *J Mol Biol* **202**, 743-57 (1988).

310. Uchida, M. et al. Site-directed coordination chemistry with P22 virus-like particles. *Langmuir* **28**, 1998-2006 (2012).

311. Botstein, D., Waddell, C.H. & King, J. Mechanism of head assembly and DNA encapsulation in Salmonella phage p22. I. Genes, proteins, structures and DNA maturation. *J Mol Biol* **80**, 669-95 (1973).

312. Matzinger, P. The danger model: a renewed sense of self. *Science* **296**, 301-5 (2002).

313. O'Neil, A., Reichhardt, C., Johnson, B., Prevelige, P.E. & Douglas, T. Genetically programmed in vivo packaging of protein cargo and its controlled release from bacteriophage P22. *Angew Chem Int Ed Engl* **50**, 7425-8 (2011).

314. Bozinovski, S. et al. Innate immune responses to LPS in mouse lung are suppressed and reversed by neutralization of GM-CSF via repression of TLR-4. *Am J Physiol Lung Cell Mol Physiol* **286**, L877-85 (2004).

315. Fujihara, M. et al. Molecular mechanisms of macrophage activation and deactivation by lipopolysaccharide: roles of the receptor complex. *Pharmacol Ther* **100**, 171-94 (2003).

316. Schwarz, T.F. & Leo, O. Immune response to human papillomavirus after prophylactic vaccination with AS04-adjuvanted HPV-16/18 vaccine: improving upon nature. *Gynecol Oncol* **110**, S1-10 (2008).

317. Kasturi, S.P. et al. Programming the magnitude and persistence of antibody responses with innate immunity. *Nature* **470**, 543-7 (2011).

318. Wang, K.L. Human papillomavirus and vaccination in cervical cancer. *Taiwan J Obstet Gynecol* **46**, 352-62 (2007).

319. Koyama, S. et al. Differential role of TLR- and RLR-signaling in the immune responses to influenza A virus infection and vaccination. *J Immunol* **179**, 4711-20 (2007).

320. Wiley, J.A. & Harmsen, A.G. Pneumocystis infection enhances antibody-mediated resistance to a subsequent influenza infection. *J Immunol* **180**, 5613-24 (2008).

321. Mackaness, G.B. The Immunological Basis of Acquired Cellular Resistance. *J Exp Med* **120**, 105-20 (1964).

322. Banchereau, J. et al. Immunobiology of dendritic cells. *Annu Rev Immunol* **18**, 767-811 (2000).

323. Forster, R. et al. CCR7 coordinates the primary immune response by establishing functional microenvironments in secondary lymphoid organs. *Cell* **99**, 23-33 (1999).

324. Randall, T.D. Pulmonary dendritic cells: thinking globally, acting locally. *J Exp Med* **207**, 451-4 (2010).

325. Foo, S.Y. & Phipps, S. Regulation of inducible BALT formation and contribution to immunity and pathology. *Mucosal Immunol* **3**, 537-44.

326. Kawamata, N. et al. Expression of endothelia and lymphocyte adhesion molecules in bronchus-associated lymphoid tissue (BALT) in adult human lung. *Respir Res* **10**, 97 (2009).

327. Kim, K.K., Kim, R. & Kim, S.H. Crystal structure of a small heat-shock protein. *Nature* **394**, 595-9 (1998).

328. Chiba, K., Matsuyuki, H., Maeda, Y. & Sugahara, K. Role of sphingosine 1-phosphate receptor type 1 in lymphocyte egress from secondary lymphoid tissues and thymus. *Cell Mol Immunol* **3**, 11-9 (2006).

329. Cyster, J.G. Chemokines, sphingosine-1-phosphate, and cell migration in secondary lymphoid organs. *Annu Rev Immunol* **23**, 127-59 (2005).

330. Hofmann, M., Brinkmann, V. & Zerwes, H.G. FTY720 preferentially depletes naive T cells from peripheral and lymphoid organs. *Int Immunopharmacol* **6**, 1902-10 (2006).

331. Holt, P.G. Development of bronchus associated lymphoid tissue (BALT) in human lung disease: a normal host defence mechanism awaiting therapeutic exploitation? *Thorax* **48**, 1097-8 (1993).

332. Holt, P.G., Strickland, D.H., Wikstrom, M.E. & Jahnsen, F.L. Regulation of immunological homeostasis in the respiratory tract. *Nat Rev Immunol* **8**, 142-52 (2008).

333. Legge, K.L. & Braciale, T.J. Accelerated migration of respiratory dendritic cells to the regional lymph nodes is limited to the early phase of pulmonary infection. *Immunity* **18**, 265-77 (2003).

334. Cook, D.N. & Bottomly, K. Innate immune control of pulmonary dendritic cell trafficking. *Proc Am Thorac Soc* **4**, 234-9 (2007).

335. Manicassamy, B. et al. Analysis of in vivo dynamics of influenza virus infection in mice using a GFP reporter virus. *Proc Natl Acad Sci U S A* **107**, 11531-6 (2010).

336. Jung, S. et al. In vivo depletion of CD11c+ dendritic cells abrogates priming of CD8+ T cells by exogenous cell-associated antigens. *Immunity* **17**, 211-20 (2002).

337. Bennett, C.L. & Clausen, B.E. DC ablation in mice: promises, pitfalls, and challenges. *Trends Immunol* **28**, 525-31 (2007).

338. Jimenez, F. et al. CCR2 plays a critical role in dendritic cell maturation: possible role of CCL2 and NF-kappa B. *J Immunol* **184**, 5571-81 (2010).

339. van Seventer, G.A. et al. Analysis of T cell stimulation by superantigen plus major histocompatibility complex class II molecules or by CD3 monoclonal antibody: costimulation by purified adhesion ligands VCAM-1, ICAM-1, but not ELAM-1. *J Exp Med* **174**, 901-13 (1991).

340. Damle, N.K. & Aruffo, A. Vascular cell adhesion molecule 1 induces T-cell antigen receptor-dependent activation of CD4+T lymphocytes. *Proc Natl Acad Sci U S A* **88**, 6403-7 (1991).

341. Damle, N.K., Klussman, K., Linsley, P.S. & Aruffo, A. Differential costimulatory effects of adhesion molecules B7, ICAM-1, LFA-3, and VCAM-1 on resting and antigen-primed CD4+ T lymphocytes. *J Immunol* **148**, 1985-92 (1992).

342. Lebedeva, T., Dustin, M.L. & Sykulev, Y. ICAM-1 co-stimulates target cells to facilitate antigen presentation. *Curr Opin Immunol* **17**, 251-8 (2005).

343. Mittelbrunn, M. et al. VLA-4 integrin concentrates at the peripheral supramolecular activation complex of the immune synapse and drives T helper 1 responses. *Proc Natl Acad Sci U S A* **101**, 11058-63 (2004).

344. Grakoui, A. et al. The immunological synapse: a molecular machine controlling T cell activation. *Science* **285**, 221-7 (1999).

345. Carrasco, Y.R. & Batista, F.D. B-cell activation by membrane-bound antigens is facilitated by the interaction of VLA-4 with VCAM-1. *EMBO J* **25**, 889-99 (2006).

346. Vermaelen, K. & Pauwels, R. Accelerated airway dendritic cell maturation, trafficking, and elimination in a mouse model of asthma. *Am J Respir Cell Mol Biol* **29**, 405-9 (2003).

347. Hollingsworth, J.W. et al. TLR4 signaling attenuates ongoing allergic inflammation. *J Immunol* **176**, 5856-62 (2006).

348. Teijaro, J.R. et al. Endothelial cells are central orchestrators of cytokine amplification during influenza virus infection. *Cell* **146**, 980-91 (2011).

349. Manicassamy, B. et al. Analysis of in vivo dynamics of influenza virus infection in mice using a GFP reporter virus. *Proc Natl Acad Sci U S A* **107**, 11531-6.

350. Wiley, J.A., Cerwenka, A., Harkema, J.R., Dutton, R.W. & Harmsen, A.G. Production of interferon-gamma by influenza hemagglutinin-specific CD8 effector T cells influences the development of pulmonary immunopathology. *Am J Pathol* **158**, 119-30 (2001).

351. Holmgren, J. & Czerkinsky, C. Mucosal immunity and vaccines. *Nat Med* **11**, S45-53 (2005).

352. Cox, R.J., Brokstad, K.A. & Ogra, P. Influenza virus: immunity and vaccination strategies. Comparison of the immune response to inactivated and live, attenuated influenza vaccines. *Scand J Immunol* **59**, 1-15 (2004).

353. Belshe, R., Lee, M.S., Walker, R.E., Stoddard, J. & Mendelman, P.M. Safety, immunogenicity and efficacy of intranasal, live attenuated influenza vaccine. *Expert Rev Vaccines* **3**, 643-54 (2004).

354. Nochi, T. Nanogel antigenic protein-delivery system for adjuvant-free intranasal vaccines. *Nature materials* **9**, 572-578 (2010).

355. Heegaard, P.M.H. Dendrimers for Vaccine and Immunostimulatory Uses. A Review. *Bioconjugate Chemistry* **21**, 405-418 (2010).

356. Stano, A. PPS nanoparticles as versatile delivery system to induce systemic and broad mucosal immunity after intranasal administration. *Vaccine* (2010).

357. Jegerlehner, A. A molecular assembly system that renders antigens of choice highly repetitive for induction of protective B cell responses. *Vaccine* **20**, 3104 (2002).

358. Peacey, M. Versatile RHDV virus-like particles: Incorporation of antigens by genetic modification and chemical conjugation. *Biotechnology and bioengineering* **98**, 968-977 (2007).

359. Chen, Z. Protective immune response in mice vaccinated with a recombinant adenovirus containing capsid precursor polypeptide P1, nonstructural protein 2A and 3C protease genes (P12A3C) of encephalomyocarditis virus. *Vaccine* **26**, 573 (2008).

360. Brennan, F.R. Chimeric plant virus particles administered nasally or orally induce systemic and mucosal immune responses in mice. *Journal of Virology* **73**, 930 (1999).

361. Caldeira, J.C. Immunogenic display of diverse peptides, including a broadly cross-type neutralizing human papillomavirus L2 epitope, on virus-like particles of the RNA bacteriophage PP7. *Vaccine* **28**, 4384 (2010).

362. Manayani, D.J. A viral nanoparticle with dual function as an anthrax antitoxin and vaccine. *PLoS pathogens* **3**, e142 (2007).

363. Lenz, P. et al. Papillomavirus-like particles induce acute activation of dendritic cells. *J Immunol* **166**, 5346-55 (2001).

364. Lenz, P. et al. Interaction of papillomavirus virus-like particles with human myeloid antigen-presenting cells. *Clin Immunol* **106**, 231-7 (2003).

365. Savard, C. et al. Improvement of the Trivalent Inactivated Flu Vaccine Using PapMV Nanoparticles. *PLoS One* **6**, e21522 (2011).

366. Liepold, L.O. Supramolecular Protein Cage Composite MR Contrast Agents with Extremely Efficient Relaxivity Properties. *Nano Letters* **9**, 4520-4526 (2009).

367. Abedin, M.J., Liepold, L., Suci, P., Young, M. & Douglas, T. Synthesis of a Cross-Linked Branched Polymer Network in the Interior of a Protein Cage. *Journal of the American Chemical Society* **131**, 4346-4354 (2009).

368. Gupta, S.S. Accelerated Bioorthogonal Conjugation: A Practical Method for the Ligation of Diverse Functional Molecules to a Polyvalent Virus Scaffold. *Bioconjugate Chemistry* **16**, 1572-1579 (2005).

369. Chatterji, A. Chemical Conjugation of Heterologous Proteins on the Surface of Cowpea Mosaic Virus. *Bioconjugate Chemistry* **15**, 807-813 (2004).

370. Whitaker, J.R. An absolute method for protein determination based on difference in absorbance at 235 and 280 nm. *Analytical biochemistry* **109**, 156 (1980).

371. Hansen, R.E. Quantification of protein thiols and dithiols in the picomolar range using sodium borohydride and 4, 4'-dithiodipyridine. *Analytical biochemistry* **363**, 77 (2007).

372. Martos, G. Egg White Ovalbumin Digestion Mimicking Physiological Conditions. *Journal of agricultural and food chemistry* **58**, 5640-5648 (2010).

373. Matzinger, P. & Kamala, T. Tissue-based class control: the other side of tolerance. *Nat Rev Immunol* **11**, 221-30 (2011).

374. Matzinger, P. Friendly and dangerous signals: is the tissue in control? *Nat Immunol* **8**, 11-3 (2007).

375. Selin, L.K., Brehm, M.A., Kim, S.K. & Chen, H.D. Heterologous immunity and the CD8 T cell network. *Springer Semin Immunopathol* **24**, 149-68 (2002).

376. Selin, L.K., Varga, S.M., Wong, I.C. & Welsh, R.M. Protective heterologous antiviral immunity and enhanced immunopathogenesis mediated by memory T cell populations. *J Exp Med* **188**, 1705-15 (1998).

377. Venter, P.A. et al. Multivalent display of proteins on viral nanoparticles using molecular recognition and chemical ligation strategies. *Biomacromolecules* **12**, 2293-301 (2011).

378. Chackerian, B., Durfee, M.R. & Schiller, J.T. Virus-like display of a neo-self antigen reverses B cell anergy in a B cell receptor transgenic mouse model. *J Immunol* **180**, 5816-25 (2008).

379. Bhagawati-Prasad, V.N. et al. CD40mAb adjuvant induces a rapid antibody response that may be beneficial in post-exposure prophylaxis. *J Immune Based Ther Vaccines* **8**, 1 (2010).

380. Kim, K.K., Kim, R. & Kim, S.-H. Crystal structure of a small heat-shock protein. *Nature* **394**, 595-599 (1998).

381. Zhang, J.G. et al. The dendritic cell receptor Clec9A binds damaged cells via exposed actin filaments. *Immunity* **36**, 646-57 (2012).

382. Ahrens, S. et al. F-actin is an evolutionarily conserved damage-associated molecular pattern recognized by DNGR-1, a receptor for dead cells. *Immunity* **36**, 635-45 (2012).

383. Gebb, S. & Stevens, T. On lung endothelial cell heterogeneity. *Microvasc Res* **68**, 1-12 (2004).

384. Thorin, E. & Shreeve, S.M. Heterogeneity of vascular endothelial cells in normal and disease states. *Pharmacol Ther* **78**, 155-66 (1998).

385. Lukacs-Kornek, V. et al. Regulated release of nitric oxide by nonhematopoietic stroma controls expansion of the activated T cell pool in lymph nodes. *Nat Immunol* **12**, 1096-104 (2011).

386. Randall, T.D. Stromal cells put the brakes on T-cell responses. *Immunol Cell Biol* **90**, 469-70 (2011).